Polymer Reviews

ISSN: 1558-3724 (Print) 1558-3716 (Online) Journal homepage: https://www.tandfonline.com/loi/lmsc20

Electromagnetic Interference Shielding Polymers and Nanocomposites - A Review

Dawei Jiang, Vignesh Murugadoss, Ying Wang, Jing Lin, Tao Ding, Zicheng Wang, Qian Shao, Chao Wang, Hu Liu, Na Lu, Renbo Wei, Angaiah Subramania & Zhanhu Guo

To cite this article: Dawei Jiang, Vignesh Murugadoss, Ying Wang, Jing Lin, Tao Ding, Zicheng Wang, Qian Shao, Chao Wang, Hu Liu, Na Lu, Renbo Wei, Angaiah Subramania & Zhanhu Guo (2019): Electromagnetic Interference Shielding Polymers and Nanocomposites - A Review, Polymer Reviews, DOI: 10.1080/15583724.2018.1546737

To link to this article: https://doi.org/10.1080/15583724.2018.1546737

Published online: 08 Feb 2019.

POLYMER REVIEWS
https://doi.org/10.1080/15583724.2018.1546737

Taylor & Francis
Taylor & Francis Group

REVIEW

Electromagnetic Interference Shielding Polymers and Nanocomposites - A Review

Dawei Jiang[a]*, Vignesh Murugadoss[b,c]*, Ying Wang[a], Jing Lin[d], Tao Ding[e], Zicheng Wang[b,f], Qian Shao[g], Chao Wang[h], Hu Liu[b], Na Lu[f], Renbo Wei[i], Angaiah Subramania[c], and Zhanhu Guo[b]

[a]Department of Chemical Engineering and Technology, College of Science, Northeast Forestry University, Harbin, China; [b]Integrated Composites Laboratory (ICL), Department of Chemical and Biomolecular Engineering, University of Tennessee, Knoxville, TN, USA; [c]Electrochemical Energy Research Lab, Centre for Nanoscience and Technology, Pondicherry University, Puducherry, India; [d]Department of Chemical Engineering, School of Chemistry and Chemical Engineering, Guangzhou University, Guangzhou, China; [e]Department of Chemistry, College of Chemistry and Chemical Engineering, Henan University, Kaifeng, P. R. China; [f]Department of Civil Engineering, Lyles School of Civil Engineering, School of Materials Engineering, Birck Nanotechnology Center, Purdue University, West Lafayette, IN, USA; [g]Department of Applied Chemistry, College of Chemical and Environmental Engineering, Shandong University of Science and Technology, Qingdao, Shandong, China; [h]Department of Materials Science and Engineering, College of Materials Science and Engineering, North University of China, Taiyuan, China; [i]Department of Chemistry, Research Branch of Advanced Functional Materials, University of Electronic Science and Technology of China, Chengdu, China

ABSTRACT

Intrinsically conducting polymers (ICP) and conductive fillers incorporated conductive polymer-based composites (CPC) greatly facilitate the research in electromagnetic interference (EMI) shielding because they not only provide excellent EMI shielding but also have advantages of electromagnetic wave absorption rather than reflection. In this review, the latest developments in ICP and CPC based EMI shielding materials are highlighted. In particular, existing methods for adjusting the morphological structure, electric and magnetic properties of EMI shielding materials are discussed along with the future opportunities and challenges in developing ICP and CPC for EMI shielding applications.

ARTICLE HISTORY
Received 29 August 2018
Accepted 2 October 2018

KEYWORDS
Absorption dominant; Conductive polymer composites; Electromagnetic interference shielding; Intrinsically conducting polymers; lightweight materials; Multi-component systems;

1. Introduction

Electromagnetic interference (EMI) has become a severe concern owing to rapid advancement in technology and widespread usage of electronic devices.[1–3] Electromagnetic interference is an electromagnetic pollution caused by electromagnetic noise originated either from natural source (lighting, solar flares, etc.) or man-made devices (electrical circuit, electronic devices,

CONTACT Jing Lin linjing@gzhu.edu.cn Department of Chemical Engineering, School of Chemistry and Chemical Engineering, Guangzhou University, Guangzhou, China; Tao Ding dingtao@henu.edu.cn Department of Chemistry, College of Chemistry and Chemical Engineering, Henan University, Kaifeng, P. R. China; Renbo Wei weirb10@uestc.edu.cn Department of Chemistry, Research Branch of Advanced Functional Materials, University of Electronic Science and Technology of China, Chengdu, China; Zhanhu Guo zguo10@utk.edu Integrated Composites Laboratory (ICL), Department of Chemical and Biomolecular Engineering, University of Tennessee, Knoxville 37996, TN, USA.
*Dawei Jiang and Vignesh Murugadoss contributed equally and should be treated as the co-first authors.
Color versions of one or more of the figures in the article can be found online at www.tandfonline.com/lmsc

etc.) over a frequency range (depends on the source) that affects or degrades the performance of another electronic device/electrical circuit and loss of stored data.[4] The disturbance may be caused by electromagnetic coupling, electromagnetic induction or conduction. Anthropogenic electromagnetic noise also affects biological processes, including human health.[5,6] These major issues have spurred researchers to develop materials for EMI shielding (or EMI attenuation), having a broad range of applications ranging from the electronic systems to biological systems.[7–10] In order to avoid serious problems of EMI, some organizations have standardized electromagnetic compatibility (EMC) regulations.[11] Electromagnetic compatibility refers to the *ABILITY OF AN EQUIPMENT* or an EMI shielding material that does not affect itself or any other equipment due to EM radiation.[12,13]

The usage of traditional metal and metallic composites as an EMI shielding materials is restricted by their high density, poor mechanical flexibility, corrosiveness, and tedious and expensive processing costs. Hence, the advanced EMI shielding materials are now mainly focused on carbon matrix, polymeric matrix, and ceramic matrix composites.[14–24] The necessities for a standard EMI shielding material are high electrical conductivity, excellent thermal stability, and low density.[25–27] Carbon nanostructures have extended their interests over metals due to their good electrical conductivity, corrosion resistance, and flexibility.[28,29] Even though carbon nanostructures suffer from high cost, tedious synthesis procedures, and poor EM absorption properties, the dielectric loss of carbon nanostructures is ascribed to electron polarization rather than natural resonance and Debye dipolar relaxation. Also, their high electron mobility causes considerable skin effect on EM wave irradiation. It has been reported that the addition of polymers to the carbon nanostructures can overcome these limitations and improve their EM absorption properties.[30–33] For example, Yu et al. demonstrated that deposition of polyaniline (PANI) nanoarray onto the graphene improved their EM absorption.[34] Bera et al. demonstrated that the electromagnetic wave absorption of the FRS [Fe_3O_4 coated reduced graphene oxide (RGO)/single wall carbon nanohorn (SWCNH)] was increased after incorporation into polydimethylsiloxane (PDMS) matrix. The dipole polarization and interfacial polarization along with the reduction in surface reflectivity due to skin effect contributed to this enhanced EM absorption.[35]

In that context, the intrinsic conducting polymers (ICP) and the conductive polymer composites (CPC) (insulating polymers filled with conducting fillers) play an important role in the development of commercially viable EMI shielding materials.[36–38]

The radar plots representing the properties of ICP based composites and CPC are given in Figure 1. To be more specific, ICP and CPC based EMI shielding materials with both corrosion resistance and lightweight have desirable electrical conductivity and excellent properties for the absorption or reflection of the electromagnetic radiation over a wide range of frequency.[39–42] Eventually, polymers composited with nanostructured materials have also enhanced their physical properties and prevent their agglomeration, without affecting EMI shielding performance.[43–46]

The number of publications associated with EMC shows an increasing trend in the last 5 years (2013–2018) by ~64% (Fig. 2a). This indicates the importance in the development of EMI shielding material. Figure 2b presents the importance of polymer in EMI shielding as it comprises more than the half of EMI shielding publication.

Although there are many reviews on ICP- and CPC- based EMI shielding materials,[47–50] reviews on the effects of process parameters on the physical as well as EMI

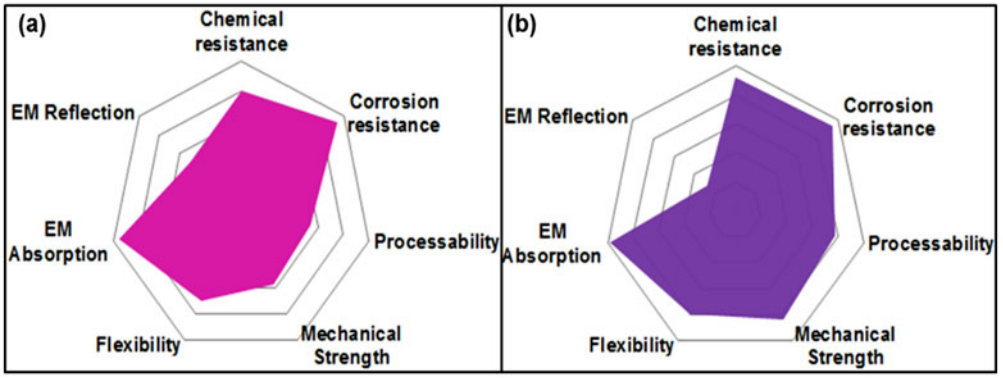

Figure 1. Radar plots representing the performance of (a) ICP based composites and (b) conductive polymer composites (CPC).

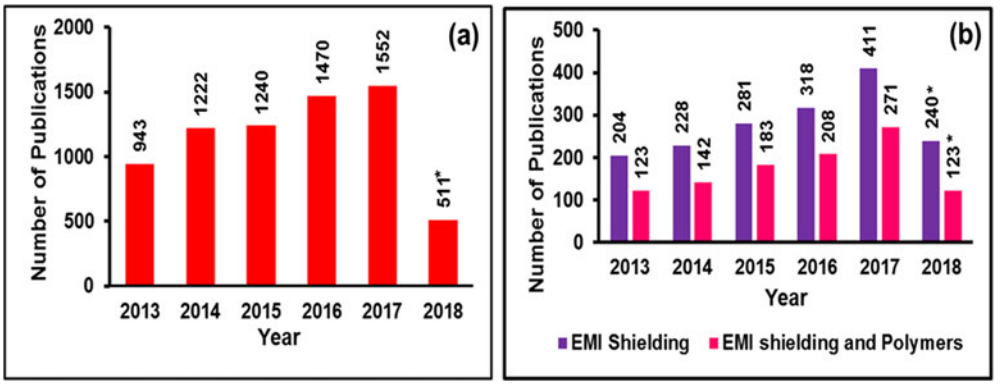

Figure 2. Graph representing a number of publications containing the keywords (a) "electromagnetic compatibility", (b) "electromagnetic interference shielding" and Electromagnetic interference shielding and polymers" in the last 5 years (*Till July 2018) obtained from Scopus.

shielding properties of ICP and CPC have not been reported. In this review, the interaction between the polymer and conductive fillers, filler concentration and their arrangement in the polymer matrix, percolation threshold theory, thermodynamics of polymer blends, and EMI mechanism of various advanced polymeric materials are introduced in detail. Besides, current research on ICP and CPC based EMI shielding materials are also discussed.

2. Basic principles of EMI shielding

2.1. EMI shielding effectiveness (EMI SE)

The capability of an EMI shielding material in attenuation or reduction of EM signal is defined by the term electromagnetic shielding effectiveness (*SE*). It is the ratio between incident field strength and transmitted field strength and expressed as in Equations (1–3);[51]

$$SE_P = 10\log(P_{in}/P_{out}) \tag{1}$$

$$SE_E = 20\log(E_{in}/E_{out}) \tag{2}$$

$$SE_H = 20\log(H_{in}/H_{out}) \tag{3}$$

where *P, E,* and *H* are the strength of plane wave, electric field, and magnetic field, respectively of the EM wave. The subscripts *in* and *out* represent the magnitude of the field strength that is *incident on* and *transmitted through* an EMI shielding material, respectively. EMI SE is expressed in decibels (dB). All electromagnetic waves include an electric (*E*) and a magnetic (*H*) fields orthogonal to each other. An EM wave propagates at a right angle to the plane containing electric field and magnetic field, and its characteristics depend on their frequency and associated photon energies. The ratio between the electric field strength and the magnetic field strength is called wave impedance. Based on the distance (*r*) of the EMI shielding material from an EM wave source, the region of measurement is separated into the *far-field* and the *near-field* region. In the *far-field* region, where the distance between EM wave source and shielding material (*r*) is greater than $\lambda/2\pi$, the ratio of the *E* to *H* (EM wave impedance) is equal to the intrinsic impedance of free space ($Z_o = 377\ \Omega$). So in the far-field region, plane wave exists and $SE_E = SE_H$. In the *near-field* region where *r* is less than $\lambda/2\pi$, the EM wave impedance is not equal to the intrinsic impedance of the free space. In this region, an EM wave is either electrical field dominant (large EM wave impedance) or magnetic field dominant (small EM wave impedance) that depends on its source and distance. If the EM wave impedance is higher than the Z_o, then it is electric field dominant and vice-versa. Thus $SE_E \neq SE_H$. The transition point occurs where the distance is less than $\lambda/2\pi$. The region of a transition is known as the transition region at which *r* is approximately equal to $\lambda/2\pi$.[52,53]

2.2. EMI shielding mechanism

For an EMI shielding material, the total EMI *SE* is contributed from three mechanisms, namely, absorption, reflection, and multiple-internal reflections as illustrated in Figure 3. When an EM wave approaches the shielding material's surface, whose intrinsic impedance is different from the impedance of EM wave propagating medium, the wave gets reflected away from the surface and also transmitted inside the material. The strength of the reflected and transmitted waves is governed by the impedance of the medium and material. Further, the strength of the transmitted waves will decrease exponentially as it travels inside the material. The distance at which its strength becomes equal to *1/e* (*e* is the Euler's number and *1/e = 0.37*) is known as skin depth (δ). When the transmitted reaches another surface of the material, a portion of it will get re-reflected (multiple-internal reflection) and another portion will get transmitted.

The skin depth of a good conductor (*i.e.*, when $\sigma \gg 2\pi\omega\varepsilon_o$) can be expressed as Equation (4);

$$\delta = \sqrt{\frac{1}{\pi\omega\mu\sigma}} \tag{4}$$

where ω is the frequency, μ is the relative magnetic permeability of shielding material, σ is electrical conductivity of shielding material, ε_o is the permittivity of free space (8.854×10^{-12} F/m). According to Equation (4), the skin depth will vary inversely with respect to electric conductivity, magnetic permeability, and frequency. This implies that

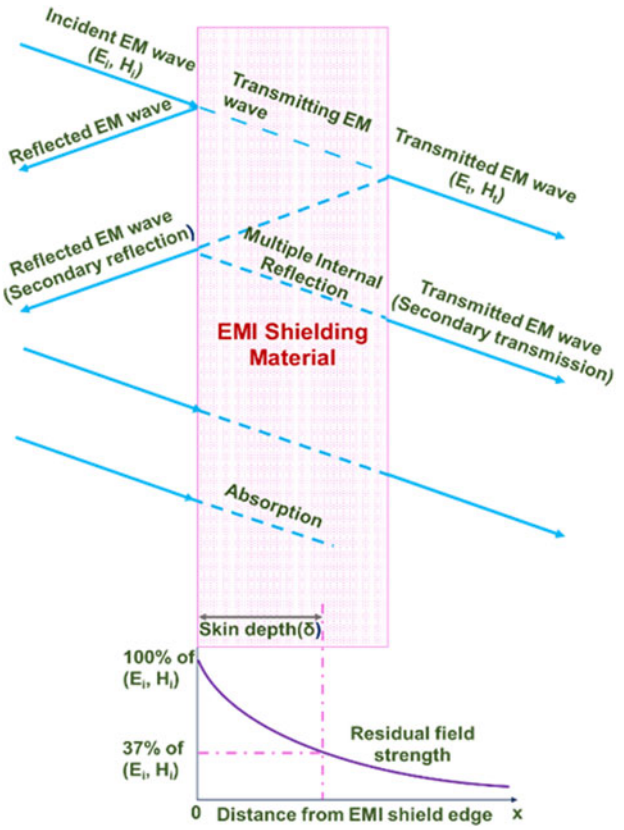

Figure 3. Pictorial depiction of the EMI shielding mechanism and the skin depth of an EMI shielding material.

an increase in the electric conductivity, magnetic permeability, and frequency increases the reflection rather than the absorption.[54]

Thus, the total *SE* of an EMI shielding material (SE_T) is the total of three *SE* contributed from reflection (SE_R), absorption (SE_A), and multiple-internal reflections (SE_M) as depicted in Equation (5);

$$\mathrm{SE_T} = \mathrm{SE_A} + \mathrm{SE_R} + \mathrm{SE_M} \tag{5}$$

The losses due to reflection and multiple-internal reflection mechanisms are the function of impedance and hence their values are different for the electric field, magnetic field, and a plane wave. On contrary, absorption phenomenon does not depend on the impedance and hence the absorption loss will have the same value for all these three fields.[55] SE_M is negligible when SE_A is greater than 10 dB.

2.3. Properties governing EMI shielding mechanism

EMI shielding mechanisms of an EMI shielding material can be understood by measuring their dielectric (relative complex permittivity, $\varepsilon_r = \varepsilon_r' - j\varepsilon_r''$) and magnetic (relative complex permeability, $\mu_r = \mu_r' - j\mu_r''$) properties.[56] The real parts ε_r' and μ_r' indicate the charge storage and magnetic storage of the EM waves, whereas their imaginary parts ε_r''

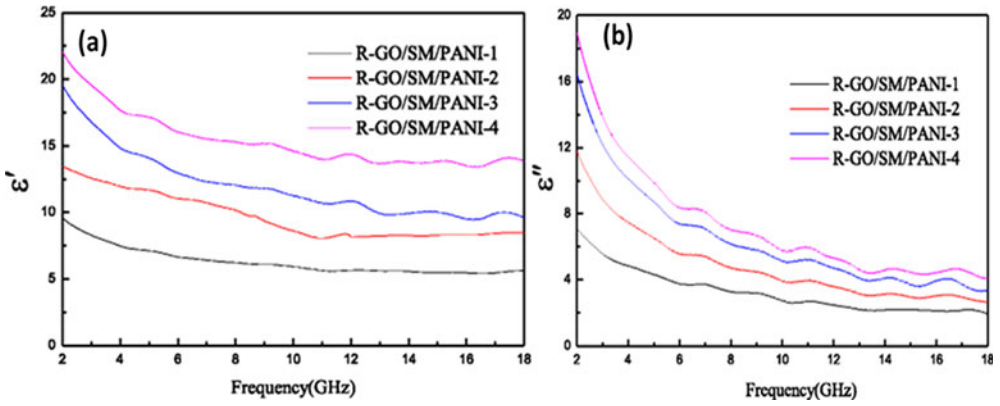

Figure 4. ε'_r and ε''_r values of r-GO/Strontium ferrite/polyaniline composites in the X-band. Reproduced with permission from ref.[62]

and μ''_r indicate dielectric loss and magnetic loss during the interaction with EM waves, respectively. The amount of losses can be calculated from the tangent of dielectric loss ($\tan\delta_\varepsilon = \frac{\varepsilon''_r}{\varepsilon'_r}$) and magnetic loss ($\tan\delta_\mu = \frac{\mu''_r}{\mu'_r}$).[57]

2.3.1. Dielectric property

The dielectric loss is mostly governed by ionic, orientational, electronic, and interfacial polarization. The ionic and orientational polarization attributed to the bound charges in the material. Interfacial polarization arises from space charges that mount up owing to the dissimilarity in the electrical conductivity/dielectric constant at the interface of two different materials, according to Maxwell-Wagner-Sillars (MWS) theory.[58]

The ε'_r and ε''_r can be related by the following Cole-Cole Equation (6);[59]

$$\left(\varepsilon'_r - \frac{\varepsilon_s + \varepsilon_\infty}{2}\right)^2 + \left(\varepsilon''_r\right)^2 = \left(\frac{\varepsilon_s - \varepsilon_\infty}{2}\right)^2 \tag{6}$$

where ε_s is the static dielectric constant and ε_∞ is the relative dielectric constant.

When the Cole-Cole plot is a semicircle, then the semicircle is related to a Debye relaxation process. For composite materials, more than one semicircle or distorted semicircle may be observed. These are attributed to more than one Debye relaxation and other mechanisms such as interfacial polarizations. For highly conducting materials, semicircle may not be observed, as the loss results mainly from conduction loss, which can be expressed as Equation (7);

$$\varepsilon''_r = \frac{\sigma}{2\pi\omega\varepsilon_o} \tag{7}$$

The ε'_r and ε''_r values will decrease with an increase in the frequency as shown in Figure 4 and obey the relation given by Equation (8),[60]

$$\varepsilon''_r = \sigma_{AC} - \sigma_{DC}\left(\varepsilon'_r \times \omega\right) \tag{8}$$

where σ_{AC} is AC electrical conductivity, σ_{DC} is DC electrical conductivity, and ω is frequency. This is because of both the decrease in the space charge polarization and the lack of dipole orientation with varying the field at higher frequencies.[61]

2.3.2. Magnetic property

The magnetic loss arises from domain wall loss, hysteresis loss, eddy current loss, and residual loss.[63] The hysteresis loss results from the hysteresis (*i.e.*, time lag of magnetization vector M, behind the magnetic field vector H), where magnetic energy is dissipated as heat. The eddy current loss is expressed as Equation (9);[64]

$$C_o = {\mu_r''}\Big/{\omega.(\mu_r')^2} = \frac{2\pi}{3}\mu_o\sigma D^2 \tag{9}$$

where μ_o is vacuum permeability and D is the diameter of the magnetic nanoparticle. The eddy current loss (C_o) remains constant with changing the frequency. For highly conducting materials, the eddy current loss is negligible and expressed as in Equation (10);

$$\frac{\mu_r''}{\mu_r'} \propto \frac{\mu_r'' D^2 \omega}{\rho} \tag{10}$$

where ρ is the electrical resistivity. The other losses include natural resonance and exchange resonance. The natural resonance usually occurs at a lower frequency and nano-sized particles will enhance the exchange resonance.[65,66] Ferromagnetic resonance theory states that the effective magnetic field (anisotropic energy) governs the natural resonance as expressed in Equations (11 and 12);[67]

$$\omega_r = \frac{\gamma}{2\pi} H_e \tag{11}$$

$$H_e = \frac{4\kappa_1}{3\mu_o M_s} \tag{12}$$

where $\frac{\gamma}{2\pi}$ is the gyromagnetic ratio (equals to 28 GHz T^{-1}), H_e is the effective magnetic field, κ_1 is magnetic crystalline anisotropy co-efficient for a magnetic material, and $\mu_o M_s$ is the saturation magnetization. A higher the effective magnetic field (Anisotropic energy) favors a higher the EM wave absorption in the higher frequency range.[68] A lower value of μ_r' (magnetic storage) than the value of μ_r'' (magnetic loss) is desirable for the absorption of EM wave.

The reflection loss of a material depends on the mobile charge carriers. Reflection does not need interconnected conducting filler network, but it possibly will improve with the presence of the interconnected network. On the other hand, electric and magnetic dipoles dominate the absorption loss. In absence of magnetic property, the EMI shielding depends solely on dielectric property and vice versa.[69] Multiple-internal reflections originate from the reflections at the interfaces and in-homogeneities of the shielded material.

2.4. EM absorption

Since the reflection loss causes secondary EM pollution, EMI shielding materials exhibiting strong absorption have attracted the research interests. For the EMI shielding materials, SE_A, SE_R, and SE_M as a function of their electromagnetic properties can be expressed as Equations (13–15);[70]

$$SE_A = 20d\sqrt{\sigma_{AC}\cdot/_2} \tag{13}$$

$$SE_R = 10\log\left[\frac{\sigma_{AC}}{16.\varepsilon_o.\mu_r.\omega}\right] \tag{14}$$

$$SE_M = 20\log 1 - e^{-2\frac{d}{\delta}} \ . \ e^{-j\frac{2}{\delta}} \tag{15}$$

where d is the distance traveled by the EM waves inside the EMI shielding material. The above Equations (13–15) imply that the reflection of an EMI shielding material is a function of $\frac{\sigma_{AC}}{\mu_r}$ and will decrease with an increase in frequency, whereas the absorption loss is a function $\sigma_{AC}.\mu_r$ and will increase with an increase in frequency. Multiple-internal reflection can be neglected for the EMI shielding materials whose thickness is larger than its skin depth (δ).[71] For a shielding material with a thickness less than the value of δ, the multiple-internal reflection decreases the EMI *SE*. Their EMI *SE* will increase with an increase in thickness.[72]

As per the transmission line theory, for an EMI shielding material having a perfect conductor at its back, reflection loss (RL) at its surface as a function of impedance is defined as Equation (16),

$$RL(dB) = 20\log\left[\frac{Z_{in} - Z_o}{Z_{in} + Z_o}\right] \tag{16}$$

where Z_{in} is the input impedance of the EMI shielding material at the surface and Z_o is the intrinsic impedance of free space (377 Ω). The Z_{in} is given by Equation (17);

$$Z_{in} = \sqrt{\mu_r/\varepsilon_r}\tanh\left[j(2\pi\omega d/c)\sqrt{\mu_r.\varepsilon_r}\right] \tag{17}$$

where c is the velocity of light.

EM absorption ability of an EMI shielding material can be confirmed by calculating the attenuation constant (α) using Equation (18);

$$\alpha = \frac{\sqrt{2}\pi\omega}{c} \times \sqrt{(\varepsilon''\mu'' - \varepsilon'\mu') + \sqrt{(\varepsilon''\mu'' - \varepsilon'\mu')^2 + (\varepsilon''\mu'' + \varepsilon'\mu')^2}} \tag{18}$$

These above equations imply that to achieve good EMI absorbing materials, the following two criteria needed be satisfied: (1) excellent impedance matching and (2) good balance between the dielectric loss ($\tan\delta_\varepsilon = {}^{\varepsilon''}/_{\varepsilon'}$) and magnetic loss ($\tan\delta_\mu = {}^{\mu''}/_{\mu'}$). Figure 5 represents the attenuation constant in the X-band range for PVdF/TPU blends (50/50) containing different loadings of Fe-Ni alloy@MWCNT. It can be observed that the EM attenuation for polymer blends containing pristine MWCNT and pristine Fe-Ni alloy is lower than other composites containing both Fe-Ni alloy@ MWCNT due to their poor permeability and poor permittivity, respectively. The PVdF/TPU polymer blend containing Fe-Ni alloy@ MWCNT in the 3:1 ratio exhibited a higher α, attributed to the impedance matching and a balance between the dielectric and magnetic properties. These results portrayed that the importance of energy conservation and impedance matching instead of materials' superior property.[73]

For highly conducting materials, its electrical conductivity (σ) is the only key parameter for *SE* because of their high $\tan\delta_\varepsilon$ (greater than 1). On the other hand, for the materials whose conductivity is weak ($\tan\delta_\varepsilon \ll 1$), both electrical conductivity and permittivity are important parameters for ICP and CPC.[74] Therefore, optimizing the

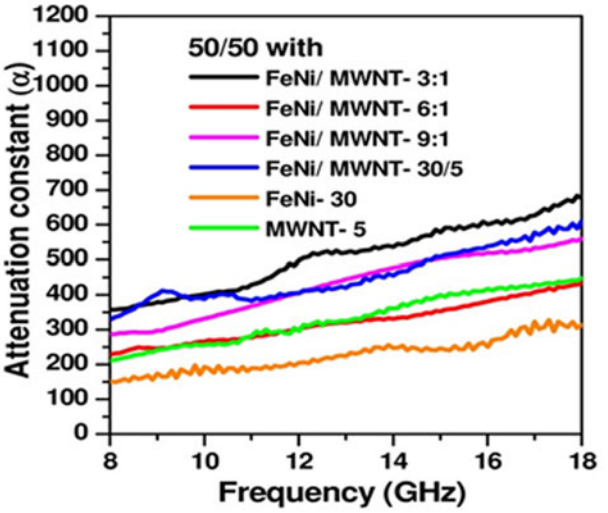

Figure 5. Attenuation constant of the PVdF/TPU (50/50) blends containing a different ratio of Fe-Ni@MWCNT in the X-band range. Reproduced with permission from ref.[73] Copyright © Wiley-VCH Verlag GmbH & Co. KGaA, Weinheim.

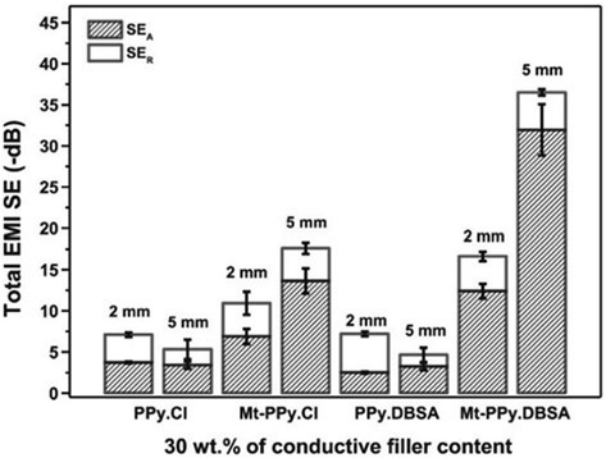

Figure 6. EMI SE of TPU based CPC incorporated with HCl doped PPy (PPy.Cl); Montmorillonite/HCl doped PPy (Mt-PPy.Cl), DBSA doped PPy (PPy.DBSA) and Montmorillonite/DBSA doped PPy (Mt-PPy.DBSA) with respect to the shielding material thickness. *DBSA: Dodecyl benzene sulfonic acid. Reproduced with permission from ref.[76] Copyright © 2018 John Wiley & Sons, Ltd.

thickness and electromagnetic properties of EMI shielding materials is important to achieve effective EMI shielding and to govern the corresponding mechanism.[75] Figure 6 depicts the influence of shielding material's thickness on its SE_T of thermoplastic polyurethane (TPU) based CPC. It is apparent that the SE_T increases with an increase in the thickness of the shielding material. The higher EMI *SE* for the montmorillonite/DBSA doped PPy (Mt-PPy.DBSA) is attributed to a better dispersion of Mt-PPy. DBSA that provides enhanced dipole and interface polarization and improved electrical conductivity.[76]

2.5. Experimental determination of shielding effectiveness

Experimentally, EMI SE_T of an EMI shielding material is obtained from complex scattering parameters (S-parameters), S11 (or S22), and S12 (or S21), of a network analyzer. (1) Shield box method (dual chamber method), (2) Shield room method, and (3) Coaxial transmission line test are three methods that have been employed for investigating the EMI shielding performance of a material. The shield box method (dual chamber) is used to compare the EMI shielding performance of different test samples made up of different materials. This method comprises of a receiving antenna inside a metal box having a sample port in one wall and a transmitting antenna outside the box. The shield box method is preferred for near-field measurements. However, it is limited by its small frequency ranges for measurement (up to 500 MHz) and poor correlations between the results. The shield room method is similar in principle to the shield box method that is designed in such a way to overcome the limitations of a shield box method. In this method, the components such as receiving antenna, transmitting antenna, and EM source generator are isolated to eliminate the possibilities of interference and thereby improve the reliability of data. The coaxial transmission line setup comprises of two sample holders (or coaxial adapters) and a network analyzer with the signals transmitted through a coaxial cable that is coupled with the attenuators. It is based on transmission line theory and preferred for far-field measurements. In addition to the above-mentioned methods, Open shield (or) Free space method is used to measure the EMI *SE* for a designed shielding of an electronic system. This method is widely used to evaluate the EMI *SE* for an assembled electronic system rather than a specific material. Figure 7 illustrates the S-parameters from a two-port vector network analyzer (VNA) representing the incident and transmitted EM waves.

From the S-parameters, the absorption factor (A), transmission factor (T), and reflection factor (R) of EM wave through an EMI shielding material can be expressed as Equations (19–21):[77]

$$R = {S_{11}}^2 \tag{19}$$

$$T = {S_{21}}^2 \tag{20}$$

$$A = 1 - R - T \tag{21}$$

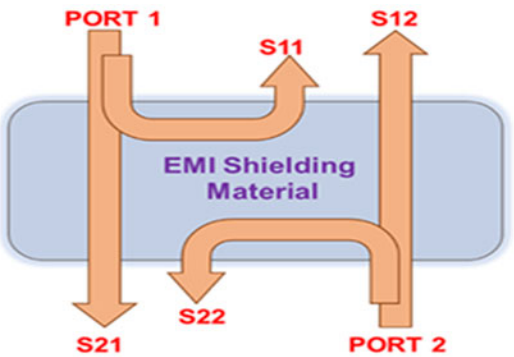

Figure 7. Complex scattering parameters of an EMI shielding material from a two-port VNA.

The corresponding SE_A, SE_R, and SE_T can be calculated from Equations (22–24):

$$SE_R = -\log_{10}(1-R) \tag{22}$$

$$SE_A = -\log_{10}\left(\frac{T}{1-R}\right) \tag{23}$$

$$SE_T = SE_A + SE_R \ (\mathrm{SE_M \ is \ negligible}). \tag{24}$$

A better understanding of the absorption by an EMI shielding material can be obtained by calculating its effective absorption (A_{eff}) percentage using Equation (25):[78]

$$A_{eff} = \frac{(1-R-T)}{(1-R)} \times 100 \ (\%) \tag{25}$$

while, A_{eff} determines the power that is absorbed by the EMI shielding material.

3. Intrinsically conducting polymers (ICPs)

Delocalization of π-electrons in a conjugated structure of ICP such as polyacetylene (Pan), polyaniline (PANI), polypyrrole (PPy), etc. has drawn their attention for EMI applications, as it provides a unique electronic property which can be tuned by doping/dedoping during their synthesis. However, extensive delocalization of π-electrons hinders their processability.[79] Also, they suffer from swelling, contraction, cracking, or softening that in turn affect their mechanical and electrical properties. These properties can be improved by introducing a second phase materials such as metal nanoparticles, magnetic materials, carbon nanostructures, metal oxides, etc.[80] The second phase materials improve the dielectric and magnetic property and thermal stability of the ICP without deteriorating their electrical conductivity, thereby enhancing the EMI *SE* or EM wave absorption. The ε_r' of the ICP composites is greater than that of pristine ICP. This increment is the result of enhanced interfacial polarization of large interfacial area and incongruity in the dielectric property between the ICP and second phase materials.

3.1. Parameter influencing the properties of ICP for EMI shielding

The EMI shielding ability of the ICP (both reflection and absorption) arises from the mobile charges (polarons and bipolarons) and bound charges (dipoles) at their backbone.[81] The ability to control their electrical conductivity by governing their oxidation state, doping, chemical structure, and morphology makes them an efficient candidate for EMI shielding.[82]

The electrical conductivity for the ICP composites depends on the reaction conditions during polymerization. For example, Wan et al. demonstrated that the electrical conductivity of bacterial cellulose/graphene/PANI (BC/GN/PANI) nanocomposites decreases from 0.82 to 0.74 $S.cm^{-1}$ on increasing the reaction temperature from 0 to 25 °C, whereas, increases from 8.5×10^{-5} to ~1 $S.cm^{-1}$ on increasing the reaction time from 2 to 10 hr.[83] The tendency of conducting polymers to agglomerate at a higher reaction temperature decreases their electrical conductivity. On contrary, an increased electrical conductivity at a longer reaction time is attributed to the increase in the amount of conducting polymers.[84] Doping of surfactants onto conducting polymers

improves the electron mobility by increasing the polarons and bipolarons concentration. For example, Bhardwaj et al. reported that sodium lauryl sulfate (SLS) doping restricts the bias dependency for interchain hopping of charge carriers and thereby enhances the electrical conductivity and EMI *SE*.[81] The morphology, chemical composition, and electrical conductivity can be modified by doping acids, that in turn affect the EMI *SE*.[85,86] Qiu et al. demonstrated that the phosphoric acid (H_3PO_4) yielded nanofiber-like structure whereas hydrochloric acid (HCl), and L(-)-camphor sulfonic acid (CSA), yielded holothurian-like structures for PANI.[87] The CSA doped PANI exhibited highest electrical conductivity that results from the increased delocalization of electrons by their hydroxyl group and morphological effect. He et al.[88] demonstrated that the σ of wood/PANI composites increased with increasing the concentration of phosphoric acid (PA). Here, the wood refers to the Wood veneers obtained from the tree, *Entandrophragma cylindricum*. However, the addition of PA beyond the optimum concentration of 0.6 M, decreased their electrical conductivity. The wood/PANI composites with 0.6 M PA exhibited the σ of 9.53×10^{-3} S cm^{-1} and EMI *SE* of ~45–60 dB between 10 and 1.5 GHz.[88] Tantawy et al. demonstrated that HCl doped PANI prepared by the solid-state reaction exhibited higher range of σ and EMI *SE* than that are prepared by conventional solution method.[89] Gahlout et al. demonstrated the effect of oxidant ($FeCl_3$) and concentration of dopant on the σ and EMI *SE* of PPy. Various dopants such as sodium lauryl sulfate (SLS), sodium dodecylbenzene sulfonate (SDBS), and naphthalene disulphonic acid (NDSA) were used. PPy prepared at pyrrole: oxidant: dopant ratio of 1:2:1 with SLS as dopant exhibited the highest σ of 42 S.cm^{-1}. The EMI *SE* exhibited by the same is ~126 dB in the X-band range.[90] Kaur et al. found that the increase in the surfactant concentration (SLS) from 5 to 30 mM, decreased the particle size from 53 to 28 nm, increased the electrical conductivity from 3 to 22 S.cm^{-1} and increased the EMI *SE* from 23 to 49 dB for PPy nanoparticles.[91] The observation from these studies revealed that the chemical formulation also can influence the properties of conducting polymers. Ebrahimi et al. compared σ and EMI *SE* of Ag incorporated PPy-MWNCTs composites prepared by UV-reduction and chemical reduction method. The composites prepared by UV-reduction methods exhibited higher σ and EMI *SE* due to higher content (57%) and homogenous distribution of silver nanoparticles at the PPy-MWCNT interfaces in comparison to that prepared by chemically reduced composites (40%).[92]

3.2. ICP based composites in EMI shielding

Metal nanoparticles such as copper, nickel, etc. were used as a second phase material with the ICP.[93] 20 wt% of silver nanowires has been incorporated into PPy to achieve a flexible EMI shielding film. The conductivity of PPy/AgNWs film increased from 0.02 S/cm for pure PPy to 62.73 S/cm, and thus its SE_T increased to 22.38 dB.[94] The higher SE_T is attributed to the electron scattering at the interfaces and surface plasmon resonances of the metal nanoparticles. However, metal nanoparticles suffer from heavy-weight and corrosion.

Metal oxides are used as the second phase material in the ICP matrix for enhancing their dielectric properties. A modified phase generated by the metal oxides at the interface restricts the movement of charge carriers in the ICP backbone. This accumulation

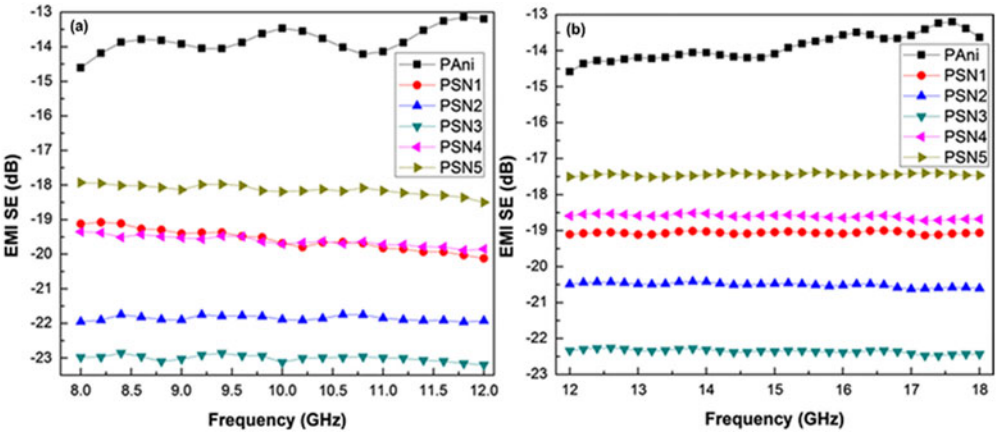

Figure 8. EMI SE of the different PANI/SnO composites in (a) X-band and (b) Ku-band. Reproduced with permission from ref.[96] Copyrights © Springer Science + Business Media New York 2013.

of charges will enhance the capacitance of ICP/metal oxide composites thereby increases the dielectric constant. Further, metal oxide fillers can overcome the drawbacks of metal fillers such as heavyweight and poor corrosion resistance, as they possess excellent corrosion resistance and thermal stability. For example, Faisal et al. reported PANI/Sb_2O_3 composites with the EMI *SE* ranging from −18 to −21 dB in the X-band and ranging from −17.5 to −20.5 dB in the Ku band.[95] Figure 8 shows the EMI SE of various wt% of SnO dispersed PANI. It is observed that the EMI *SE* increased with the increase of SnO up to a critical concentration and then decreased at a higher concentration of SnO in both X-band and Ku-band.[96] This may be due to the deterioration in the continuity of polymer chains at a higher loading of SnO.

PANI incorporated with 20 wt% Y_2O_3 exhibited an EMI *SE* of 19–20 dB in the frequency between 12.4 and 18 GHz. The anisotropy generated by the incorporating Y_2O_3 contributed to various polarization loss with a subsequent increase in the EM absorption.[97] Saini et al. demonstrated that the introduction of tetragonal $BaTiO_3$ improved the EM absorption of the DBSA-doped PANI nanocomposites. The suppression of reflection resulted from the decrement in the concentration of polarons with the addition of $BaTiO_3$ as it decreased the static conductivity.[98]

Carbon nanostructures are used as efficient second phase material with ICP due to their lightweight, well-regulated aspect ratio, and flexibility.[81] Saini et al. reported the enhancement in the σ of PANI by coating it onto the multi-walled carbon nanotube (MWCNT) by the in-situ polymerization technique. The nanotubes acted as an interconnecting bridge for the PANI grains coated on the MWCNT. This increased the coherence and coupling between the chains and enhanced the interchain transport. The π-π^* interaction between the MWCNT and PANI quinoid rings increased the delocalized electrons in the composites and thereby improved the σ.[99] The σ achieved with 25% MWCNT-polyaniline nanocomposites (19.7 $S.cm^{-1}$) is higher than that of pristine MWCNT (19.1 $S.cm^{-1}$) and PANI (2.0 $S.cm^{-1}$). The highly entangled tubes with poor packing are the reason for the lower conductivity of bulk MWCNT. The uniform coating of PANI improved the intertubular charge transport by reducing the void/disorder

in the composites. The absorption dominated SE_T of −27.5 to −39.2 dB was achieved in the frequency range of 12.4–18.0 GHz.[100]

The σ of ICP/magnetic material composites is lower than that of pristine ICP. This is due to the dissociation in the conducting chains of the ICP upon the addition of magnetic material. Similarly, the saturation magnetization (*Ms*) and coercivity field (*Hc*) of the ICP/magnetic material composites are lower than that of the pristine magnetic material due to the separation of magnetic particles by the intermittent non-magnetic ICP. Despite these, the ICP/magnetic material composites exhibited higher thermal stability and EMI *SE* than that of pure ICP. The increased thermal stability of the ICP/magnetic material composites is attributed to the inhibition of polymer chain motion at a higher temperature by magnetic particles. The increased EMI *SE* of ICP/magnetic material composites is the result of the synergic effect of dielectric loss (contributed by ICP) and magnetic loss (contributed by magnetic material).[101,102] Hence, the optimization of the σ and μ of ICP/magnetic material composite is significant to achieve efficient EMI attenuation. The optimization can be achieved by choosing the appropriate concentration of the materials. Belaabed et al. demonstrated that the reflection loss (*RL*) of PANI/Fe_3O_4 in the epoxy matrix (1 mm thick) varied with changing the wt% of either PANI or/and Fe_3O_4. The composites with 15 wt% PANI and 10 wt% Fe_3O_4 exhibited a *RL* of −42 dB at 16.3 GHz, whereas it is −37.4 dB at 14.85 GHz for 15% of PANI and 25% of Fe_3O_4. The composites containing only 20% of PANI showed a *RL* of −11 dB at 18 GHz.[103] Choudhary et al.[104] investigated the EMI behavior of coral–shaped yttrium–iron–garnet (YIG) particles/PANI-wax and found that the values of ε_r' and ε_r'' increased with an increase in the weight percentage of YIG, but become zero at higher concentrations (50 wt.%) as shown in Figure 9. The incorporated magnetic material enhanced the orientation polarization and accumulation of space charge due to the variation in the relative dielectric constant between them and ICP. This in turn led to the increased dielectric values.[105] The PANI/YIG composites exhibited higher values at 15 wt% and 20 wt%. The composites with 15 and 20 wt.% of YIG also exhibited resonance peaks at 9 and 14.8 GHz. Garnets are soft ferrimagnetic materials and exhibits a high saturation magnetization (contribute to anisotropic magnetic loss) and narrow

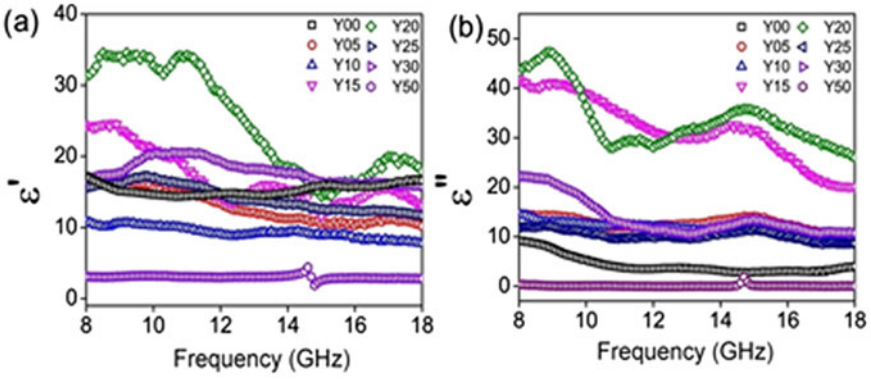

Figure 9. (a) ε′ and (b) ε″ as a function of YIS content in PANI/YIG composite in the frequency range between 8 and 18 GHz. Reproduced with permission from ref.[104] Copyrights © 2011 2018 Wiley-VCH Verlag GmbH & Co. KGaA, Weinheim.

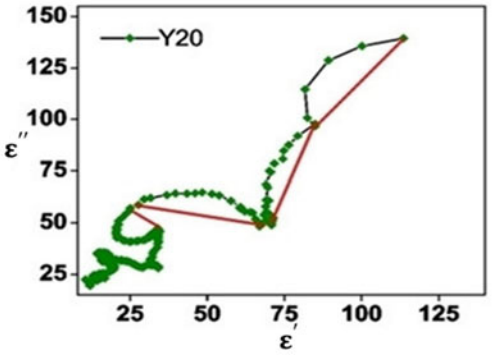

Figure 10. (a) Cole-Cole plot for the 20 wt% of YIS containing PANI. Reproduced with permission from ref.[104] Copyrights © 2011 2018 Wiley-VCH Verlag GmbH & Co. KGaA, Weinheim.

ferromagnetic resonance and hence contributes to the magnetic loss. At a critical concentration of 20 wt%, maximum SE_T of −44.8 dB was achieved for PANI/YIG composites. Further, the Cole–Cole plot of 20 wt% YIG loaded PANI (Fig. 10) displayed many semicircles resulting from the inhomogeneity-induced large interfacial polarization.

Zhang et al. found that the coating of PANI on to Fe_3O_4 provided an appropriate dielectric loss while preserving the magnetic loss of the Fe_3O_4/polyaniline core/shell microspheres. Also, the RL varies with changing the PANI shell thickness, which increased from −17.2 dB (15.6 GHz) at 60 nm to −37.4 dB (15.4 GHz) at 100 nm and decreased at 120 nm to −24.7 dB (14.8GHz). The maximum *RL* shifted towards a lower frequency with an increase in the shell thickness.[106]

Wu et al. studied the influence of carbon black (CB) content on the EMI shielding properties of PANI and demonstrated that PANI/CB (20 and 30 wt%) composites exhibited absorption dominant performances over the radar band (2–40 GHz).[107] Gopakumar et al. adopted the in-situ polymerization technique to prepare flexible cellulose nanofiber/PANI composites.[108] The cellulose nanofiber solution provided adequate hydrogen bonding for the formation of flexible film. The 1.0 mm thick cellulose nanofiber/PANI composites (1:1) exhibited σ and EMI *SE* of 0.831 $S.cm^{-1}$ and −23 dB, respectively. The EMI absorption properties of various ICP composites are tabulated in Table 1.

4. Conductive polymer composite (CPC)

Nonconducting polymers containing conductive fillers, known as extrinsic conducting polymer composite/conductive polymer composite (CPC), are excellent materials for EMI shielding because of their lightweight, corrosion resistance, appropriate electrical, and dielectric characteristics to avert electrostatic discharge, disturbance, and interference between the electronic systems. It has also been reported that the uniquely structured CPCs, such as segregated structures,[134] double percolation structures,[135] layer-by-layer assembly,[136] multilayer structures,[137] and foam structures,[138] help to enhance the EM absorption. Among various conducting fillers, such as ICP, metal nanoparticles, and carbon nanostructures, nanocarbons are widely used as effective fillers due to their large surface area, high aspect ratio, high σ, and easy processability.[75,139] In this section, we discuss the parameters influencing the properties CPC,

thermodynamics, and morphological evolution in biphasic polymer blends and EMI performance and corresponding mechanism of various CPC.

4.1. Parameter influencing the properties of CPC for EMI shielding

A substantial enhancement in the permittivity of insulator matrices can be attained by adding electrically conducting materials as fillers. The conducting fillers distributed in insulating mediums act as "micro-capacitors", thereby improve their ability to store the electric energy. When the conducting fillers are added to insulator matrices, they are linked with each other and form a conducting network. The formation of an interconnected conducting network in CPC is explained by the theory of electrical percolation threshold. When the amount of conducting fillers in the insulating polymer reaches a critical concentration, the interconnected network of conducting fillers is constructed up, and the corresponding insulating polymer is converted to a conducting polymer composite. This transition is termed as "percolation transition" and the critical concentration of conducting fillers at percolation transition is known as "percolation threshold". σ of the CPC at the percolation threshold can be described as Equation (26 and 27):[140,141]

$$\sigma = \sigma_1(\varphi_c - \varphi)^t, \text{ when } \varphi < \varphi_c \tag{26}$$

$$\sigma = \sigma_2(\varphi - \varphi_c)^{-s}, \text{ when } \varphi > \varphi_c \tag{27}$$

where σ_1 and σ_2 are the conductivities of fillers and insulating polymer matrix, φ is the filler concentration (volume fraction), φ_c is the filler concentration at percolation transition, and t and s are the parameters (describing the number of connections between the fillers at the percolation threshold along with the arrangement of the conductive network, *i.e.*, the particles dispersion and 2-, or 3- dimensional systems). Generally, $t = 1.1$–1.3 and $s = 1.1$–1.3 for 2- dimensional network and $t = 1.6$–2.0 and $s = 0.7$–1.0 for 3- dimensional networks. But the experimental t values are in the range of 1–12. The reason for this deviation still remains unclear. The most satisfactory elucidation is that the $t > 2$ represents 3- dimensional networks while $t < 2$ represents 2-dimensional networks of conducting fillers in the CPC.

For the CPC having a filler content below φ_c, the influence of the frequency on their dielectric constant and dielectric loss factor in a measured frequency range is very limited and their values increase as the content of the conductive filler increases. However, they are frequency dependent beyond the φ_c.[142] Furthermore, the φ_c is closely associated to the geometrical parameters of the conducting fillers, such as size, shape and orientation, and their electrical conductivity. For the CPC with randomly distributed fillers, the φ_c decreases with an increase in the fillers' aspect ratio.[143] In the conductive network of an insulating polymer, the σ occurs by the migrating transport of electron in the conductive nanofillers, hopping/tunneling transport of electrons between the conductive fillers separated by the polymer matrix.[144,145]

The potential required to hop/tunnel between the conductive fillers depends on the polymer properties and processing/fabrication conditions of the composites. After an optimum concentration of conductive fillers, the σ remains the same while the current

Table 1. EMI Absorption characteristics of ICP and their composites.

Materials	Absorber loading (wt.%)	Maximum RL (dB)	Frequency at Maximum RL (GHz)	Bandwidth range (GHz) RL < -10 dB	d @ RL Maxima (mm)	Ref.
Epoxy-PPy/Fe_3O_4-ZnO	—	−32.53 dB	9.96	8.8–12.4 (<−10dB) & 9.7–10.9 (< −20dB)	2.0	[109]
Fe_3O_4/GNPs-NH-PANI	—	−40.31	—	7.85–17.47	2.6	[110]
GN-PANI-Fe_3O_4 in paraffin	50%	−43.9	11.4	5.4–16.4	2.5	[111]
Ni/PANI/rGO	—	−51.3	4.9	3.3–6.4	3.5	[112]
PANI-rGO-Co_3O_4 in paraffin	50%	−32.6	6.3	3.4–11.8 & 12.9–18	3.0	[113]
PPy-rGO-Co_3O_4 in paraffin	50%	−33.5	15.8	6.6–18.0	2.5	[114]
PPy-$BaFe_{12}O_{19}$/ $Ni_{0.8}Zn_{0.2}Fe_2O_4$ in paraffin	70%	−25.5	9.8	7.8–11.6	3.0	[115]
$FeNi_3$@SiO_2@rGO–PANI in paraffin	25%	−40.18	14.0	10.08–10.8 & 12.08–18.0	2.4	[116]
FeCo@SnO2@GN@PANI in paraffin	30%	−39.8	6.4	4.6–7.7	3.0	[117]
RGO/$CoFe_2O_4$/ MWCNT	—	−46.8	11.6	4.9–18	1.6	[118]
GN@Fe3O4@C@PANI in paraffin	25%	−44.2	11.4	9.7–15.5	3.0	[119]
N-GN@PANI nanorod in paraffin	25%	−38.8	7.3	6.5–8.8	3.0	[120]
GN@Fe_3O_4@PANI@TiO_2 nanosheets in paraffin	50%	−41.8	14.4	7.0–8.5 & 10.2–16.2	1.4	[121]
FeCo@GNe@PPy in paraffin	30%	−40.7	5.7	3.1–6 & 12.8–15.6	2.5	[122]
Cl/RGO/PVP in paraffin	50%	−27.59	6.88	4.2–18	2.5	[123]
GN/PEDOT/$CoFe_2O_4$ in paraffin	50%	−43.2	9.4	8.2–11.3	2.4	[124]
PPy/rGO aerogel in paraffin	15%	−54.4	12.76	10.20–16.96	3.0	[125]
Fe_3O_4/PPy/carbon in epoxy	20%	−25.9	10.2	8.0–12.5	3.0	[126]
RGO/p-Fe_3O_4/PANI in paraffin	70%	−29.51	14.69	—	1.0	[127]
Cubic $NiFe_2O_4$/GN-PANI	—	−50.5	12.5	11.0–16.3	2.5	[128]
GN@$CoFe_2O_4$@polyaniline in paraffin	50%	−47.7	14.9	12.3–18 (< −10dB) & 14–16(< −20dB)	1.6	[129]
PANI/Nanoflower-like CuS in paraffin	20%	−45.2	2.78	0.3–3	3.0	[130]
PANI/RGO in paraffin	50%	−41.4	13.8	11.7–15.9 (< −10dB) & 12.8–14.3 (< −20dB)	2.0	[131]
PANI in paraffin	30%	−40.5	5.8	3.2–18	5.0	[132]
PANI/$Ba(CoTi)_{0.25}Fe_{11.75}O_{19}$ in paraffin	50%	−45.2	11.2	∼10–13.8	2.5	[133]

carrying capability of the polymer composites increases. The dependency of the σ on the distance between the two conductive fillers in a polymer matrix is given by Equation (28):[146]

$$\sigma \sim \mathrm{x}\ \exp\left(-\frac{x}{a}\right) \tag{28}$$

where x is the gap between the two conducting fillers in a polymer matrix and a is the characteristic tunneling distance. Figure 11 shows the change in σ and the EMI SE with respect to the filler loading for Printex black (P-CB) loaded polymer blend of two

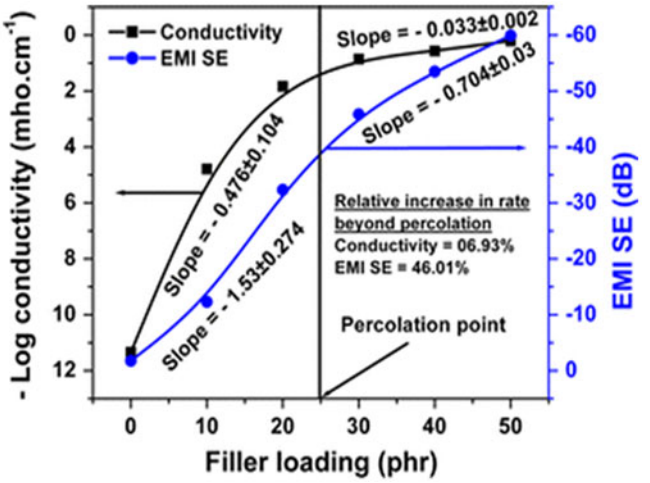

Figure 11. σ and EMI SE with respect to the filler loading for Printex black (P-CB) loaded EVA/NBR polymer blend (75/25). Reproduced with permission from ref.[147] Copyright © Springer Science + Business Media, LLC 2011. (*phr-part per hundred parts of rubber).

copolymers, namely ethylene-vinyl acetate (EVA) and acrylonitrile-butadiene (NBR) in the ratio of 75:25. It is found that the relative increase in the σ (6.93%) is less than that of EMI *SE* (46.01%).[147] This signifies that apart from σ there are many factors that are crucial for controlling the EMI *SE*.

The migration of electrons depends on the intrinsic conductivity of the fillers. Also, it has been reported that the reflection or absorption mechanisms of the CPC are associated with the properties of the fillers. For example, Yilmaz et al. claimed that the increasing concentration of vapor grown carbon nanofibers (VGCNF) in PVdF matrix improved their absorption capability towards the EM waves rather than the reflection, attributed to the absorption capability of VGCNF.[148] Additionally, the decrease in the gap between fillers at higher concentration contributed to the absorption rather than reflection.[149] Arjmand et al. compared the EMI SE of the polystyrene/MWCNT composites fabricated by the compression molding technique with the same composites prepared by the injection molding technique.[150] It has been observed that the EMI shielding by reflection was almost the same for both composites, and it increased with increasing the concentration of MWCNT. But composites prepared by compression molding technique exhibited a better EMI shielding by absorption than that of the composites prepared by injection molding. This is due to the increased connectivity between the fillers in the composites prepared by compression molding technique. The increase in connectivity led to a higher polarization of thinner polystyrene matrix region between the MWCNT. Therefore, the composites prepared by compression molding showed higher values of real permittivity than the composites prepared by injection molding.[151] Higher polarization results increased EMI shielding by absorption for the compression molded composites. The decrease in the connectivity of MWCNT for injection molded composites is due to the increased MWCNT alignment. From the above results, it can be seen that the absorption of the EM wave depends on the gap/connectivity between the conductive fillers, whereas the reflection of EM wave is influenced by the concentration of conductive fillers.

However, the addition of conducting fillers reduces the mechanical performance of CPC, because the conductive network formed by the conducting fillers greatly constrains the motion of the polymers' molecular chain, resulting in the inferior toughness and ductility of the CPC. Some works are focused on using the hybrid fillers to enhance the mechanical performance of CPC as the incorporation of hybrid fillers with better conductivity decreases the φ_c. The shape, size, and dispersibility of the conductive fillers also play a vital role in defining the φ_c. For example, Joseph et al. demonstrated that the 2 wt% carbon nanofiber (CNF) filled silicone rubber (SR) exhibited an EMI *SE* higher than the 2 wt% of MWCNT filled SR in the frequency range of 2.0–18.4 GHz. This is due to that in the measured frequency region, the wavelength is nearly equal to the length of CNF but higher than the length of MWCNT. The SR filled with CNF wafer exhibited a higher EMI *SE* than SR filled with 2 wt% of CNF due to the improved electrical contact. Also, when the thickness of the CNF wafer was increased from 0.73 to 0.75 mm, an increase in EMI *SE* from 35.08 to 38.95 dB was observed.[152] For the composites containing the fillers whose length is less than the wavelength of EM wave, the EMI *SE* depends more on conductivity than the imaginary permittivity due to the lack of interaction between them. Satisfactory dispersion of the conducting filler in the polymer is associated with the appropriate selection of process parameters and the filler-polymer compatibility. The efficient filler-polymer interaction prevents the aggregation of conducting fillers, which in turn provides superior EMI *SE*. The filler-polymer interaction can be investigated by a parameter, Bound Rubber content (BRC), which can be calculated using the Equation (29):[153,154]

$$BRC = 100 \times \frac{\left[W_{fg} - W_t\left\{m_f/(m_f + m_f)\right\}\right]}{W_t\left\{m_f/(m_f + m_r)\right\}} \tag{29}$$

where W_{fg} and W_t are the weight of rubber filler gel and rubber sample, respectively, and m_f and m_r are weight fraction of the filler and rubber, respectively. A higher BRC value corresponds to a higher interaction between the polymers and conducting fillers.[155] The BRC will increase with the increase in weight percentage of the conductive fillers. Figure 12a and b shows that BRC of chlorinated polyethylene and ethylene

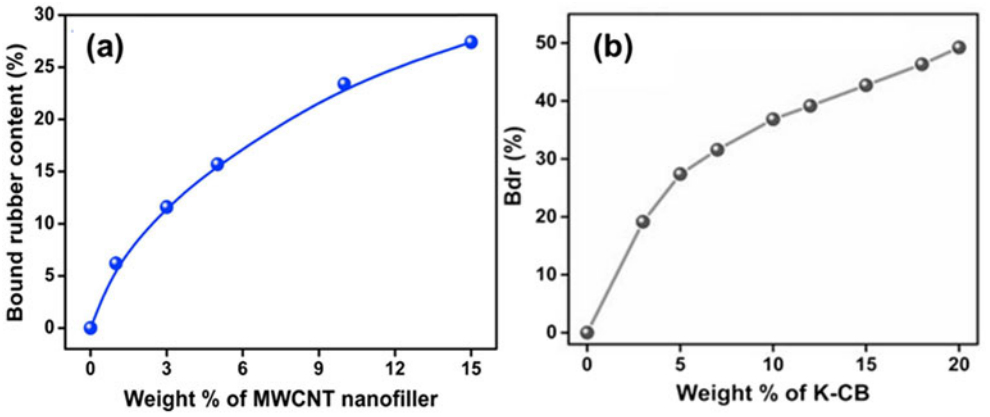

Figure 12. BRC of (a) chlorinated polyethylene and (b) ethylene methyl acrylate as a function of wt.% of MWCNT and K-CB, respectively. Modified from ref.[153,155]

methyl acrylate increases with an increase in the weight percentage of the corresponding fillers (MWCNT and Ketjen carbon black (K-CB), respectively). More interaction will increase the permittivity of the CPC due to the collected charges at their interface, attributed to the alteration in relaxation time of polymer and fillers.[156]

Altering the chemical vicinity and the functionalization of the carbonaceous fillers improves their dispersion and interaction with the polymer matrices which in turn influence the φ_c, impedance matching as well as EMI shielding performance.[157–161] For example, Bose et al. constructed a ternary continuous structure in which the pristine MWCNTs (p-MWCNTs) were confined in the PVDF phase whereas, PMMA wrapped MWCNTs (PMMA-MWCNTs) were confined at the interface of PVDF/ABS (50/50) co-continuous blends. An EMI *SE* of −24 dB (at 18 GHz frequency) was obtained for 50/50 blends with 3 wt% MWCNTs.[162] The same group also reported a high RL of −61 dB at 12.7 GHz for PVdF/PC blends containing PMMA-MWCNT. Higher dielectric relaxation losses due to the accumulation of virtual charges in the interfacial region of heterogeneous dielectrics increase the complex permittivity and result in higher reflection losses.[163] Wu et al. functionalized the graphene foam (GF) with DBSA to improve its wettability and bond formation with PEDOT: PSS.[164] The prepared PEDOT: PSS/GF exhibited negative permittivity ascribed to the delocalization of polarized charges at the interfaces.[165] The optimized PEDOT: PSS/GF composites exhibited the largest EMI SEs of 91.9 dB, attributed to the enhanced interaction between the constituents by the addition of DBSA. Liang et al. revealed that the functionalized graphene exhibited low φ_c of 0.52 vol.% in the epoxy matrix and achieved an EMI *SE* of ∼21 dB at 8.8 vol.% in X-band.[166] Zhang et al. studied the effect of carbon to oxygen (C/O) ratio on the dispersion of graphene in PMMA matrix and their corresponding EMI *SE*.[167] The graphene with highest C/O ratio (13.2) displayed a better dispersion in PMMA than the graphene with the lowest ratio, with an EMI *SE* of ∼30 dB at 4.2 vol%. Li et al. prepared thermally reduced functionalized graphene incorporated polystyrene foam and achieved σ and EMI *SE* of 1.1×10^{-2} S.m^{-1} and ∼18 dB, respectively at 10 wt%.[168] Hsiao et al. achieved homogenous dispersion of graphene in a water-borne polyurethane (WPU) matrix by covalently modification using aminoethyl methacrylate. At 5 vol.% loading, the prepared CPC exhibited an σ of 43.64 S.m^{-1} and EMI *SE* of 38 dB in X-band.[169] They also demonstrated that the noncovalent functionalization of graphene sheets (GNS) with stearyl trimethyl ammonium chloride improved their interaction with sulfonated WPU and decreased the φ_c. At 5 vol.% of GNS, the CPC achieved an EMI *SE* of 32 dB.[170] Further, the same research group also composited positively charged cationic surfactant (didodecyl dimethyl ammonium bromide, DDAB) adsorbed graphene oxide and negatively charged sulfonated functional group containing electrospun WPU using electrostatic attraction between them by layer-by-layer assembly method, which exhibited EMI *SE* of ∼34 dB in the X-band for a sample with a thickness of 1.0 mm.[171] Poothanari et al. used polar copolymer, polypropylene-grafted maleic anhydride (PP-g-MA), as compatibilizer for polycarbonate (PC)/polypropylene (PP) polymer blend.[172] The addition of PP-g-MA provided co-continuous morphology for PC/PP blend due to the reduced interfacial tension and diffused interface, which is unaffected by the inclusion of MWCNT. Also, it improved the dispersion of MWCNT. The compatibilized

PC/PP blend of 2 mm thickness displayed an EMI *SE* of 54.78 dB at 3 GHz for 10 wt% MWCNT loading. Tian et al. described that the nitrogen-doped reduced graphene oxide (N-RGO) obtained using diethylenetriamine (DETA) exhibited uniform dispersion in WPU matrix with σ of 0.08 S.cm^{-1} and EMI *SE* of 28.3 dB at 9 GHz at 12 wt% N-RGO content.[173] However, the chemical modifications depreciate the intrinsic properties of the CPC's constituents.[174]

Distribution of conducting fillers in the polymer matrix is influenced by filler loading and filler-polymer interaction. There will be no specific interaction between the filler and polymer at lower concentrations, whereas higher concentrations will greatly change the distribution, polarity matching, polymer-filler interactions, and resulting in conductive network structures. But the aggregation of fillers due to the Vander Waals' interaction at the higher loading will negatively affect the mechanical and thermal properties, processing and cost.[175,176] Interestingly, the φ_c can be reduced by selective/preferential localization of conducting fillers in the polymer system, which is based on classical thermodynamics. The preferential localization of the conductive fillers increases their concentration at the local level and thereby generates effective conductive networks.[177] The segregated structure and double percolation structure are two main strategies to achieve selective localization, thereby depress the concentration of conductive fillers. Yan et al. achieved EMI *SE* ranging between 28.3 and 32.4 dB for polyethylene/graphene composites with the segregated structure at an ultralow filler content of 0.660 vol.%.[178] Multi-facet segregated structured RGO/polystyrene composites presented an admirable EMI *SE* of 45.1 dB than their conventional structures at 2.5 mm sample thickness and 3.47 vol.% of filler loading.[179] The multi-facet segregated structure provides more interfaces that enhance the EM attenuation. In segregated structure, the conducting fillers are found at the polymer interfaces and form compact conductive structure, whereas, in double percolation structures, the conductive fillers are added to one continuous component of two immiscible polymer blend to form complicated conductive structures.[180,181] In spite of the advantages, the segregated and double threshold CPCs suffer from following demerits: (a) In segregated CPC, the conductive layers formed by the conductive fillers hinder the molecular diffusion between the polymer matrix granules, resulting in an extremely weak adhesive interaction, (b) In double threshold structures, the immiscible interface between the polymer blends leads to poor interfacial interactions in CPC with a double-percolated structure. It is, therefore, necessary to eliminate the structural defects at the interfaces, which can be achieved by varying process/fabrication conditions. Wu et al. demonstrated that segregated CNT/PP prepared at the elevated temperature and pressure of 180 °C and 100 MPa, respectively using solid phase molding suppressed the interfacial defects and improved the connectivity of CNT than that prepared by melt mixing.[182] The segregated CNT/PP composites prepared by solid phase molding exhibited a SE_T of 17.1 dB at 0.3 wt% CNT, whereas CNT/PP prepared by melt mixing exhibited a similar SE_T at 5 wt% CNT/PP composites with segregated structures. Compared to the single-phase CPCs, two-phase CPCs has a lower φ_c and higher σ along with higher EMI *SE*. The blend of two polymers having different polarity can form a well-defined interface where the fillers were expected to accumulate easily.[183]

4.1.1. Conditions for miscibility of two polymers

The condition for miscibility of the two polymers can be inferred from the Gibbs energy of mixing (ΔG_m) by Equation (30):

$$\Delta G_m = \Delta H_m - T\Delta S_m \tag{30}$$

where ΔH_m and ΔS_m are enthalpy and entropy of mixing, respectively. For miscibility of the polymer blend, the following conditions must be satisfied: $\Delta G_m < 0$ and $(\emptyset_i)_{T,P} > 0$ where $\emptyset_i$ is the amount (volume fraction) of the component i in the mixture.

In the equilibrium state, the distribution and position of fillers in CPC are controlled by their interfacial energy. The thermodynamic tendency of the conducting fillers at the polymer interface was reported by Sumita et al. as Equation (31):[180]

$$\omega_{12} = \frac{\gamma_{Filler-Polymer_1} - \gamma_{Filler-Polymer_2}}{\gamma_{Polymer}} \tag{31}$$

where γ in the numerator indicates different interfacial tension between constituent fillers and polymers, and the denominator is the interfacial tension between the constituents. When $\omega_{12} > 1$, filler would prefer polymer 2, when $\omega_{12} < -1$, the filler would prefer polymer 1, when $-1 < \omega_{12} < 1$, the filler is expected to confine at the interface.[184–186] Interfacial tension between the components is given by Wu's Equation as follows:[187]

$$\gamma_{AB} = \gamma_A + \gamma_B - 4\left[\frac{\gamma_A^d \cdot \gamma_B^d}{\gamma_A^d + \gamma_B^d} + \frac{\gamma_A^p \cdot \gamma_B^p}{\gamma_A^p + \gamma_B^p}\right] \tag{32}$$

where γ, γ^d and γ^p are total surface tension, the dispersive and polar components of the surface tension, respectively.

Biswas et al. investigated the influence of conducting filler localization on the EMI *SE* of the PC and polyvinylidene fluoride (PVDF) (50/50) blends.[188] The localization of two different fillers separately in two polymer phases enhanced the SE_T comparing to that of composites containing two different fillers in the same polymer or in both the phases. This enhancement in the SE_T accounts for SE_A while SE_R remains for all the samples remain the same. Figure 13 demonstrates the above-explained conception. The polymer blend composites that contain 3 wt% MWCNT in PVdF phase and $BaTiO_3$ (BT) in PC phase (Fig. 13a) and 3 wt% MWCNT in PVdF phase and $NiFe_2O_4$ (NF) in PC phase (Fig. 13b) exhibited a maximum SE_T than the composites that are containing BT/NF in PVdF phase and BT/NF in both PVdF phase or PC. This is attributed to the synergetic effect arising from both phases containing nanosized fillers. Figure 13c and d displays that the percentage of absorption follows the same trend as SE_T.

Further, the conducting fillers can easily form a closely packed interconnect conductive network in a polymer with amorphous phase compared with their semi-crystalline counterparts.[147] Figure 14 shows the morphological evolution and preferential localization of the biphasic polymers with respect to their mass ratio. It can be observed that the co-continuous phases exist and double percolation structures are formed for the polymer blends with a mass ratio close to 1 (Fig. 14b–d). For higher mass ratio (Fig. 14a and e), both the polymers are existing as droplets. More details on the

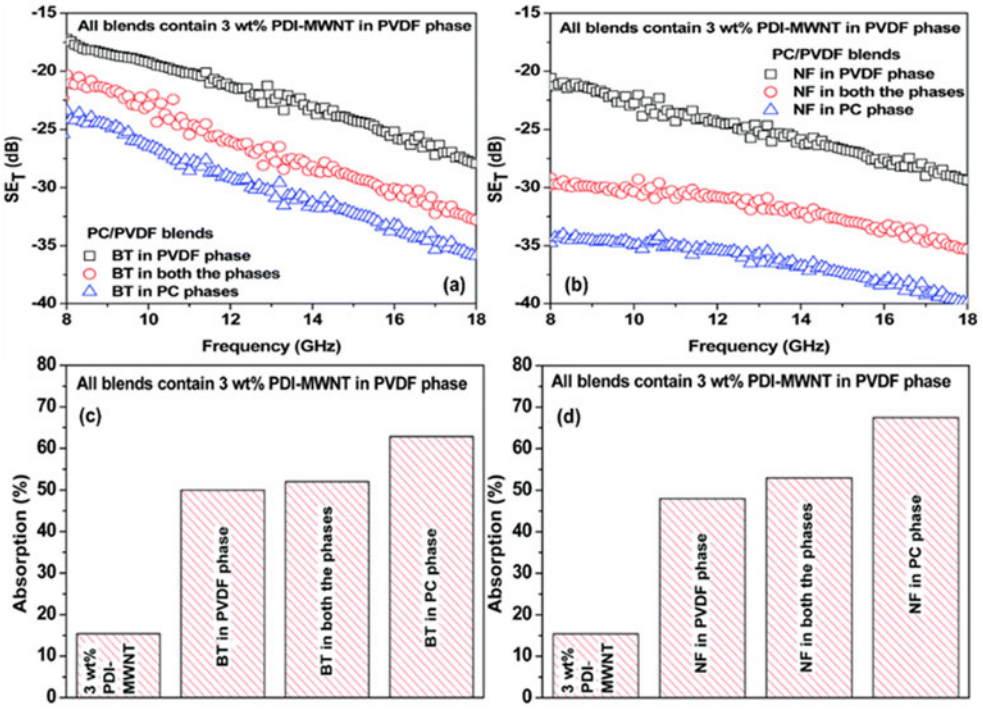

Figure 13. (a) SET values of MWCNT and $BaTiO_3$ containing PVdF/PC blend, (b) (a) SET values of MWCNT and $NiFe_2O_4$ containing PVdF/PC blend, (c) Absorption percentage of MWCNT and $BaTiO_3$ containing PVdF/PC blend and (d) Absorption percentage of MWCNT and $NiFe_2O_4$ containing PVdF/PC blend. Reproduced with permission from ref.[188] Copyright © The Royal Society of Chemistry 2015.

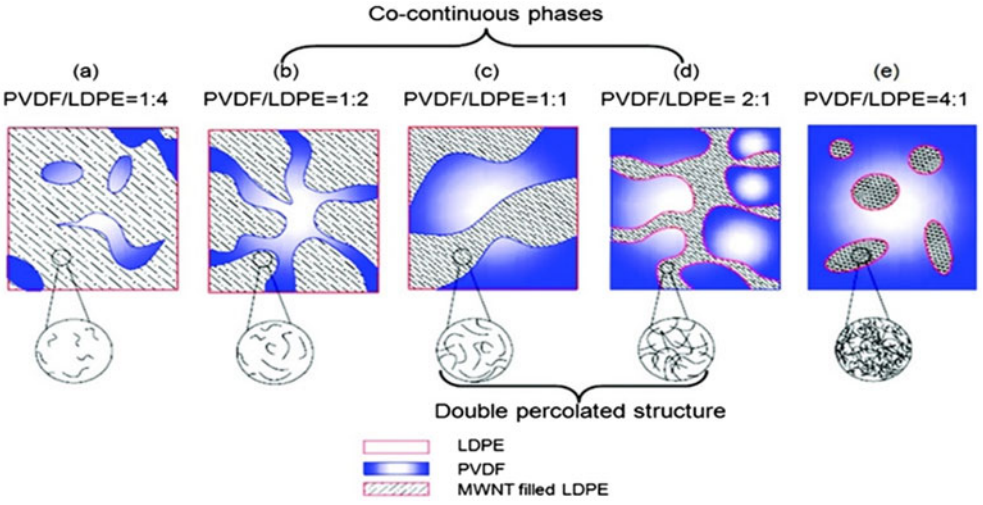

Figure 14. Morphological evolution and preferential localization of the biphasic polymers (PVDF/LDPE) blend with respect to their mass ratio. Reproduced with permission from ref.[138] Copyrights © 2011 American Chemical Society.

thermodynamics, morphologies of the polymer blends, and their dependency on polymer ratio are found in the earlier works.[189–193] Further, an ultra-high-density polymer matrix conductive fillers have also been reported. In this type, the conductive filler containing polymer phase can also act as an effective binder that attributes to the reduced interfacial flaws.[194]

4.2. Single-phase CPCs

Schmitz et al. prepared poly(acrylonitrile-co-butadiene-co-styrene) (ABS) based CPCs comprising CB/MWCNT hybrid as a conducting filler and compared their properties with ABS/MWCNT and ABS/CB. The hybridization of MWCNT with CB reduced the quantity of MWCNT required to attain good EMI *SE*. It was reported that CNTs can exhibit reduced percolation threshold than CB in the ABS matrix. This is because the CNTs prefer styrene-acrylonitrile phase to butadiene phase for distribution that arises from thermodynamic affinity.[195] In this study, the MWCNT: CB hybrid fillers are distributed in both the phases with a stronger influence on butadiene phase. The 3 wt% loaded ABS comprising MWCNT.CB hybrid fillers in the 50:50 ratio showed a good amalgamation of melt flow index (MFI) and EMI *SE*, 12.10 g/10 min and 23.77 dB, respectively. In addition, a higher EMI *SE* of 29.37 dB was achieved for ABS comprising 3 wt% MWCNT.CB hybrid fillers in the 75:25 ratio, without compromising the MFI.[196] This research group also prepared ABS/carbon composites by fused deposition modeling (FDM), where CNTs, CB, and CNT/CB hybrid are carbon conducting fillers. At 3 wt% of filler loading, the EMI *SE* of the CPC follows the order of ABS/CNT > ABS/HYB > ABS/CB > neat ABS regardless of the growing direction. SE_T of ABS CPCs with respect to the growing direction is shown in Figure 15. It can be observed that when the EM waves incident at the respective faces of the ABS/carbon composites, the samples prepared along the PC direction exhibited an enhanced attenuation, because of their highest volume electrical conductivity.[197]

Ji et al. achieved selective localization of MWCNT in thermoplastic polyurethane (TPU) using intumescent flame retardant (IFR) particles. The IFR forms solid phases in the polymer matrix, and hence the localization of MWCNT is achieved at the remaining space. The IFRs also contributed to the uniform distribution of MWCNT without agglomeration. This, in turn, established a continuous conductive network between the IFR particles. With 1% of CNT and 10 wt% of IFR, the TPU exhibited an EMI *SE* of 20 dB.[198] Xu et al. prepared CPC comprises furan-grafted poly (styrene-(ethylene-co-butylene)-styrene) (Fur-SEBS) containing furan-grafted-graphene (FG) and MWCNTs as conducting fillers. The introduction of FG also improves chemical resistance and EM absorption without the loss of CPC moldability. The CPC with 4 wt% FG and 12 wt% MWCNTs achieved an EMI *SE* of 36 dB.[199] Flexible sponge-like CNTs consisting of self-assembled CNTs with interconnected structures and their composites with polydimethylsiloxane (PDMS) (CNT/PDMS) exhibited an excellent EMI shielding performance.[200] The freestanding sponge-like CNTs at a thickness of 1.8 mm reached the SE_T of 54.8 dB in the entire 8–12 GHz range, with very small SE_R (about 0.3–0.7 dB). 1.0 wt% CNT sponge loaded PDMS exhibited the SE_T value of 46.3 dB (with SE_R of about 0.5dB). Figure 16a shows the SE_T, SE_A, and SE_R values of both the CNT sponge and

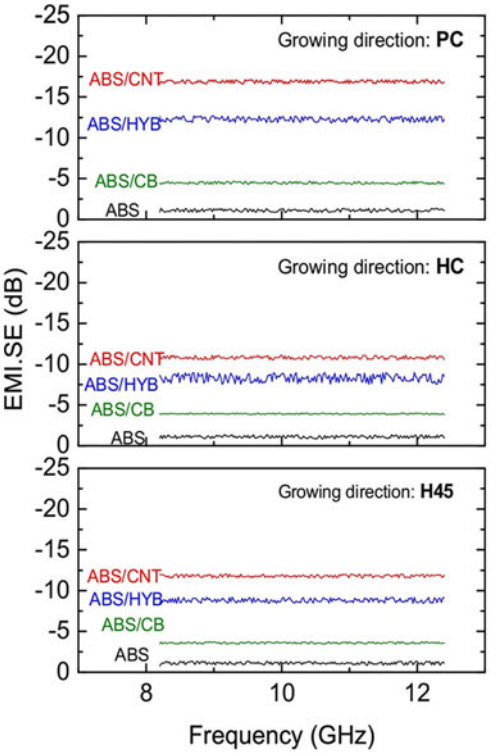

Figure 15. EMI SE of ABS/ carbon composites as a function of growing directions: perpendicular direction (Top graph), horizontal concentric direction (middle graph) & horizontal alternate direction (bottom graph). Reproduced with permission from ref.[197] Copyright © 2018 Elsevier Ltd.

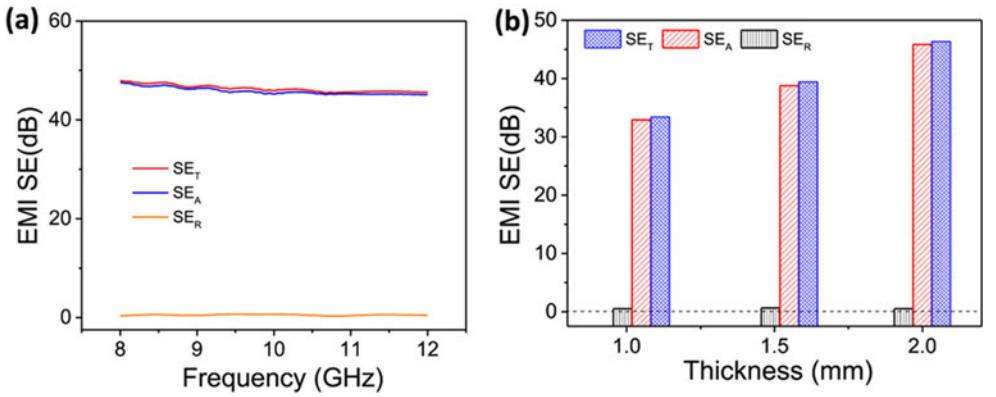

Figure 16. (a) SET, SEA, and SER of the CNT/PDMS composite in the X-band and (b) SET, SEA and SER of the CNT/PDMS composite of different thickness. Reproduced with permission from ref.[200] Copyright © 2018 Elsevier B.V.

CNT/PDMS composites almost constant for the entire frequency range of X-band. Figure 16b shows the SE_T, SE_A, and SE_R values for the samples of different thickness. It can be observed that the SE_T and SE_A increases as the thickness is increased, while the SE_R deviations are comparatively negligible. This is because, with the increase in

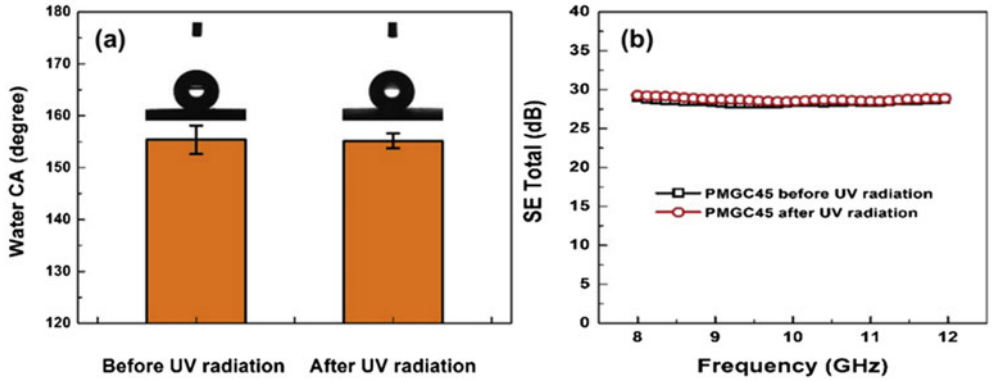

Figure 17. (a) Water contact angle and (b) SET for non-radiated and UV radiated PMGC45. Reproduced with permission from ref.[201] Copyright © 2018 Elsevier Ltd.

thickness, the amount of CNT in the sponges gradually increases, which improves the internal multi-reflection, scattering, and absorption that lead to an improved SE_A. The infiltration of PDMS into the sponge had a very little effect on the internal connection structure of CNTs. Interfacial effects and dielectric relaxations are the attenuation mechanisms of the CNT/PDMS film. After repeated stretching or bending for 1000 cycles, the EMI *SE* of the CPC hardly changed.[200]

Ma et al. reported porous super-hydrophobic PVdF/MWCNT/graphene composites (PMGC) as self-cleaning EMI shielding material. PMGC having multi-scaled raspy-like morphology exhibited a water contact angle of 155.4° ± 2.7° and SE_T of ~28.5 dB at 4.5 vol.% of carbon fillers (MWCNT: Graphene =1:1) and ~2 mm thickness. Figure 17a and b shows that their contact angle and EMI shielding performance of PMGC are not affected under UV-radiation.[201] Wu et al. prepared a segregated CNT/PP composite with an excellent EMI SE of 48.3 dB at 5.0 wt.% of filler loading and 2.2 mm thickness.[182] Nimbalkar et al. described that the EMI *SE* of the polycarbonate (PC)/graphite nanoplatelets (GNP) increased with increasing the GNP content and the thickness of nanocomposite samples. The EMI *SE* was 35.0 and 47.2 dB for 1 and 2 mm thick PC/GNP nanocomposites in the X-band. The increased EMI *SE* is due to the increased interfacial polarizations and multiple-internal reflections at the higher GNP content and thickness.[202]

Bai et al. demonstrated that poly(ethylene oxide) (PEO) matrix dispersed with 2.6 Vol.% chemically reduced graphene exhibited a min. *RL* of −38.8 dB for 1.5 mm thick sample as depicted in Figure 18. It has been observed that the peak frequency varies with varying the thickness (1.8–4.0 mm). At 2 mm thickness, the bandwidth of $RL <$ −10 dB covers a broad range between 12.4 and 18 GHz with a maximum *RL* of −32.4 dB. The excellent microwave absorption was attributed to the conduction loss arising from the interconnected network of large surface area graphene and dielectric loss arising from the dipole relaxation, interfacial polarization, and multiple scattering at the heterogeneous interface.[203]

Nasouri et al. demonstrated an EMI *SE* of 22 dB in the X-band for the 4 wt% Fe_3O_4 incorporated electrospun polyvinylpyrrolidone (PVP).[204] Chauhan et al. studied the performance of poly(ether ketone) (PEK)/$BaTiO_3$ in X-band region.[205] The dielectric

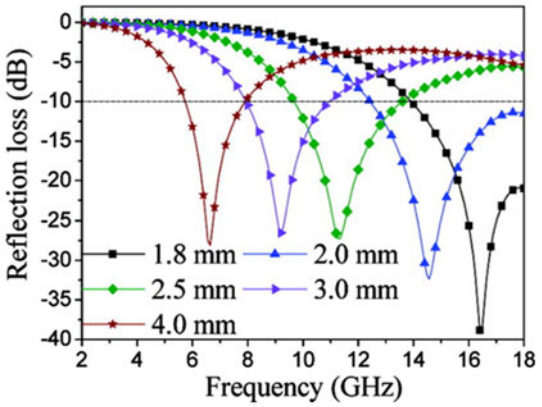

Figure 18. Reflection as a function of frequency for 12 vol.% of chemically reduced graphene loaded PEO. Reproduced with permission from ref.[203] Copyright © 2011 American Chemical Society.

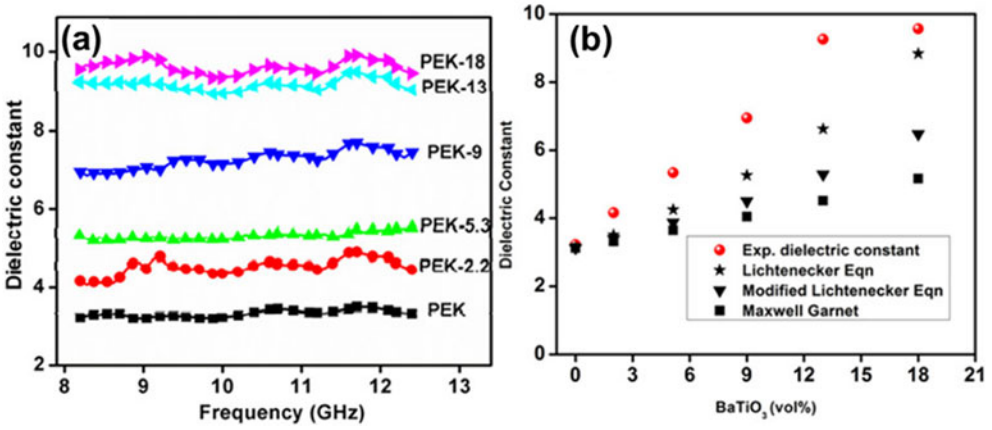

Figure 19. Dielectric constant of different weight percentages of $BaTiO_3$ loaded PEK in the X-band, (b) comparison of theoretical models with experimental results. Reproduced with permission from ref.[205] Copyright © 2018 Wiley Periodicals, Inc.

constant of the prepared PEK/$BaTiO_3$ increases with an increase in the filler loading ($BaTiO_3$). The rate of increment is significant at a lower loading whereas it becomes negligible at higher loadings. This is because of the aggregation of fillers at the higher wt% (Fig. 19a). Figure 19b shows that the experimental value of dielectric constant fits well with modified Lichtenecker equation. The PEK containing 16 wt% of $BaTiO_3$ exhibited a SE_T of 11 dB with absorption as the dominant mechanism (SE_A = 8.1 dB), due to enhanced dielectric properties attributed to $BaTiO_3$.

4.3. Polymer blend-based CPCs

Wang et al. fabricated hollow glass microspheres (HGMs) incorporated poly(vinylidene fluoride) (PVDF)/polystyrene (PS)/MWCNT composites. The prepared samples with 10 wt% MWCNT and 2 wt% HGMs displayed an average EMI *SE* of 43.03 dB, which is

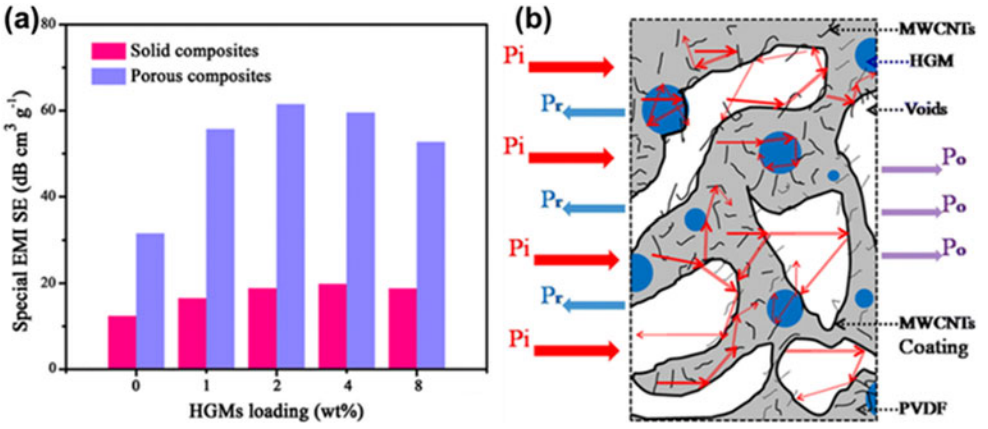

Figure 20. (a) Specific EMI SE (SSE) and (b) EMI Shielding mechanism of the P/CNT/HGM composites. Reproduced with permission from ref.[206] Copyright © Springer Science + Business Media, LLC, part of Springer Nature 2018.

greater than that for the composites with no HGMs (25.27 dB) in the frequency range between 8.0 and 12.0 GHz (X-band). The porous composites showed better EMI shielding performance than the solid composites (Fig. 20a). It was observed that the incorporated HGMs endorsed the interlink between conducting fillers along with the scattering and reflection of the electromagnetic incident wave (Fig. 20b), that improved its EMI *SE*.[206] The segregated PVDF/MWCNT composites fabricated by mechanical mixing followed by hot compaction exhibited high electrical conductivity and EMI *SE* of 6 S m^{-1} and 30.89 dB with absorption as dominant mechanism in the X-band. A significant increase in EMI SE was observed over the entire frequency range as the sample thickness increased from 0.6 to 3.0 mm.[207]

Wang et al. demonstrated a morphological control of the MWCNT conducting network in two phasic blends of poly(L-lactide) [PLLA] and poly(ε-caprolactone) [PCL] by the formation of stereo-complex crystallites (SC) during melt processing. The composites of (48PLLA +12PDLA)/PCL/MWCNT containing 0.2 wt% and 0.8 wt% MWCNTs, displayed the EMI *SE* of about 7.2–11.4 dB and ~17 dB, respectively. The improved EMI shielding performance is mainly related to the enhanced electrical conductivity of the (48PLLA +12PDLA)/PCL/MWCNT composites with co-continuous morphology and the increased MWCNT loadings.[208] However, the poor compatibility between these two different polymers limits their mechanical properties. To address this problem, the same research group constructed segregated CPCs with two polymers of the same molecular structures and different viscosities. They prepared biodegradable with segregated PLLA/MWCNT nanocomposites (S-PLLA/MWCNT) using PLLA polymers of two different viscosities and compared their EMI shielding performance with a random PLLA/MWCNT nanocomposites (R-PLLA/MWCNT). The dimensional parameter value (t) of the threshold percolation equation for the S-PLLA/MWCNT and R-PLLA/MWCNT was found to be 1.63 and 3.89, respectively. Thus, S-PLLA/MWCNT exhibited superior electrical conductivity at an ultra low φ_c of 0.019 vol.% than that of the R-PLLA/MWCNT (φ_c ~0.22 vol.%). At 0.8 vol.% of MWCNT loading, S- PLLA/MWCNT displayed three orders and 36% higher values for electrical conductivity (25 S m^{-1}) and

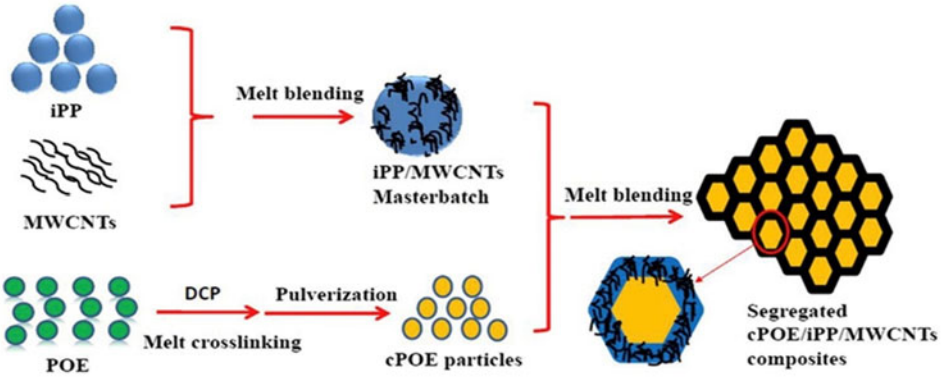

Figure 21. Illustration of the construction of S-POE/iPP/MWCNT CPC. Reproduced with permission from ref.[210] Copyright © The Royal Society of Chemistry 2017.

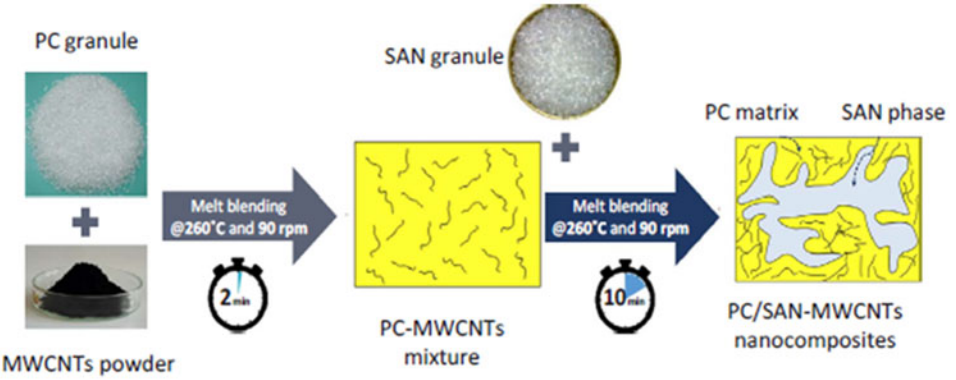

Figure 22. Schematic of the preparation procedure of PC/SAN–MWCNTs nanocomposites. Reproduced with permission from ref.[211] Copyright © 2018 Elsevier Ltd.

EMI *SE* (~30 dB), respectively, compared to R-PLLA/MWCNT. The calculated skin depth values of S- PLLA/MWCNT are lower than the sample thickness, indicating their high efficiency for attenuating microwaves.[209] Liu et al. prepared segregated CPC comprising of isotactic polypropylene (iPP) and poly(ethylene-co-1-octene) [POE] blends having MWCNT dispersed in continuous iPP phase by melt binding technique. Figure 21 explains the construction of S-POE/iPP/MWCNT CPC. A high-efficiently conductive network was formed with a low φ_c of 0.24 vol.%. The EMI *SE* of ~25 dB was achieved with 3.0 vol.% MWCNTs and a thickness of 1.2 mm.[210]

Bizhani et al. prepared double percolated CPCs containing PC and SAN loaded with MWCNT by melt compounding technique at 260 °C, as shown in Figure 22 and achieved a maximum *SE* of 25–29 dB for 10 mm thick sample loaded with 1 wt% of MWCNT over the X-band.[211]

Yu et al. prepared CNT/UHMWPE composites with oriented segregated structure by a solid extrusion method and compared its electrical conductivity, percolation threshold, tensile strength, and EMI *SE* with CNT/UHMWPE composites prepared by compression molding having conventional segregated structure.[212] The oriented segregated structure results from the strong shear flow produced in the solid extrusion method.

The strong shear force causes deformation of the UHMWPE particles in the extrusion direction, resulting in the formation of an oriented segregated structure. Li et al. revealed the selective distribution of Fe_3O_4 nanoparticles and MWCNT in the ternary polymer blend of PVdF/PS/HDPE by melt blending technique.[213] MWCNT are localized in the PS shell of PS/HDPE core-shell structure and Fe_3O_4 nanoparticles are localized in the PVdF matrix (F-F) and HDPE core (E-F). The conductive network was formed at 1 vol.% and unaffected by the volume percentage of Fe_3O_4 and their localization either in PVdF or HDPE. However, the F-F composites with Fe_3O_4 nanoparticles localized in the PVdF matrix exhibited higher permittivity values than the E-F composites with Fe_3O_4 nanoparticles localized in HDPE core as shown in Figure 23. This is due to the increased interaction between the Fe_3O_4 and PVdF than that of Fe_3O_4 and HDPE. It can also be observed that the values of permittivity vary linearly with the vol.% of Fe_3O_4 from 0 to 2.0 vol.%. Subsequently, F-F composites have shown a higher EMI *SE* (20.5 dB–26.5 dB) than E-F composites (17 dB–23.7 dB) at the same Fe_3O_4 loading (2 vol.%) in X-band range.

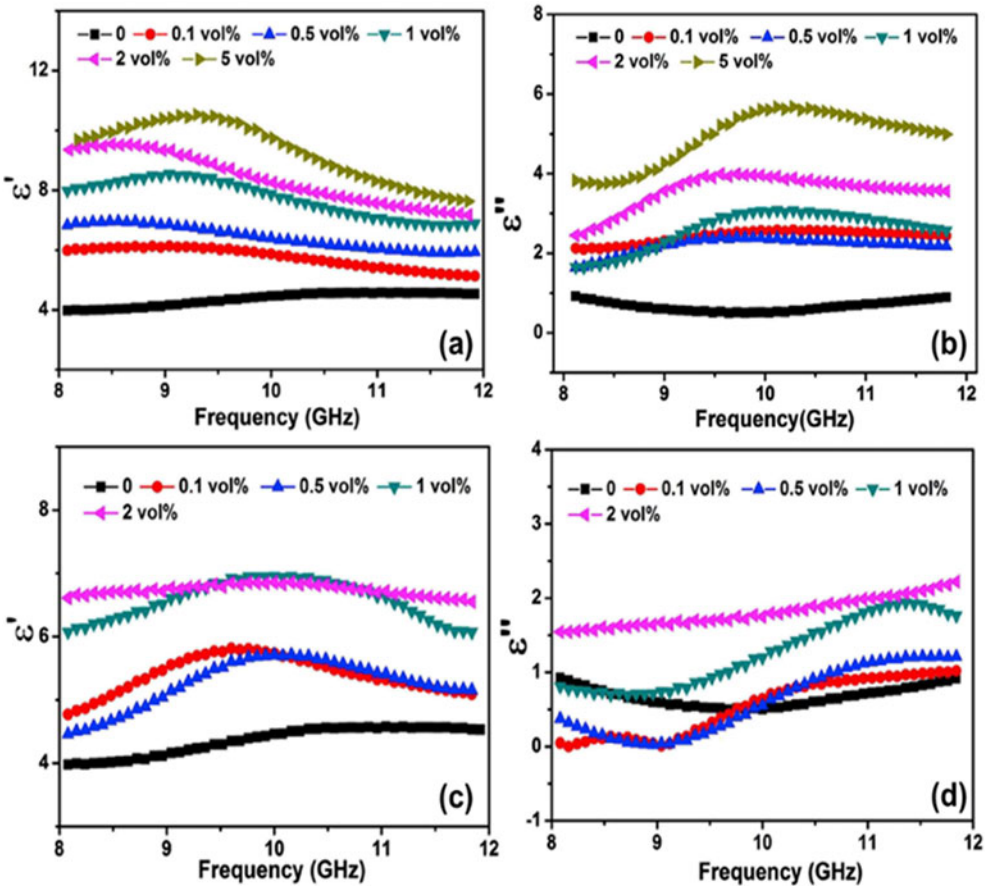

Figure 23. ε′ and ε″ of F-F (a & b) and E-F composites (c & d), respectively, for different vol.% of Fe_3O_4 loading in the X-band. Reproduced with permission from ref.[213] Copyrights © 2018 Elsevier B.V.

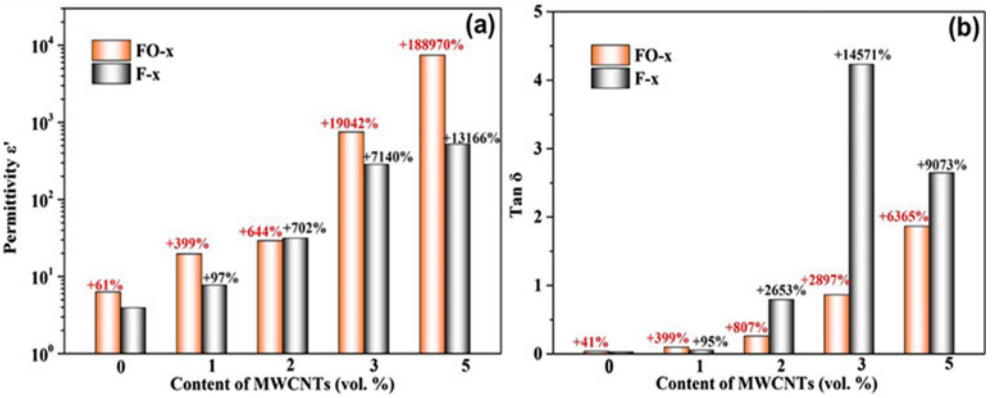

Figure 24. Value of (a) ε'_r and (b) tan δ as a function of MWCNT content for PVDF/OBC/MWCNT and PVdF/MWCNT nanocomposites. Reproduced with permission from ref.[214] Copyrights © 2017 Elsevier Ltd.

Zha et al. described that the selective confinement of MWCNT at the interface of PVDF and OBC (ethylene-α-octene block copolymer) reduces the φ_c by 23% compared to the PVdF/MWCNT nanocomposites. Figures 24 shows that the ε'_r (Fig. 23a) and tan δ (Fig. 23b) increases with increase in the MWCNT content and their values are higher for PVDF/OBC/MWCNT nanocomposites than the PVdF/MWCNT nanocomposites. An EMI *SE* of ~34 dB was attained for PVDF/OBC/MWCNT at 2.7 vol.% MWCNT.[214] The enhancement in the dielectric property and EMI *SE* is attributed to the strong interfacial polarization arising from the charge carrier built up at the interfaces.

4.4. Conductive anisotropic CPC

Normally, CPCs exhibit conductive (electrical) isotropy because of the randomly distributed conducting fillers in their polymer matrix. Conductive anisotropy can be achieved by alignment of fillers using a magnetic or shear or electric field. Conductive anisotropy results in electrical conductivity in one direction and insulating in another direction. The percolation threshold for conductive filler concentration in CPCs can be further reduced by achieving conductive anisotropy.[215] For example, Mao et al. demonstrated that the graphene stripes aligned in the polypropylene/(styrene-ethylene/butadiene-styrene) triblock by using shear force exhibited the four orders of higher σ in parallel direction than the perpendicular direction.[216] Shi et al. achieved conductive anisotropy in S-PLLA/PCL/MWCNT/Ni CPC by applying a magnetic field of ~47.5 mT for 30 min at 100 °C.[215] After achieving conductive anisotropy, higher values of σ was observed in the direction parallel to the alignment attributed to the Ni-particle chains. This alignment also enhanced the value of EMI *SE* as depicted in Figure 25. The segregated structured composites with a random distribution of nickel exhibited an EMI *SE* of 7–9 dB, whereas the composites with aligned nickel chains exhibited an EMI *SE* of 24–19 dB. This enhanced EMI shielding with respect to the alignment of nickel particles was attributed to the increased absorption and reflection of EM radiation inside the nanocomposites, which were caused by the formation of Ni particle chains and higher electrical conductivity. The segregated structured PLLA/PCL/MWCNT/Ni

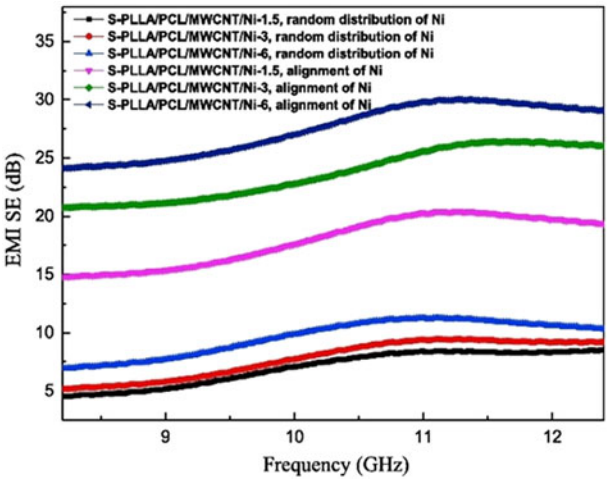

Figure 25. EMI SE values of the Segregated PLLA/PCL/MWCNT/Ni CPC with respect to the alignment of Ni particles over the X-band. Reproduced with permission from ref.[215] Copyright © 2018 Elsevier B.V.

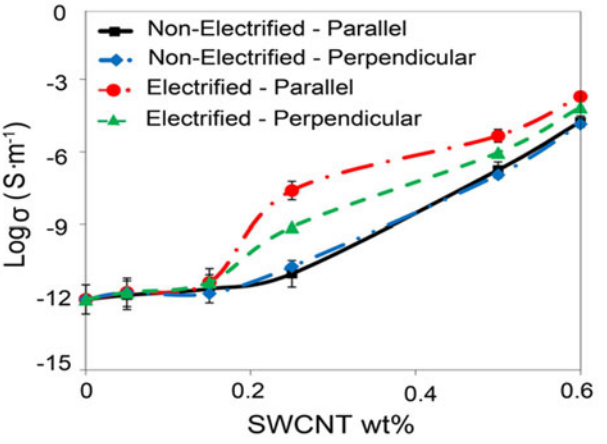

Figure 26. Deviation of σ for electrified and non-electrified epoxy composites with respect to wt.% of SWCNT. Reproduced with permission from ref.[217] Copyright © 2017 Society of Plastics Engineers.

nanocomposites exhibited higher mechanical properties than the conventionally structured nanocomposites.

Hashemi et al. achieved epoxy/SWCNT composites with aligned SWCNT using DC electric field. Figure 26 shows the change in the values of σ for electrified and nonelectrified epoxy composites with respect to wt% of SWCNT. The σ of the epoxy composites with aligned SWCNT is higher than that of randomly distributed SWCNT. SWCNT showed higher tendency to align in a parallel direction on electrifying with DC electric field and hence higher electrical conductivity in the parallel direction (4.6×10^{-6} $S.m^{-1}$) than that of perpendicular direction (9.3×10^{-9} $S.cm^{-1}$) at 0.5 wt% of SWCNT. The EMI *SE* of 12.8 and 9.1 dB was achieved for the electrified and nonelectrified composites with 0.6 wt% SWCNT loading and 3.0 mm thickness.[217]

5. Lightweight polymer composites

Further, low density, flexibility, thermal insulation, impact damping, and good structural stability have attracted the applications of conductive fillers filled polymer foam for EMI shielding applications.[218,219] Flexible materials possess high recovery properties with a low percolation threshold whereas rigid materials have less recovery.[220,221]

Ghosh et al. prepared Ketjen carbon black (K-CB) incorporated PU foam by dip coating. Further, PEG 4000 has been used as the ionic surfactant to prevent the coalescence of K-CB during the dipping of PU foam. The surfactants are found to have a negligible effect on the σ of PU foam nanocomposite. At 2 wt% K-CB loading, PU foam composites exhibited an EMI *SE* of 65.6 dB.[222] Eswaraiah et al. demonstrated an EMI *SE* of ~20 and 18 dB over the frequency range of 1–8 GHz for 5 wt% of functionalized graphene(fG) in fG-PVdF foam in the X-band.[223] Thomassin et al. showed that the foaming of the nanocomposites allowed to significantly decrease the reflectivity below −15 dB (only 3% of the initial radiation is reflected).[224] Xu et al. reported that the density influenced the microstructure of the CNT-PU composites.[225] The decrease in the density decreases the cell wall thickness and changes the three-dimensional conduction to two dimensional (Fig. 27). This, in turn, increases the φ_c and decreases the σ of the cell.[226,227] The CNT content in the cell walls decreases with a decrease in the density of the foam that attributes to the decrease in the electrical conductivity.[228]

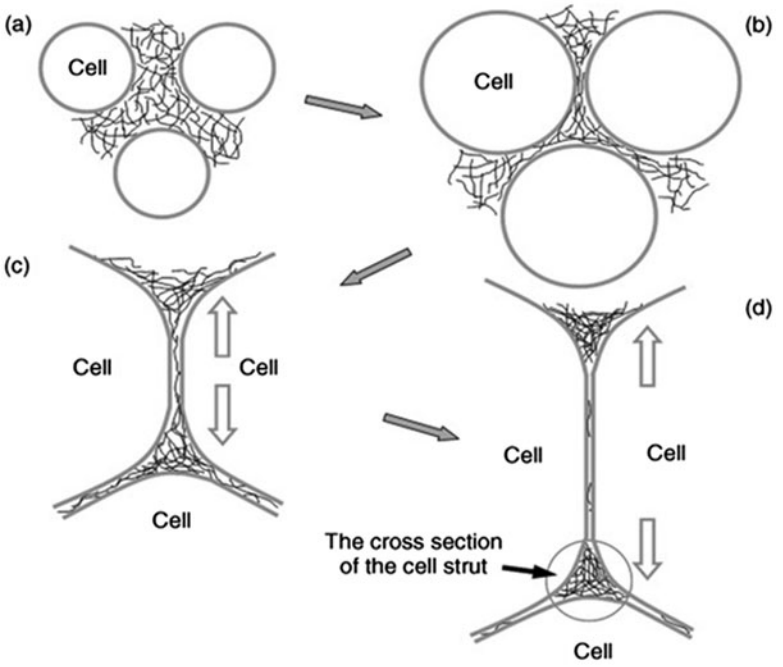

Figure 27. Schematic illustration of changes in the microstructural changes with the gradually from (a) to (d) for CNT/PU foam composites. CNT is represented by the thin black lines and the cell boundaries are represented by wide lines. The growth directions of the air bubbles during foaming are represented by the arrows. Reproduced with permission from ref.[225] Copyright © 2007 Wiley-VCH Verlag GmbH & Co. KGaA, Weinheim.

Wang et al. compared the foaming behavior and EMI *SE* of PLA/graphite prepared by regular foam injection molding (RFIM) and mold-opening foam injection molding (MOFIM).[229] The foams fabricated using the MOFIM method possess a uniform microcellular structure, whereas foams fabricated using the RFIM possess a collapsed microcellular structure. The EMI *SE* of the MOFIM foams is ~45 dB, which is higher than that RFIM foams (~30 dB). Yang et al. reported that the CNT/PS and CNF/PS foam exhibited the EMI *SE* of 18.56 and 20.51 at 7 wt% and 20 wt%, respectively.[230] Chen et al. demonstrated that the 0.8 wt% graphene (GN) incorporated PDMS foam exhibited the nearly similar EMI *SE* (~20 dB) to the 7 wt% of CNT incorporated polystyrene foam.[230,231] Xu et al. demonstrated that the CNT/HDPE foam exhibited an SE_T of 21.2 dB at low φ_c of 1.66 vol.%, whereas solid CNT/HDPE required a higher CNT content of about 2.31 vol.%.[232] Yan et al. prepared porous graphene/polystyrene foams (GPS) using $CaCo_3$ particles using compression molding followed by the salt-leaching method.[233] The average EMI *SE* of the GPS samples of 2.5 mm thickness at 0.45 and 0.27 $g.cm^{-3}$ are found to be approximately 29.3 and 17.3 dB, respectively. Zhang et al. demonstrated SE_T, SE_A, and SE_R of 19, 18, and 1 dB, respectively, for 1.8 vol.% of GN loaded microcellular PMMA foam using subcritical CO_2.[234] Zheng et al. prepared low density (0.28–0.4 g/cm^3) polyetherimide (PEI) composites containing GN@Fe_3O_4 by phase inversion method with outstanding specific shielding effectiveness (SSE) of ~41.5 dB/(g/cm^3) in the X-band at 10 wt% loading.[235] The excellent EMI *SE* attributed to the spherical micro-scale bubbles in the foam that can depreciate the EM waves by scattering and multi-internal reflection between the nanofillers and the cell walls. In addition, the micro-scale bubbles of the foam prevent the EM waves from escaping easily before being attenuated by absorption and heat transfer as illustrated in Figure 28a–b. TEM image (Fig. 28c) showing two parallel G@ Fe_3O_4 in PEI matrix supports the illustrated shielding mechanism of multi-internal reflection. The same research group has also demonstrated a higher *SE* value of 57.7 dB for the 10 wt% graphene loaded PU foam of ~6 cm thick. Also, the G/PU foams exhibited excellent compressibility. It is also observed that their shielding performance can be modified by compressing the foams. Figure 29 shows that the SE_T of the 6 mm thick G(10 wt.%)/PU foam decreases with increasing the compression percentage. It can be observed that the SE_R remains almost the same for all compression rates, whereas SE_A decreases. This can be ascribed to the decrease in the cell-matrix interface area during compression that deteriorates the multiple-internal reflection and scattering of EM waves.[236]

Ling et al. reported low-density microcellular PEI/GN foams with accumulation and alignment of graphene on the cell wall and SSE ranging from 17 to 44 dB/(g/cm^3).[237] Zheng et al. assembled an aligned porous MWCNT/WPU composites with low and well-regulated densities by the unidirectional freeze-drying and demonstrated an outstanding SSE up to 1148 dB cm^3 g^{-1}.[238] Fu et al. fabricated self-healing hydrogel by dispersing MWCNT into the hydrophobic polyacrylamide (PAM) and demonstrated a SE_T of ~28.5 dB. The cellulose nanofiber (CNF) is used as the dispersant. The prepared hydrogels (Fig. 30a) exhibited excellent capacity to withstand deformations such as convolving (Fig. 30b), bending (Fig. 30c), knotting (Fig. 30d), and knotted stretching (Fig. 30e), without change in its shape (Fig. 30f).[239] However, since it is difficult to control the porous shape by these preparation methods, the preparation of prevailing pores is still unsatisfactory.

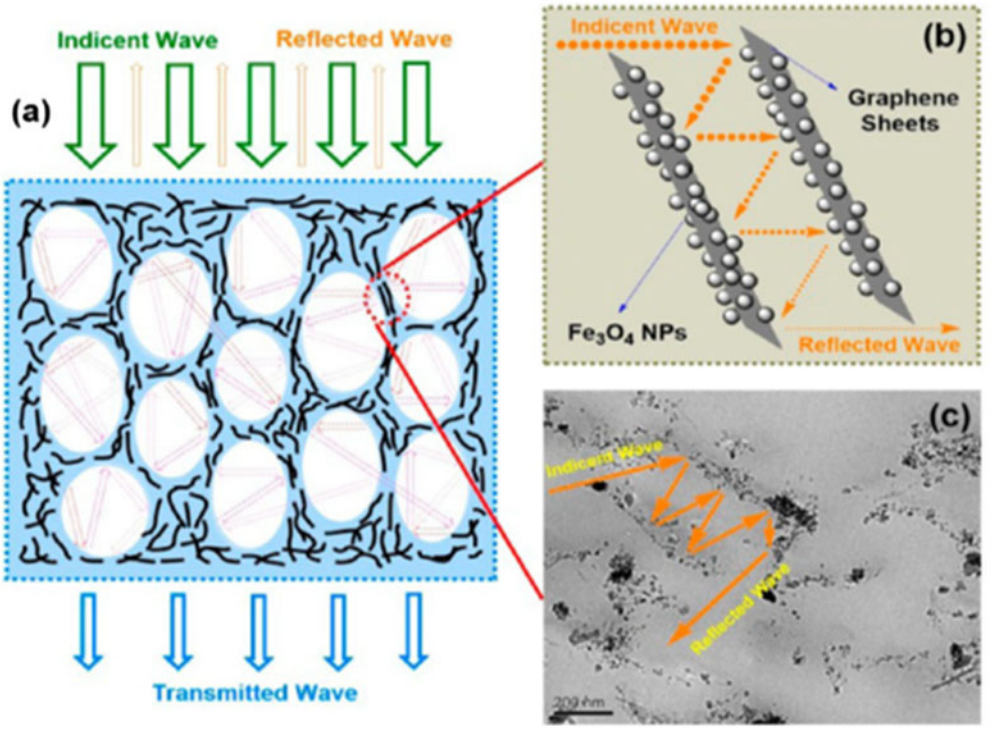

Figure 28. (a) Schematic illustration of EM attenuation and (b) multi-internal reflection route in the PEI/G@Fe_3O_4 foams; (c) TEM image demonstrating the illustrated EM attenuation mechanism. Reproduced with permission from ref.[235] Copyright © 2013 American Chemical Society.

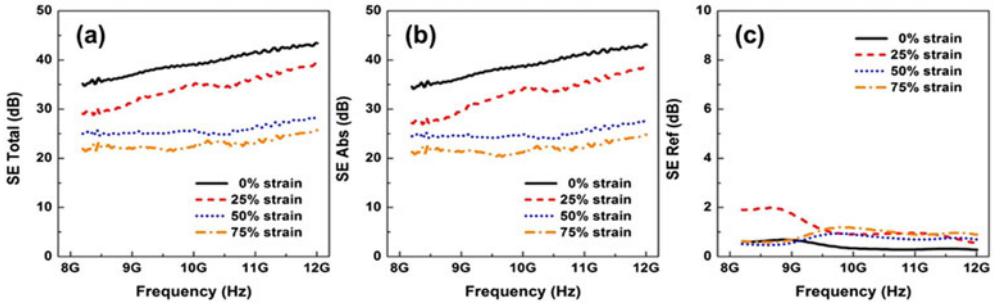

Figure 29. SET, (b) SEA, (c) SER of the 6 mm thick G (10 wt.%)/PU under various compression strain in the frequency range of 8–12 GHz. Modified from ref.[236]

Xing et al. assembled flexible sandwich structures by laminating Ni-coated carbon fibers in between polycarbonate films. The resultant structures exhibited an EMI *SE* of 72.7 dB at the thickness of 0.31 mm. The density and electrical conductivity of the structures prepared at an optimum condition is 1.7 g.cm^{-3} and 376.6 S.cm^{-1}, respectively.[240] Na et al. fabricated poly(ether ether ketone) (PEEK) composite flexible films comprised of MWCNT.

To improve the disperion of MWCNT, the MWCNT were coated with poly(ether sulfone) (PES). The PES coating prevented the agglomeration of MWCNT and improved

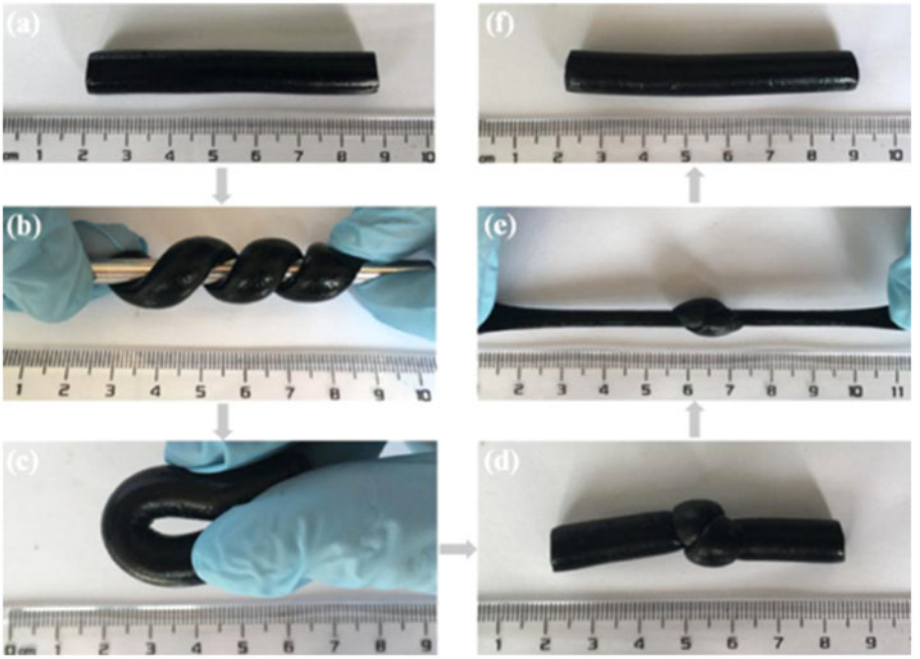

Figure 30. Pictures displaying outstanding mechanical property of $PAMF_{0.3}T_1$: (a) original shape, (b) convolving, (c) twisting, (d) knotting, (e) stretching, and (f) recovering. Reproduced from ref.[239] Copyright © 2018 American Chemical Society.

the dispersion as their molecular structure was similar to that of PEEK. Further, GENIOPLAST® pellets (GPPS) were added to improve the dispersion and to reduce the melt viscosity of PEEK for easy processing. The PEEK/MWCNT-GPPS exhibits a higher electrical conductivity than PEEK/MWCNT. At a critical concentration of 1.0 wt.% for GPPS, an EMI *SE* of about 10.5 dB over 8.2–12.4 GHz and 16.2 dB at 40 GHz was achieved.[241] Jia et al. fabricated a flexible and transparent EMI shielding film of PU containing calcium alginate (CA) and silver nanowires (Ag NW). The PU and CA are transparent to EM wave and hence the EMI *SE* depends on the Ag NW. The highest EMI *SE* of 31.3 dB in between the 4 and 18 GHz was achieved for the CA/Ag NW/PU film, whose area density of Ag NW and transmittance were 174 $mg{\cdot}m^{-2}$ and 81%, respectively.[242] Oh et al. investigated the EMI shielding performance of silver nanoparticles (Ag-NP) coated polyethylene terephthalate (PET) film between 0.1 and 1 GHz. The Ag NP/PET film exhibited the highest SE_T values of 60.49 at 0.1 GHz and 54.72 dB at 1.0 GHz.[243] Ozen et al. prepared Ag-NP deposited polyamide (PA66) nonwoven fabrics with excellent weight normalized SSE of over 1200 $dB{\cdot}cm^3{\cdot}g^{-1}$ in the 0.015–3 GHz range.[244] Sabira et al. reported freestanding and flexible PVdF-Graphene film of thickness 20 μm and 15 wt% graphene, exhibiting an absorption dominant EMI *SE* of 47 dB ($SE_A = 45.36$ dB; $SE_R = 2.17$ dB) in the X-band.[245] Kim et al. demonstrated thin and flexible CPC composed of 40 wt% of MWCNT containing Fe catalyst and PMMA with an EMI *SE* of ~27 dB.[246] Xu et al. prepared nickel (Ni)/nylon porous membrane (NPM) composite film, in which nickel is deposited on both sides of the NPM to get sandwich structure by electroless deposition technique.[247] The prepared Ni/NPM film exhibited

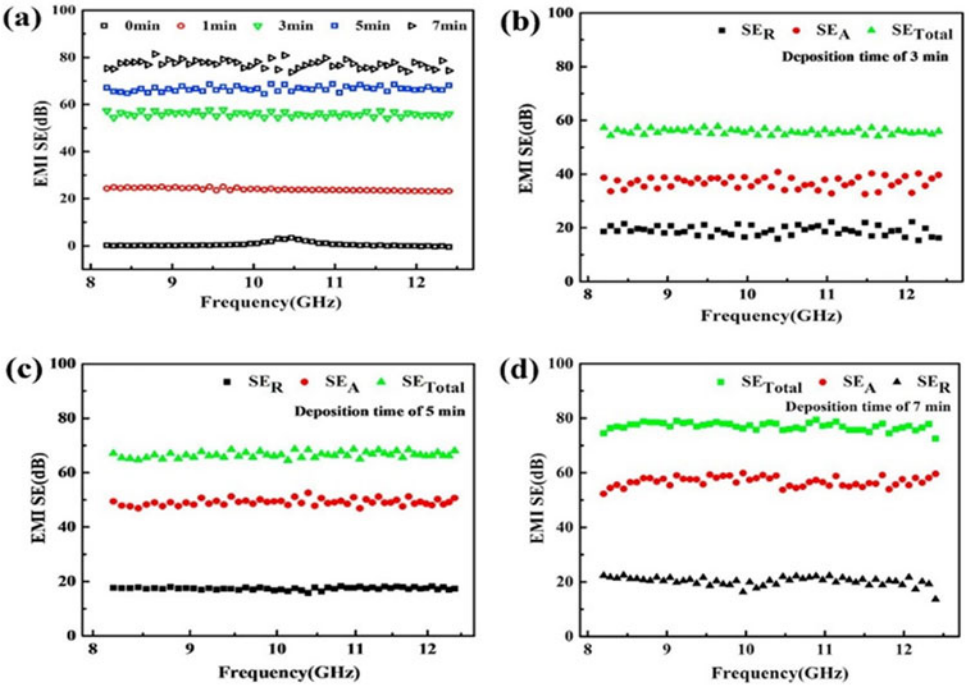

Figure 31. SE_T, SE_A, and SE_R of the NPM/Ni films prepared at different deposition times. Reproduced with permission from ref.[247] Copyright © 2018 Elsevier B.V.

an EMI *SE* of 77 dB and retained 85% of its initial value after 300 bending cycles. Figure 31a–d shows that SE_T increases with an increase in the deposition time of nickel films, while the SE_A increases whereas SE_R remains the same. The EMI *SE* values are not changing with increasing the frequency in the entire range.

Thus, the polymer/carbon composites could serve as lightweight, economic, processable, and mechanically strong composites. EMI shielding performance of the various CPC is summarized in Table 2.

6. Multicomponent systems

The amalgamation convention has recently changed from simple to hybrid nanomaterials to accumulate every single fundamental property in a solitaire composite for better shielding efficiency.[259] Sambyal et al. prepared PPy/RGO/barium strontium titanate (BST)/Fe_3O_4 as demonstrated in Figure 32a, adopting chemical oxidative polymerization. The nonuniformities (heterogeneities) in the prepared multi-component composites led to space charge polarization. The charge accumulation at the interface between components promoted the formation of dipole and interfacial polarization as presented in Figure 32b. The value of EMI *SE* for the prepared PPy/RGO/BST/Fe_3O_4 composites is ~48 dB in the X-band, with absorption as the dominant mechanism.[260]

Zhan et al. prepared flexible segregated CPCs comprising natural rubber (NR), Fe_3O_4, and RGO (S-NRMG) by self-assembly technique in NR as displayed in Figure 33. The highest σ values for NRG-10 and NRMG-10 composites respectively are achieved after

Table 2. EMI shielding performance of various CPC.

Materials	Filler loading (wt.%)	σ (S.cm^{-1})	SE_T (dB)	SE_A (dB)	SE_R (dB)	d (mm)	Investigated Frequency range	Ref.
MWCNT/chlorinated PE	15 %	~ 0.01	36.0	—	—	2.0	X-band	[153]
TPV/NCGF	1.2%	0.066	34.4	30.1	4.0	2.0	X-band	[248]
ABS/ CB:CNT (25:75)	3.0%	0.029	29.37	23.99	4.91	2.0	X-band	[196]
S-PLLA/MWCNT	1.1%	0.25	30.0	26.0	4.0	1.5	X-band	[209]
R-PLLA/MWCNT	1.1%	3×10^{-5}	22.0	19.5	2.5	1.5	X-band	
S-PLLA/PCL/MWCNT/Ni	6.0% (Ni)	—	24–29	—	—	—	X-band	[215]
RGO-GF/UP	20.0% (GF)	—	21.3	18.2	2.7	10.0	X-band	[249]
Microcellular Polyimide (PI) /RGO/ MWCNTs composite	8% (RGO & MWCNT)	18.7×10^{-3}	16.6	14.7	2.1	—	X-band	[250]
CF/polyacrylamide/ wood fiber (CPW) composite	7.5% (CF)	$\sim 10^{-3}$	41.03	—	—	—	X-band	[251]
PVDF/PS/ HDPE-MWCNTs	1.6%	0.9×10^{-3} @σ_c of 0.3%	31.7 @9.5 GHz	29.1 @9.5GHz	2.6 @9.5GHz	—	X-band	
MWCNTs/waterborne polyurethane	10%	0.124	29	21.5	7.5	0.8	X-band	[252]
PPCP/MWCNT	4.6%	7.2×10^{-3}	47.8	42.5	5.4	2.0	X-band	[253]
Microcellular PI/ RGO/MWCNTs	8%	0.0187	16.6–18.2	14.7	2.1	0.5	X-band	[250]
Ni coated RGO/PC/SAN	3%	—	29.4	—	—	—	8–18 GHz	[254]
MWCNT/PP	7.5 vol.%	—	34.8	26.8	8.0	1.0	X-band	[255]
Polyamide 6/EG	2.27 vol.%	5.5×10^{-3}	25.0	23.54	1.48	2.0	X-band	[256]
PP/MWCNT	20%	0.66	57.0	39.9	17.1	2.0	S-band	[257]
	20%	0.66	47.0	70% SE_T	30% SE_T	2.0	X-band	
	20%	0.66	44.0	70% SE_T	30% SE_T	2.0	Ku-band	
PMMA/Graphene foam	1.8 vol.%	31.1×10^{-3}	19.0	18.0	1.0	2.4	X-band	[234]
PI/RGO	16%	8.0×10^{-3}	20.0	17.6	2.4	0.8	X-band	[258]

*X- band: 8–12 GHz.

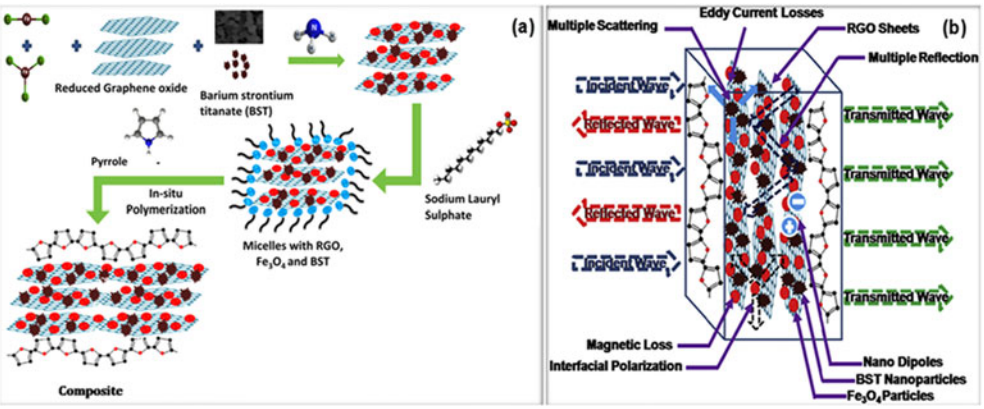

Figure 32. (a) Pictorial illustration of the synthesis of PPy/RGO/BST/Fe_3O_4 composite by chemical oxidative polymerization process and (b) Schematic representation of possible mechanism of EMI Shielding in PBRF composite. Reproduced with permission from ref.[260] Copyright © 2018 Published by Elsevier B.V. on behalf of Korean Physical Society.

thermal treatment at 150 °C, which is ascribed to the established perfect conducting network of RGO sheets. However, the electrical conductivity of NRMG-10 is slightly less than that of NRG-10 due to the negative effect of iron oxide nanoparticles. The

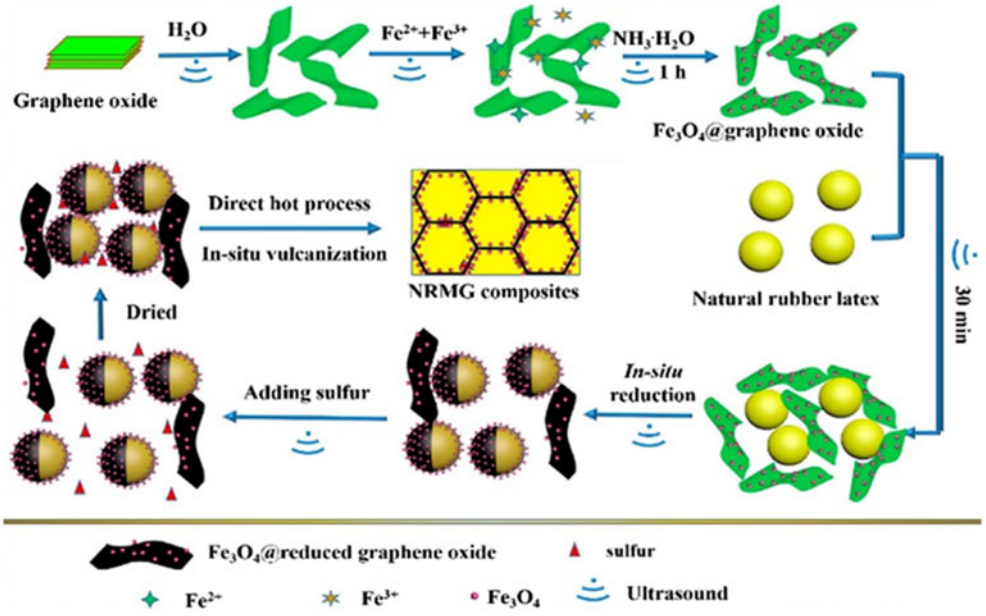

Figure 33. Schematic illustration of the preparation process of NRMG composites. Reproduced with permission from ref.[261] Copyright © 2018 Elsevier B.V.

heat treatment also contributed to the enhanced EMI. However, the S-NRMG exhibited an EMI *SE* (42.4 dB) higher than the NRG (34.0 dB) at 10 phr of RGO. The *SE* values vary directly with the content of RGO. The higher *SE* values are accredited to the combination of numerous free charge carriers, electric dipoles, and an excellent conducting network of RGO and the magnetic resonances and eddy currents of Fe_3O_4 magnetic nanoparticles. In NRMG, the large interfacial area between the RGO and Fe_3O_4 provided an extensive interfacial polarization and thereby proliferated the pathway for EM waves which consecutively upturned the EM attenuation. NRMG-10 exhibited excellent bending stability, injecting brilliance into the next generation of flexible EMI shielding materials.[261]

Biswas et al. demonstrated "absorption–multiple reflections–absorption" multi-layered structure in which absorption layer (top and bottom) composed of MWCNT-MnO_2 and RGO-Fe nanostructures in the PVdF matrix and the reflection layer (middle) composed of MWCNT in PC/PVdF blend. These multilayered structures exhibited a SE_T of 57 dB at a thickness of 0.9 mm with 92% absorption.[262] In another study, the SE_T was improved to 64 dB by improving impedance matching of the top layer using functionalized MWCNT.[263] Xu et al. demonstrated "absorb-reflect-reabsorb process" by generating gradient layered structure in WPU comprising of RGO@Fe_3O_4 distributed throughout the matrix and a thin tetraneedle-like ZnO (T-ZnO)/Ag bottom layer.[264] The thick layer of rGO@Fe_3O_4 distributed throughout the PU matrix contributed to the impedance matching and EM absorption and the thin T-ZnO/Ag layer at the bottom re-reflected the EM wave and thereby increased the absorption further, as illustrated in Figure 34. At 0.8 vol.% of rGO@Fe_3O_4 and 5.7 vol.% of rGO@Fe_3O_4, the prepared PU gradient structured composites exhibited an extraordinary SE_T of 87.2 dB with only 2.4 dB of SE_R with a sample thickness of 0.5 mm.

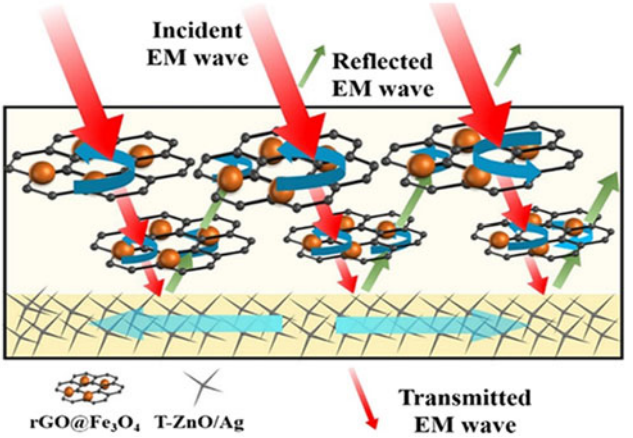

Figure 34. Schematic illustration of gradient structured waterborne polyurethane comprising of rGO@Fe_3O_4 and T-ZnO/Ag. Reproduced with permission from ref.[264]

Wang et al. prepared silver (Ag)/RGO coated polyester (PET) fabric. Prior to the addition of silver and RGO, PET fabric surface was functionalized with poly (diallyl dimethyl ammonium chloride) (PDDA) to improve the adhesive strength between the PET fabric substrate and the additives. The weight of Ag/RGO deposited on the PET fabric surface with and without PDDA functionalization was found to be 2.47 and 3.68 $mg{\cdot}cm^{-2}$, respectively. Also, the PDDA functionalized PET fabric retained 85.6% of Ag/RGO after washing, whereas bare PET fabric retained only 38.5%. The positive charges offered by the PDDA on the surface of PET fabric are due to the increased particle loading and adhesion. Subsequently, PDDA modified PET-Ag/RGO exhibited relatively higher EMI *SE* that ranges from 52 to 57 dB between 1 and 18 GHz.[265] Vyas et al. investigated the EMI shielding performance of inorganic salt ($LiBF_4$) and organic salt ($EMIMBF_4$) containing PVdF-HFP polymer gel electrolyte with Fe_3O_4 and MWCNT as fillers.[266] The ion conducting salts in the PVdF-HFP increased the charge storage capacity of the polymer matrix by generating more mobile ions and thereby improved the dielectric property. MWCNT contributed to dielectric loss and Fe_3O_4 contributed to the magnetic loss. The SE_T of the polymer nanocomposite gel electrolytes reached ~43.5 dB. Jin et al. prepared methyl vinyl silicone rubber (VMQ) based nanocomposites that consisted of MWCNT decorated graphene nanoplatelet/Fe_3O_4@$BaTiO_3$ (GFBTM) as conductive fillers. The VMQ/16 wt% GFBTM exhibited a σ of 1 $S.m^{-1}$ and EMI *SE* of 26.7 dB over a broad bandwidth ranging from 1.0 to 20.0 GHz.[267] Zhang et al. reported that 5 wt% RGO/MnF_eO_4 containing PVdF nanocomposites exhibited a min. *RL* of −29.0 dB at 9.2 GHz with a wide band of 8.00–12.88 GHz for $RL < -10$ dB. The improved EM absorption is the result of dielectric loss (PVdF and RGO), magnetic loss ($MnFe_2O_4$) and synergetic effect (PVdF + RGO; PVdF + $MnFe_2O_4$ and $MnFe_2O_4$+RGO).[268] Hua et al. reported that 2.6 mm thick sample of CPCs composed of GN/MWCNT/poly(p-phenylenebenzobisoxazole) [GMP] exhibited a *RL* of −50.17 dB at 12.58 GHz.[269] The improved EM absorption was attributed to the impedance matching at the interface of free space and surface of the multi-phase composites and the heterogeneities along with strong dielectric properties.

7 Conclusion and future perspectives

Recent advances in EMI shielding using ICP and CPC have clearly indicated that polymers and their hybrids/multi-structural composites are very promising for EMI shielding applications. The frequency-dependent characteristics, as well as the adjustment of the morphological structure and processing parameters, are discussed to achieve enhanced EMI shielding along with to understand its corresponding mechanisms. It is worth mentioning that all of these studies aim to introduce nonuniformities (heterogeneities) inside the EMI shielding materials to enhance EM absorption. In the case of biphasic polymer blends, engineering of filler localization and morphology greatly improved the EM absorption. The attractive features of the polymer-based materials such as lightweight and high EM absorption demonstrated their potentials in EMI shielding.

Despite considerable advancements, they face many obvious challenges. The significant limitations include: Insulating nature of polymers that may lead to the enlargement of skin depth for EM attenuation (if sufficient conducting network is not established by the conductive fillers); Difficult in processing and reconstruction of defects; Surface-functionalization of fillers that harms the physical properties of the composites and processing; Poor thermal stability that hinders their applications in high-temperature operation; Understanding the thermodynamics of polymer blends and corresponding preferential localization of fillers; tailoring of morphology and physical properties of the fillers, etc. Even though, multi-component structures and lightweight foams are reported as efficient EM absorbers, the factors that determine their bandwidth of EM absorption and skin depth are still not clearly explained and it is not clear how the temperature influences the electromagnetic properties of materials in the nanoscale polymer nanocomposites or nanohybrids. Hence, more investigations are needed in this direction. However, we envision that light-weight multi-component nanostructures and three-dimensional architectures of polymer-based materials with good mechanical properties and high thermal stability will lead toward the realization of highly efficient EMI shielding for various applications.

Acknowledgments

The authors appreciate the supports from Heilongjiang Natural Science Foundation (QC2017038), Fundamental Research Funds for the Central Universities (No. 2572018BC27), China Postdoctoral Science Foundation (No. 2016M601402) Heilongjiang Postdoctoral Fund (No. LBH-Z16004, LBH-Z16089). Mr. MV is grateful to the Indo-US Science and Technology Forum (IUSSTF), Department of Science and Technology (DST), New Delhi for providing a fellowship under BASE program (IUSSTF BASE Internships 2018/12/Vignesh M, dt. 09/04/2018).

References

1. Gurusiddesh, M.; Madhu, B. J.; Shankaramurthy, G. J. Structural, Dielectric, Magnetic and Electromagnetic Interference Shielding Investigations of Polyaniline Decorated $Co_{0.5}Ni_{0.5}Fe_2O_4$ Nanoferrites. *J. Mater. Sci: Mater. Electron*. **2018**, *29*, 3502–3509. doi: 10.1007/s10854-017-8285-4.
2. Gong, S.; Zhu Zheng, H.; Arjmand, M.; Sundararaj, U.; Yeow, J.; T. W.; Zheng, W. Effect of Carbon Nanotubes on Electromagnetic Interference Shielding of Carbon Fiber Reinforced Polymer Composites. *Polym. Compos*. **2018**, *39*, E655–E663. doi:10.1002/pc.24084.

3. Biao, Z.; Deng, J.; Zhang, R.; Liang, L.; Fan, B.; Bai, Z.; Shao, G.; Park, C. B. Recent Advances on the Electromagnetic Wave Absorption Properties of Ni Based Materials. *Eng.Sci.* doi: **2018**, *3*, 5–40. doi:10.30919/es8d735.
4. Li, T.-T.; Chen, A.-P.; Hwang, P.-W.; Pan, Y.-J.; Hsing, W.-H.; Lou, C.-W.; Chen, Y.-S.; Lin, J.-H. Synergistic Effects of Micro-/Nano-fillers on Conductive and Electromagnetic Shielding Properties of Polypropylene Nanocomposites. *Mater. Manuf. Processes* **2018**, *33*, 149–155. doi:10.1080/10426914.2016.1269924.
5. Engels, S.; Schneider, N.-L.; Lefeldt, N.; Hein, C. M.; Zapka, M.; Michalik, A.; Elbers, D.; Kittel, A.; Hore, P. J.; Mouritsen, H. Anthropogenic Electromagnetic Noise Disrupts Magnetic Compass Orientation in a Migratory Bird. *Nature* **2014**, *509*, 353. doi:10.1038/nature13290.
6. Erogul, O.; Oztas, E.; Yildirim, I.; Kir, T.; Aydur, E.; Komesli, G.; Irkilata, H. C.; Irmak, M. K.; Peker, A. F. Effects of Electromagnetic Radiation from a Cellular Phone on Human Sperm Motility: An in Vitro Study. *Arch. Med. Res.* **2006**, *37*, 840–843. doi:10.1016/j.arcmed.2006.05.003.
7. Ding, Z.; Shi, S. Q.; Zhang, H.; Cai, L. Electromagnetic Shielding Properties of Iron Oxide Impregnated Kenaf Bast Fiberboard. *Composites, Part B*. **2015**, *78*, 266–271. doi:10.1016/j.compositesb.2015.03.044.
8. Tang, H.; Jian, X.; Wu, B.; Liu, S.; Jiang, Z.; Chen, X.; Lv, W.; He, W.; Tian, W.; Wei, Y.; et al. Fe3C/helical Carbon Nanotube Hybrid: Facile Synthesis and Spin-Induced Enhancement in Microwave-absorbing Properties. *Composites, Part B* **2016**, *107*, 51–58. doi:10.1016/j.compositesb.2016.09.003.
9. Tugirumubano, A.; Vijay, S. J.; Go, S. H.; Kwac, L. K.; Kim, H. G. Investigation of Mechanical and Electromagnetic Interference Shielding Properties of Nickel–CFRP Textile Composites. *J. Mater. Eng. Perform*. **2018**, *27*, 2255–2262. doi:10.1007/s11665-018-3334-6.
10. Bhawal, P.; Ganguly, S.; Das Tushar, K.; Mondal, S.; Das, N. C. Mechanically Robust Conductive Carbon Clusters Confined Ethylene Methyl Acrylate–based Flexible Composites for Superior Shielding Effectiveness. *Polym. Adv. Technol.* **2018**, *29*, 95–110. doi:10.1002/pat.4092.
11. Sawai, P.; Chattopadhaya, P. P.; Banerjee, S. Synthesized Reduce Graphene Oxide (rGO) Filled Polyetherimide Based Nanocomposites for EMI Shielding Applications. *Mater. Today: Proc*. **2018**, *5*, 9989–9999. doi:10.1016/j.matpr.2017.10.197.
12. Singh, A. K.; Shishkin, A.; Koppel, T.; Gupta, N. A Review of Porous Lightweight Composite Materials for Electromagnetic Interference Shielding. *Comp., Part B* **2018**, *149*, 188–197. doi:10.1016/j.compositesb.2018.05.027.
13. Huang, J.-C. EMI Shielding Plastics: A Review. *Adv. Polym. Technol*. **1995**, *14*, 137–150. doi:10.1002/adv.1995.060140205.
14. Zhang, Y.; Wang, X.; Cao, M. Confinedly Implanted $NiFe_2O_4$-rGO: Cluster Tailoring and Highly Tunable Electromagnetic Properties for Selective-frequency Microwave Absorption. *Nano Res*. **2018**, *11*, 1426–1436. doi:10.1007/s12274-017-1758-1.
15. Xiang, C.; Pan, Y.; Liu, X.; Sun, X.; Shi, X.; Guo, J. Microwave Attenuation of Multiwalled Carbon Nanotube-fused Silica Composites. *Appl. Phys. Lett*. **2005**, *87*, 123103. doi:10.1063/1.2051806.
16. Cao, M.-S.; Wang, X.-X.; Cao, W.-Q.; Yuan, J. Ultrathin Graphene: Electrical Properties and Highly Efficient Electromagnetic Interference Shielding. *J. Mater. Chem. C*. **2015**, *3*, 6589–6599. doi:10.1039/C5TC01354B.
17. Yang, C. C.; Gung, Y. J.; Hung, W. C.; Ting, T. H.; Wu, K. H. Infrared and Microwave Absorbing Properties of $BaTiO_3$/polyaniline and $BaFe_{12}O_{19}$/polyaniline Composites. *Compos. Sci. Technol*. **2010**, *70*, 466–471. doi:10.1016/j.compscitech.2009.11.021.
18. Luo, C.; Duan, W.; Yin, X.; Kong, J. Microwave-Absorbing Polymer-Derived Ceramics from Cobalt-Coordinated Poly(dimethylsilylene)Diacetylenes. *J. Phys. Chem. C*. **2016**, *120*, 18721–18732. doi:10.1021/acs.jpcc.6b03995.

19. Jiang, X.; Li, S.; He, S.; Bai, Y.; Shao, L. Interface Manipulation of CO_2–philic Composite Membranes Containing Designed UiO-66 Derivatives towards Highly Efficient CO_2 Capture. *J. Mater. Chem. A*. **2018**, *6*, 15064–15073. doi:10.1039/C8TA03872D.
20. Song, Y.; He, L.; Zhang, X.; Liu, F.; Tian, N.; Tang, Y.; Kong, J. Highly Efficient Electromagnetic Wave Absorbing Metal-Free and Carbon-Rich Ceramics Derived from Hyperbranched Polycarbosilazanes. *J. Phys. Chem. C*. **2017**, *121*, 24774–24785. doi:10.1021/acs.jpcc.7b07646.
21. Sun, H.; Yang, X.; Zhang, Y.; Cheng, X.; Xu, Y.; Bai, Y.; Shao, L. Segregation-Induced in Situ Hydrophilic Modification of Poly (vinylidene Fluoride) ultrafiltration Membranes via Sticky Poly (ethylene Glycol) Blending. *J. Membr. Sci*. **2018**, *563*, 22–30. doi:10.1016/j.memsci.2018.05.046.
22. Yang, X.; Wang, Z.; Shao, L. Construction of Oil-unidirectional Membrane for Integrated Oil Collection with Lossless Transportation and Oil-in-water Emulsion Purification. *J. Membr. Sci*. **2018**, *549*, 67–74. doi:10.1016/j.memsci.2017.11.071.
23. Gu, J.; Li, Y.; Liang, C.; Tang, Y.; Tang, L.; Zhang, Y.; Kong, J.; Liu, H.; Guo, Z. Synchronously Improved Dielectric and Mechanical Properties of Wave-transparent Laminated Composites Combined with Outstanding Thermal Stability by Incorporating Iysozyme/POSS Functionalized PBO Fibers. *J. Mater. Chem. C* **2018**, *6*, 7652–7660. doi:10.1039/C8TC02391C.
24. Wu, N.; Liu, C.; Xu, D.; Liu, J.; Liu, W.; Shao, Q.; Guo, Z. Enhanced Electromagnetic Wave Absorption of Three-Dimensional Porous Fe_3O_4/C Composite Flowers. *ACS Sustainable Chem. Eng*. **2018**, *6*, 12471–12480. doi:10.1021/acssuschemeng.8b03097.
25. Cao, M.; Han, C.; Wang, X.; Zhang, M.; Zhang, Y.; Shu, J.; Yang, H.; Fang, X.; Yuan, J. Graphene Nanohybrids: excellent Electromagnetic Properties for the Absorbing and Shielding of Electromagnetic Waves. *J. Mater. Chem. C*. **2018**, *6*, 4586–4602. doi:10.1039/C7TC05869A.
26. Ren, F.; Guo, Z.-Z.; Guo, H.; Jia, L.-C.; Zhao, Y.-C.; Ren, P.-G.; Yan, D.-X. Layer-Structured Design and Fabrication of Cyanate Ester Nanocomposites for Excellent Electromagnetic Shielding with Absorption-Dominated Characteristic. *Polymers* **2018**, *10*, 933.
27. Zhou, S.; Wang, J.; Wang, S.; Ma, X.; Huang, J.; Zhao, G.; Liu, Y. Facile Preparation of Multiscale Graphene-basalt Fiber Reinforcements and Their Enhanced Mechanical and Tribological Properties for Polyamide 6 Composites. *Mater. Chem. Phys*. **2018**, *217*, 315–322. doi:10.1016/j.matchemphys.2018.06.080.
28. Wang, C.; Murugadoss, V.; Kong, J.; He, Z.; Mai, X.; Shao, Q.; Chen, Y.; Guo, L.; Liu, C.; Angaiah, S.; Guo, Z. Overview of Carbon Nanostructures and Nanocomposites for Electromagnetic Wave Shielding. *Carbon* **2018**, *140*, 696–733. doi:10.1016/j.carbon.2018.09.006.
29. Yang, Z.; Hao, X.; Chen, S.; Ma, Z.; Wang, W.; Wang, C.; Yue, L.; Sun, H.; Shao, Q.; Murugadoss, V.; Guo, Z. Long-term Antibacterial Stable Reduced Graphene Oxide Nanocomposites Loaded with Cuprous Oxide Nanoparticles. *J. Colloid Interface Sci*. **2019**, *533*, 13–23. doi:10.1016/j.jcis.2018.08.053.
30. Ren, F.; Guo, Z.; Shi, Y.; Jia, L.; Qing, Y.; Ren, P.; Yan, D. Lightweight and Highly Efficient Electromagnetic Wave-absorbing of 3D CNTs/GNS@$CoFe_2O_4$ Ternary Composite Aerogels. *J. Alloys Compd*. **2018**, *768*, 6–14. doi:10.1016/j.jallcom.2018.07.209.
31. Wu, H.-Y.; Zhang, Y.-P.; Jia, L.-C.; Yan, D.-X.; Gao, J.-F.; Li, Z.-M. Injection Molded Segregated Carbon Nanotube/Polypropylene Composite for Efficient Electromagnetic Interference Shielding. *Ind. Eng. Chem. Res*. **2018**, *57*, 12378–12385. doi:10.1021/acs.iecr.8b02293.
32. Jia, L.-C.; Yan, D.-X.; Jiang, X.; Pang, H.; Gao, J.-F.; Ren, P.-G.; Li, Z.-M. Synergistic Effect of Graphite and Carbon Nanotubes on Improved Electromagnetic Interference Shielding Performance in Segregated Composites. *Ind. Eng. Chem. Res*. **2018**, *57*, 11929–11938. doi:10.1021/acs.iecr.8b03238.

33. Li, M.-Z.; Jia, L.-C.; Zhang, X.-P.; Yan, D.-X.; Zhang, Q.-C.; Li, Z.-M. Robust Carbon Nanotube Foam for Efficient Electromagnetic Interference Shielding and Microwave Absorption. *J. Colloid Interface Sci.* **2018**, *530*, 113–119. doi:10.1016/j.jcis.2018.06.052.
34. Yu, H.; Wang, T.; Wen, B.; Lu, M.; Xu, Z.; Zhu, C.; Chen, Y.; Xue, X.; Sun, C.; Cao, M. Graphene/polyaniline Nanorod Arrays: Synthesis and Excellent Electromagnetic Absorption Properties. *J. Mater. Chem.* **2012**, *22*, 21679–21685. doi:10.1039/c2jm34273a.
35. Bera, R.; Maitra, A.; Paria, S.; Karan, S. K.; Das, A. K.; Bera, A.; Si, S. K.; Halder, L.; De, A.; Khatua, B. B. An Approach to Widen the Electromagnetic Shielding Efficiency in PDMS/ferrous Ferric Oxide Decorated RGO-SWCNH Composite through Pressure Induced Tunability. *Chem. Eng. J.* **2018**, *335*, 501–509. doi:10.1016/j.cej.2017.10.178.
36. Song, W.-L.; Cao, M.-S.; Lu, M.-M.; Bi, S.; Wang, C.-Y.; Liu, J.; Yuan, J.; Fan, L.-Z. Flexible Graphene/polymer Composite Films in Sandwich Structures for Effective Electromagnetic Interference Shielding. *Carbon* **2014**, *66*, 67–76. doi:10.1016/j.carbon.2013.08.043.
37. Chen, Y.-H.; Huang, C.-Y.; Roan, M.-L.; Lai, F.-D.; Chen, K.-N.; Yeh, J.-T. The Copper Sulfide Coating on Polyacrylonitrile with a Chelating Agent of Ethylenediaminetetraacetic Acid by an Electroless Deposition Method and Its EMI Shielding Effectiveness. *J. Appl. Polym. Sci.* **2010**, *115*, 570–578. doi:10.1002/app.31009.
38. Onar, N.; Aks¸It, A. C.; Ebeoglugil, M. F.; Birlik, I.; Celik, E.;.; Ozdemir, I. Structural, Electrical, and Electromagnetic Properties of Cotton Fabrics Coated with Polyaniline and Polypyrrole. *J. Appl. Polym. Sci.* **2009**, *114*, 2003–2010. doi:10.1002/app.30652.
39. Wang, C.; Zhao, M.; Li, J.; Yu, J.; Sun, S.; Ge, S.; Guo, X.; Xie, F.; Jiang, B.; Wujcik, E. K.; et al. Silver Nanoparticles/Graphene Oxide Decorated Carbon Fiber Synergistic Reinforcement in Epoxy-Based Composites. *Polym.* **2017**, *131*, 263–271. doi:10.1016/j.polymer.2017.10.049.
40. Kuang, T.; Chang, L.; Chen, F.; Sheng, Y.; Fu, D.; Peng, X. Facile Preparation of Lightweight High-strength Biodegradable Polymer/multi-walled Carbon Nanotubes Nanocomposite Foams for Electromagnetic Interference Shielding. *Carbon* **2016**, *105*, 305–313. doi:10.1016/j.carbon.2016.04.052.
41. Nam, Y.-W.; Sathish Kumar, S. K.; Ankem, V. A.; Kim, C.-G. Multi-functional Aramid/Epoxy Composite for Stealth Space Hypervelocity Impact Shielding System. *Compos. Struct.* **2018**, *193*, 113–120. doi:10.1016/j.compstruct.2018.03.046.
42. Gyergyek, S.; Pahovnik, D.; Žagar, E.; Mertelj, A.; Kostanjšek, R.; Beković, M.; Jagodič, M.; Hofmann, H.; Makovec, D. Nanocomposites Comprised of Homogeneously Dispersed Magnetic Iron-oxide Nanoparticles and Poly(methyl Methacrylate). *Beilstein J. Nanotechnol.* **2018**, *9*, 1613–1622. doi:10.3762/bjnano.9.153.
43. Li, Y.; Jing, T.; Xu, G.; Tian, J.; Dong, M.; Shao, Q.; Wang, B.; Wang, Z.; Zheng, Y.; Yang, C.; Guo, Z. 3-D Magnetic Graphene Oxide-Magnetite Poly(vinyl Alcohol) Nanocomposite Substrates for Immobilizing Enzyme. *Polym* **2018**, *149*, 13–22. doi:10.1016/j.polymer.2018.06.046.
44. Sun, Y.; Luo, S.; Sun, H.; Zeng, W.; Ling, C.; Chen, D.; Chan, V.; Liao, K. Engineering Closed-Cell Structure in Lightweight and Flexible Carbon Foam Composite for High-Efficient Electromagnetic Interference Shielding. *Carbon* **2018**, *136*, 299–308. doi:10.1016/j.carbon.2018.04.084.
45. Muzaffar, A.; Ahamed, M. B.; Deshmukh, K.; Faisal, M.; Pasha, S. K. K. Enhanced Electromagnetic Absorption in NiO and BaTiO3 Based Polyvinylidenefluoride Nanocomposites. *Mater. Lett.* **2018**, *218*, 217–220. doi:10.1016/j.matlet.2018.02.029.
46. Jana, P. B.; Mallick, A. K.; De, S. K. Effects of Sample Thickness and Fiber Aspect Ratio on EMI Shielding Effectiveness of Carbon Fiber Filled Polychloroprene Composites in the X-band Frequency Range. *IEEE Trans. Electromagn. Compat.* **1992**, *34*, 478–481. doi:10.1109/15.179281.
47. Lv, L.; Liu, J.; Liu, H.; Liu, C.; Lu, Y.; Sun, K.; Fan, R.; Wang, N.; Lu, N.; Guo, Z.; Wujcik, E. K. An Overview of Electrically Conductive Polymer Nanocomposites toward Electromagnetic Interference Shielding. *Eng. Sci.* **2018**, *2*, 26–42. doi:10.30919/es8d615.

48. Geetha, S.; Satheesh Kumar, K. K.; Rao Chepuri, R. K.; Vijayan, M.; Trivedi, D. C. EMI Shielding: Methods and Materials-A Review. *J. Appl. Polym. Sci.* **2009**, *112*, 2073–2086. doi:10.1002/app.29812.
49. Biswas, S.; Panja, S. S.; Bose, S. Tailored Distribution of Nanoparticles in bi-phasic Polymeric Blends as Emerging Materials for Suppressing Electromagnetic Radiation: Challenges and Prospects. *J. Mater. Chem. C.* **2018**, *6*, 3120–3142. doi:10.1039/C8TC00002F.
50. Qin, F.; Brosseau, C. A Review and Analysis of Microwave Absorption in Polymer Composites Filled with Carbonaceous Particles. *J. Appl. Phys.* **2012**, *111*, 061301.
51. Ohlan, A.; Singh, K.; Chandra, A.; Dhawan, S. K. Microwave Absorption Behavior of Core − Shell Structured Poly (3,4-Ethylenedioxy Thiophene)−Barium Ferrite Nanocomposites. *ACS Appl. Mater. Interfaces* **2010**, *2*, 927–933. doi:10.1021/am900893d.
52. Parveen, S.; Manju, A. "Microwave Absorption and EMI Shielding Behavior of Nanocomposites Based on Intrinsically Conducting Polymers, Graphene and Carbon Nanotubes", In New Polymers for Special Applications, 1st edition; Gomes, A. D. S., (Ed.); Ivona Lovric: Croatia, **2012**; pp 71–112.
53. Chiang, W.-Y.; Chiang, Y.-S. Effect of Titanate Coupling Agent on Electromagnetic Interference Shielding Effectiveness and Mechanical Properties of PC–ABS–NCF Composite. *J. Appl. Polym. Sci.* **1992**, *46*, 673–681. doi:10.1002/app.1992.070460414.
54. Abdi, M. M.; Kassim, A. B.; Ekramul Mahmud, H. N. M.; Yunus, W. M. M.; Talib, Z. A. Electromagnetic Interference Shielding Effectiveness of New Conducting Polymer Composite. *J. Macromol. Sci., Part A* **2009**, *47*, 71–75. doi:10.1080/10601320903399834.
55. Rathi, V.; Panwar, V. Electromagnetic Interference Shielding Analysis of Conducting Composites in near- and Far-Field Region. *IEEE Trans. Electromagn. Compat.* **2018**, *60*, 1–7.
56. Cheng, C.; Fan, R.; Wang, Z.; Shao, Q.; Guo, X.; Xie, P.; Yin, Y.; Zhang, Y.; An, L.; Lei, Y.; et al. Tunable and Weakly Negative Permittivity in Carbon/silicon Nitride Composites with Different Carbonizing Temperatures. *Carbon* **2017**, *125*, 103–112. doi:10.1016/j.carbon.2017.09.037.
57. Wang, Z.; Wei, R.; Gu, J.; Liu, H.; Liu, C.; Luo, C.; Kong, J.; Shao, Q.; Wang, N.; Guo, Z.; Liu, X. Ultralight, Highly Compressible and Fire-Retardant Graphene Aerogel with Self-adjustable Electromagnetic Wave Absorption. *Carbon* **2018**, *139*, 1126–1135. doi:10.1016/j.carbon.2018.08.014.
58. Zhu, J.; Gu, H.; Luo, Z.; Haldolaarachige, N.; Young, D. P.; Wei, S.; Guo, Z. Carbon Nanostructure-Derived Polyaniline Metacomposites: Electrical, Dielectric, and Giant Magnetoresistive Properties. *Langmuir* **2012**, *28*, 10246–10255. doi:10.1021/la302031f.
59. Sun, K.; Xie, P.; Wang, Z.; Su, T.; Shao, Q.; Ryu, J.; Zhang, X.; Guo, J.; Shankar, A.; Li, J.; et al. Flexible Polydimethylsiloxane/multi-walled Carbon Nanotubes Membranous Metacomposites with Negative Permittivity. *Polym* **2017**, *125*, 50–57. doi:10.1016/j.polymer.2017.07.083.
60. Soloman, M. A.; Kurian, P.; Anantharaman, M. R.; Joy, P. A. Effect of Carbon Black on the Mechanical and Dielectric Properties of Rubber Ferrite Composites Containing Barium Ferrite. *J. Appl. Polym. Sci.* **2003**, *89*, 769–778. doi:10.1002/app.12266.
61. Koops, C. G. On the Dispersion of Resistivity and Dielectric Constant of Some Semiconductors at Audiofrequencies. *Phys. Rev.* **1951**, *83*, 121–124. doi:10.1103/PhysRev.83.121.
62. Luo, J.; Shen, P.; Yao, W.; Jiang, C.; Xu, J. Synthesis, Characterization, and Microwave Absorption Properties of Reduced Graphene Oxide/Strontium Ferrite/Polyaniline Nanocomposites. *Nanoscale Res. Lett.* **2016**, *11*, 141.
63. González, M.; Pozuelo, J.; Baselga, J. Electromagnetic Shielding Materials in GHz Range. *Chem. Rec.* **2018**, *18*, 1000–1009.
64. Wu, T.; Liu, Y.; Zeng, X.; Cui, T.; Zhao, Y.; Li, Y.; Tong, G. Facile Hydrothermal Synthesis of Fe3O4/C Core-Shell Nanorings for Efficient Low-Frequency Microwave Absorption. *ACS Appl. Mater. Interfaces* **2016**, *8*, 7370–7380. doi:10.1021/acsami.6b00264.

65. Philippe, T.; Guillaume, V.; Olivier, A.; Francoise, F.-V.; Fernand, F. Monodisperse Ferromagnetic Particles for Microwave Applications. *Adv. Mater.* **1998**, *10*, 1032–1035.
66. Arias, R.; Chu, P.; Mills, D. L. Dipole Exchange Spin Waves and Microwave Response of Ferromagnetic Spheres. *Phys. Rev. B.* **2005**, *71*, 224410.
67. Kittel, C. On the Theory of Ferromagnetic Resonance Absorption. *Phys. Rev.* **1948**, *73*, 155–161. doi:10.1103/PhysRev.73.155.
68. Yang, L.; Yichun, Z.; Cheng, Z.; Benyuan, H.; Yulong, L.; Wenchuan, L.; Xu, W.; Xiangyang, L. Low Temperature Preparation of Highly Fluorinated Multiwalled Carbon Nanotubes Activated by Fe_3 O_4 to Enhance Microwave Absorbing Property. *Nanotechnology* **2018**, *29*, 365703.
69. Seng, L. Y.; Wee, F. H.; Rahim, H. A.; Malek, F.; You, K. Y.; Liyana, Z.; Jamlos, M. A.; Ezanuddin, A. A. M. EMI Shielding Based on MWCNTs/polyester Composites. *Appl. Phys. A.* **2018**, *124*, 140.
70. Ohlan, A.; Singh, K.; Chandra, A.; Dhawan, S. K. Microwave Absorption Properties of Conducting Polymer Composite with Barium Ferrite Nanoparticles in 12.4–18GHz. *Appl. Phys. Lett.* **2008**, *93*, 053114. doi:10.1063/1.2969400.
71. Chen, M.; Zhang, L.; Duan, S.; Jing, S.; Jiang, H.; Luo, M.; Li, C. Highly Conductive and Flexible Polymer Composites with Improved Mechanical and Electromagnetic Interference Shielding Performances. *Nanoscale* **2014**, *6*, 3796–3803. doi:10.1039/C3NR06092F.
72. Zhang, K.; Yu, H.-O.; Yu, K.-X.; Gao, Y.; Wang, M.; Li, J.; Guo, S. A Facile Approach to Constructing Efficiently Segregated Conductive Networks in Poly(lactic Acid)/Silver Nanocomposites via Silver Plating on Microfibers for Electromagnetic Interference Shielding. *Compos. Sci. Technol.* **2018**, *156*, 136–143. doi:10.1016/j.compscitech.2017.12.037.
73. Menon, A. V.; Madras, G.; Bose, S. Magnetic Alloy-MWNT Heterostructure as Efficient Electromagnetic Wave Suppressors in Soft Nanocomposites. *Chemistry Select* **2017**, *2*, 7831–7844. doi:10.1002/slct.201700986.
74. Liu, Z.; Bai, G.; Huang, Y.; Ma, Y.; Du, F.; Li, F.; Guo, T.; Chen, Y. Reflection and Absorption Contributions to the Electromagnetic Interference Shielding of Single-walled Carbon Nanotube/polyurethane Composites. *Carbon* **2007**, *45*, 821–827. doi:10.1016/j.carbon.2006.11.020.
75. Liu, Z.; Bai, G.; Huang, Y.; Li, F.; Ma, Y.; Guo, T.; He, X.; Lin, X.; Gao, H.; Chen, Y. Microwave Absorption of Single-Walled Carbon Nanotubes/Soluble Cross-Linked Polyurethane Composites. *J. Phys. Chem. C.* **2007**, *111*, 13696–13700. doi:10.1021/jp0731396.
76. Ramoa Sílvia, D. A. S.; Barra Guilherme, M. O.; Merlini, C.; Livi, S.; Soares Bluma, G.; Pegoretti, A. Electromagnetic Interference Shielding Effectiveness and Microwave Absorption Properties of Thermoplastic Polyurethane/Montmorillonite-polypyrrole Nanocomposites. *Polym. Adv. Technol.* **2018**, *29*, 1377–1384. doi:10.1002/pat.4249.
77. Kalkan Erdoğan, M.; Karakışla, M.; Saçak, M. Polypyrrole and Silver Particles Coated Poly(ethylene Terephthalate) Nonwoven Composite for Electromagnetic Interference Shielding. *J. Compos. Mater.* **2018**, *52*, 1353–1362. doi:10.1177/0021998317724859.
78. Gupta, A.; Choudhary, V. Electromagnetic Interference Shielding Behavior of Poly(trimethylene Terephthalate)/Multi-walled Carbon Nanotube Composites. *Compos. Sci. Technol.* **2011**, *71*, 1563–1568. doi:10.1016/j.compscitech.2011.06.014.
79. Anand, J.; Palaniappan, S.; Sathyanarayana, D. N. Conducting Polyaniline Blends and Composites. *Progr. Polym. Sci.* **1998**, *23*, 993–1018. doi:10.1016/S0079-6700(97)00040-3.
80. Huang, J.; Cao, Y.; Shao, Q.; Peng, X.; Guo, Z. Magnetic Nanocarbon Adsorbents with Enhanced Hexavalent Chromium Removal: Morphology Dependence of Fibrillar vs Particulate Structures. *Ind. Eng. Chem. Res.* **2017**, *56*, 10689–10701. doi:10.1021/acs.iecr.7b02835.
81. Bhardwaj, P.; Kaushik, S.; Gairola, P.; Gairola, S. P. Exceptional Electromagnetic Radiation Shielding Performance and Dielectric Properties of Surfactant Assisted Polypyrrole-carbon

Allotropes Composites. *Radiat. Phys. Chem.* **2018**, *151*, 156–163. doi:10.1016/j.radphyschem.2018.06.001.
82. Sastry, D. N.; Revanasiddappa, M.; Suresh, T.; Kiran, Y. T. R.; Raghavendra, S. C. Electromagnetic Shielding Effectiveness Studies on Polyaniline/CSA-WO3 Composites at KU Band Frequencies. *AIP Conf. Proc.* **2018**, *1953*, 090067.
83. Wan, Y.; Li, J.; Yang, Z.; Ao, H.; Xiong, L.; Luo, H. Simultaneously Depositing Polyaniline onto Bacterial Cellulose Nanofibers and Graphene Nanosheets toward Electrically Conductive Nanocomposites. *Curr. Appl. Phys.* **2018**, *18*, 933–940. doi:10.1016/j.cap.2018.05.008.
84. Wang, H.; Zhu, E.; Yang, J.; Zhou, P.; Sun, D.; Tang, W. Bacterial Cellulose Nanofiber-Supported Polyaniline Nanocomposites with Flake-Shaped Morphology as Supercapacitor Electrodes. *J. Phys. Chem. C.* **2012**, *116*, 13013–13019. doi:10.1021/jp301099r.
85. Bláha, M.; Varga, M.; Prokeš, J.; Zhigunov, A.; Vohlídal, J. Effects of the Polymerization Temperature on the Structure, Morphology and Conductivity of Polyaniline Prepared with Ammonium Peroxodisulfate. *Eur. Polym. J.* **2013**, *49*, 3904–3911. doi:10.1016/j.eurpolymj.2013.08.018.
86. Zhang, Z.; Wei, Z.; Zhang, L.; Wan, M. Polyaniline Nanotubes and Their Dendrites Doped with Different Naphthalene Sulfonic Acids. *Acta Mater.* **2005**, *53*, 1373–1379. doi:10.1016/j.actamat.2004.11.030.
87. Qiu, M.; Zhang, Y.; Wen, B. Facile Synthesis of Polyaniline Nanostructures with Effective Electromagnetic Interference Shielding Performance. *J. Mater. Sci: Mater. Electron.* **2018**, *29*, 10437–10444. doi:10.1007/s10854-018-9100-6.
88. He, W.; Li, J.; Tian, J.; Jing, H.; Li, Y. Characteristics and Properties of Wood/Polyaniline Electromagnetic Shielding Composites Synthesized via in Situ Polymerization. *Polym. Compos.* **2018**, *39*, 537–543. doi:10.1002/pc.23966.
89. Tantawy, H. R.; Aston, D. E.; Smith, J. R.; Young, J. L. Comparison of Electromagnetic Shielding with Polyaniline Nanopowders Produced in Solvent-Limited Conditions. *ACS Appl. Mater. Interfaces* **2013**, *5*, 4648–4658. doi:10.1021/am401695p.
90. Gahlout, P.; Choudhary, V. Tailoring of Polypyrrole Backbone by Optimizing Synthesis Parameters for Efficient EMI Shielding Properties in X-band (8.2–12.4GHz). *Synth. Met.* **2016**, *222*, 170–179. doi:10.1016/j.synthmet.2016.10.016.
91. Kaur, A.; Ishpal.; Dhawan, S. K. Tuning of EMI Shielding Properties of Polypyrrole Nanoparticles with Surfactant Concentration. *Synth. Met.* **2012**, *162*, 1471–1477.
92. Ebrahimi, I.; Gashti, M. P. Polypyrrole-MWCNT-Ag Composites for Electromagnetic Shielding: Comparison between Chemical Deposition and UV-reduction Approaches. *J. Phys. Chem. Solids* **2018**, *118*, 80–87.
93. Yu, D.; Wang, Y.; Hao, T.; Wang, W.; Liu, B. Preparation of Silver-plated Polyimide Fabric Initiated by Polyaniline with Electromagnetic Shielding Properties. *J. Ind. Text* **2018**, *47*, 1392–1406. doi:10.1177/1528083717692592.
94. Chen, J.-J.; Liu, S.-L.; Wu, H.-B.; Sowade, E.; Baumann, R. R.; Wang, Y.; Gu, F.-Q.; Liu, C.-R.-L.; Feng, Z.-S. Structural Regulation of Silver Nanowires and Their Application in Flexible Electronic Thin Films. *Mater. Design* **2018**, *154*, 266–274. doi:10.1016/j.matdes.2018.05.018.
95. Faisal, M.; Khasim, S. Polyaniline-Antimony Oxide Composites for Effective Broadband EMI Shielding. *Iran. Polym. J.* **2013**, *22*, 473–480. doi:10.1007/s13726-013-0149-z.
96. Faisal, M.; Khasim, S. Broadband Electromagnetic Shielding and Dielectric Properties of Polyaniline-stannous Oxide Composites. *J. Mater. Sci: Mater. Electron.* **2013**, *24*, 2202–2210. doi:10.1007/s10854-013-1080-y.
97. Faisal, M.; Khasim, S. Electrical Conductivity, Dielectric Behavior and EMI Shielding Effectiveness of Polyaniline-Yttrium Oxide Composites. *Bull. Korean Chem. Soc.* **2013**, *34*, 99–106. doi:10.5012/bkcs.2013.34.1.99.
98. Saini, P.; Arora, M.; Gupta, G.; Gupta, B. K.; Singh, V. N.; Choudhary, V. High Permittivity Polyaniline–Barium Titanate Nanocomposites with Excellent Electromagnetic Interference Shielding Response. *Nanoscale* **2013**, *5*, 4330–4336. doi:10.1039/c3nr00634d.

99. Koh, Y.-N.; Mokhtar, N.; Phang, S.-W. Effect of Microwave Absorption Study on Polyaniline Nanocomposites with Untreated and Treated Double Wall Carbon Nanotubes. *Polym. Compos*. **2018**, *39*, 1283–1291. doi:10.1002/pc.24064.
100. Saini, P.; Choudhary, V.; Singh, B. P.; Mathur, R. B.; Dhawan, S. K. Polyaniline-MWCNT Nanocomposites for Microwave Absorption and EMI Shielding. *Mater. Chem. Phys*. **2009**, *113*, 919–926. doi:10.1016/j.matchemphys.2008.08.065.
101. Saini, M.; Singh, S. K.; Shukla, R.; Kumar, A. Mg Doped Copper Ferrite with Polyaniline Matrix Core–Shell Ternary Nanocomposite for Electromagnetic Interference Shielding. *J. Inorg. Organomet. Polym. Mater*. **2018**, *28*, 2306–2315.
102. Gu, H.; Zhang, H.; Lin, J.; Shao, Q.; Young, D. P.; Sun, L.; Shen, T. D.; Guo, Z. Large Negative Giant Magnetoresistance at Room Temperature and Electrical Transport in Cobalt Ferrite-polyaniline Nanocomposites. *Polym* **2018**, *143*, 324–330. doi:10.1016/j.polymer.2018.04.008.
103. Belaabed, B.; Wojkiewicz, J. L.; Lamouri, S.; El Kamchi, N.; Lasri, T. Synthesis and Characterization of Hybrid Conducting Composites Based on Polyaniline/magnetite Fillers with Improved Microwave Absorption Properties. *J. Alloys Compd*. **2012**, *527*, 137–144. doi:10.1016/j.jallcom.2012.02.179.
104. Choudhary Harish, K.; Kumar, R.; Pawar Shital, P.; Anupama, A. V.; Bose, S.; Sahoo, B. Effect of Coral-Shaped Yttrium Iron Garnet Particles on the EMI Shielding Behaviour of Yttrium Iron Garnet-Polyaniline-Wax Composites. *ChemistrySelect* **2018**, *3*, 2120–2130. doi:10.1002/slct.201702698.
105. Gandhi, N.; Singh, K.; Ohlan, A.; Singh, D. P.; Dhawan, S. K. Thermal, Dielectric and Microwave Absorption Properties of Polyaniline–$CoFe_2O_4$ Nanocomposites. *Compos. Sci. Technol*. **2011**, *71*, 1754–1760. doi:10.1016/j.compscitech.2011.08.010.
106. Zhang, B.; Du, Y.; Zhang, P.; Zhao, H.; Kang, L.; Han, X.; Xu, P. Microwave Absorption Enhancement of Fe3O4/polyaniline Core/shell Hybrid Microspheres with Controlled Shell Thickness. *J. Appl. Polym. Sci*. **2013**, *130*, 1909–1916. doi:10.1002/app.39332.
107. Wu, K. H.; Ting, T. H.; Wang, G. P.; Ho, W. D.; Shih, C. C. Effect of Carbon Black Content on Electrical and Microwave Absorbing Properties of Polyaniline/carbon Black Nanocomposites. *Polym. Degrad. Stab*. **2008**, *93*, 483–488. doi:10.1016/j.polymdegradstab.2007.11.009.
108. Gopakumar, D. A.; Pai, A. R.; Pottathara, Y. B.; Pasquini, D.; Carlos de Morais, L. s.; Luke, M.; Kalarikkal, N.; Grohens, Y.; Thomas, S. Cellulose Nanofiber-Based Polyaniline Flexible Papers as Sustainable Microwave Absorbers in the X-Band. *ACS Appl. Mater. Interfaces* **2018**, *10*, 20032–20043. doi:10.1021/acsami.8b04549.
109. Olad, A.; Shakoori, S. Electromagnetic Interference Attenuation and Shielding Effect of Quaternary Epoxy-PPy/Fe_3O_4-ZnO Nanocomposite as a Broad Band Microwave-Absorber. *J. Magn. Magn. Mater*. **2018**, *458*, 335–345. doi:10.1016/j.jmmm.2018.03.050.
110. Zhang, W.; Zhang, X.; Qiao, Y.; Yan, H.; Qi, S. Covalently Bonded GNPs-NH-PANI Nanorod Arrays Modified by Fe3O4 Nanoparticles as High-performance Electromagnetic Wave Absorption Materials. *Mater. Lett*. **2018**, *216*, 101–105. doi:10.1016/j.matlet.2018.01.008.
111. Liu, P.; Huang, Y.; Zhang, X. Superparamagnetic Fe3O4 Nanoparticles on Graphene-Polyaniline: Synthesis, Characterization and Their Excellent Electromagnetic Absorption Properties. *J. Alloys Compd*. **2014**, *596*, 25–31. doi:10.1016/j.jallcom.2014.01.188.
112. Wang, Y.; Wu, X.; Zhang, W.; Huang, S. Facile Synthesis of Ni/PANI/RGO Composites and Their Excellent Electromagnetic Wave Absorption Properties. *Synth. Met*. **2015**, *210*, 165–170. doi:10.1016/j.synthmet.2015.09.022.
113. Liu, P.; Huang, Y.; Wang, L.; Zhang, W. Preparation and Excellent Microwave Absorption Property of Three Component Nanocomposites: Polyaniline-reduced Graphene oxide-Co3O4 Nanoparticles. *Synth. Met*. **2013**, *177*, 89–93. doi:10.1016/j.synthmet.2013.06.009.
114. Liu, P.; Huang, Y.; Wang, L.; Zhang, W. Synthesis and Excellent Electromagnetic Absorption Properties of Polypyrrole-Reduced Graphene oxide-Co3O4 Nanocomposites. *J. Alloys Compd*. **2013**, *573*, 151–156. doi:10.1016/j.jallcom.2013.03.280.

115. Wang, Y.; Huang, Y.; Ding, J. Synthesis and Enhanced Electromagnetic Absorption Properties of polypyrrole-$BaFe_{12}O_{19}/Ni_{0.8}Zn_{0.2}Fe_2O_4$ on Graphene Nanosheet. *Synth. Met.* **2014**, *196*, 125–130. doi:10.1016/j.synthmet.2014.07.027.
116. Ding, X.; Huang, Y.; Wang, J.; Wu, H.; Liu, P. Excellent Electromagnetic Wave Absorption Property of Quaternary Composites Consisting of Reduced Graphene Oxide, polyaniline and $FeNi_3@SiO_2$ Nanoparticles. *Appl. Surf. Sci.* **2015**, *357*, 908–914. doi:10.1016/j.apsusc.2015.09.103.
117. Wang, Y.; Zhang, W.; Luo, C.; Wu, X.; Yan, G. Superparamagnetic $FeCo@SnO_2$ Nanoparticles on Graphene-polyaniline: Synthesis and Enhanced Electromagnetic Wave Absorption Properties. *Ceram. Int.* **2016**, *42*, 12496–12502. doi:10.1016/j.ceramint.2016.05.038.
118. Zhang, K.; Gao, X.; Zhang, Q.; Li, T.; Chen, H.; Chen, X. Preparation and Microwave Absorption Properties of Asphalt Carbon Coated Reduced Graphene Oxide/magnetic $CoFe_2O_4$ Hollow Particles Modified Multi-wall Carbon Nanotube Composites. *J. Alloys Compd.* **2017**, *723*, 912–921. doi:10.1016/j.jallcom.2017.06.327.
119. Wang, L.; Huang, Y.; Li, C.; Chen, J.; Sun, X. Hierarchical Composites of Polyaniline Nanorod Arrays Covalently-grafted on the Surfaces of $Graphene@Fe_3O_4@C$ with High Microwave Absorption Performance. *Compos. Sci. Technol.* **2015**, *108*, 1–8. doi:10.1016/j.compscitech.2014.12.011.
120. Wang, L.; Huang, Y.; Huang, H. N-doped Graphene@polyaniline Nanorod Arrays Hierarchical Structures: Synthesis and Enhanced Electromagnetic Absorption Properties. *Mater. Lett.* **2014**, *124*, 89–92. doi:10.1016/j.matlet.2014.03.066.
121. Liu, P.; Huang, Y.; Yang, Y.; Yan, J.; Zhang, X. Sandwich Structures of $Graphene@Fe_3O_4@PANI$ Decorated with TiO_2 Nanosheets for Enhanced Electromagnetic Wave Absorption Properties. *J. Alloys Compd.* **2016**, *662*, 63–68. doi:10.1016/j.jallcom.2015.12.022.
122. Wang, Y.; Wu, X.; Zhang, W.; Luo, C.; Li, J. Synthesis of Ferromagnetic Sandwich FeCo@graphene@PPy and Enhanced Electromagnetic Wave Absorption Properties. *J. Magn. Magn. Mater.* **2017**, *443*, 358–365. doi:10.1016/j.jmmm.2017.07.063.
123. Weng, X.; Li, B.; Zhang, Y.; Lv, X.; Gu, G. Synthesis of Flake Shaped Carbonyl Iron/reduced Graphene Oxide/polyvinyl Pyrrolidone Ternary Nanocomposites and Their Microwave Absorbing Properties. *J. Alloys Compd.* **2017**, *695*, 508–519. doi:10.1016/j.jallcom.2016.11.083.
124. Liu, P.; Huang, Y.; Zhang, X. Preparation and Excellent Microwave Absorption Properties of Ferromagnetic Graphene/poly(3, 4-ethylenedioxythiophene)/$CoFe_2O_4$ Nanocomposites. *Powder Technol.* **2015**, *276*, 112–117. doi:10.1016/j.powtec.2014.08.045.
125. Wu, F.; Xie, A.; Sun, M.; Wang, Y.; Wang, M. Reduced Graphene Oxide (RGO) modified Spongelike Polypyrrole (PPy) aerogel for Excellent Electromagnetic Absorption. *J. Mater. Chem. A.* **2015**, *3*, 14358–14369. doi:10.1039/C5TA01577D.
126. Yang, R.-B.; Reddy, P. M.; Chang, C.-J.; Chen, P.-A.; Chen, J.-K.; Chang, C.-C. Synthesis and Characterization of Fe_3O_4/polypyrrole/carbon Nanotube Composites with Tunable Microwave Absorption Properties: Role of Carbon Nanotube and Polypyrrole Content. *Chem. Eng. J.* **2016**, *285*, 497–507. doi:10.1016/j.cej.2015.10.031.
127. Luo, J.; Xu, Y.; Yao, W.; Jiang, C.; Xu, J. Synthesis and Microwave Absorption Properties of Reduced Graphene Oxide-magnetic Porous Nanospheres-polyaniline Composites. *Compos. Sci. Technol.* **2015**, *117*, 315–321. doi:10.1016/j.compscitech.2015.07.008.
128. Liu, P.; Huang, Y.; Zhang, X. Cubic $NiFe_2O_4$ Particles on Graphene-polyaniline and Their Enhanced Microwave Absorption Properties. *Compos. Sci. Technol.* **2015**, *107*, 54–60. doi:10.1016/j.compscitech.2014.11.021.
129. Liu, P.; Huang, Y.; Zhang, X. Synthesis, characterization and Excellent Electromagnetic Wave Absorption Properties of $Graphene@CoFe_2O_4@$polyaniline Nanocomposites. *Synth. Met.* **2015**, *201*, 76–81. doi:10.1016/j.synthmet.2015.01.022.

130. Sun, J.; Shen, Y.; Hu, X.-S. Polyaniline/flower-like CuS Composites with Improved Electromagnetic Interference Shielding Effectiveness. *Polym. Bull.* **2018**, *75*, 653–667. doi:10.1007/s00289-017-2060-9.
131. Liu, P.; Huang, Y. Decoration of Reduced Graphene Oxide with Polyaniline Film and Their Enhanced Microwave Absorption Properties. *J. Polym. Res.* **2014**, *21*, 430.
132. Zhang, P.; Han, X.; Kang, L.; Qiang, R.; Liu, W.; Du, Y. Synthesis and Characterization of Polyaniline Nanoparticles with Enhanced Microwave Absorption. *RSC Adv.* **2013**, *3*, 12694–12701. doi:10.1039/c3ra40973b.
133. Du, L.; Du, Y.; Li, Y.; Wang, J.; Wang, C.; Wang, X.; Xu, P.; Han, X. Surfactant-Assisted Solvothermal Synthesis of $Ba(CoTi)_xFe_{12-2x}O_{19}$ Nanoparticles and Enhancement in Microwave Absorption Properties of Polyaniline. *J. Phys. Chem. C.* **2010**, *114*, 19600–19606. doi:10.1021/jp1067268.
134. Wang, G.; Wang, L.; Mark, L. H.; Shaayegan, V.; Wang, G.; Li, H.; Zhao, G.; Park, C. B. Ultralow-Threshold and Lightweight Biodegradable Porous PLA/MWCNT with Segregated Conductive Networks for High-Performance Thermal Insulation and Electromagnetic Interference Shielding Applications. *ACS Appl. Mater. Interfaces*. **2018**, *10*, 1195–1203. doi:10.1021/acsami.7b14111.
135. Pawar, S. P.; Rzeczkowski, P.; Pötschke, P.; Krause, B.; Bose, S. Does the Processing Method Resulting in Different States of an Interconnected Network of Multiwalled Carbon Nanotubes in Polymeric Blend Nanocomposites Affect EMI Shielding Properties? *ACS Omega* **2018**, *3*, 5771–5782. doi:10.1021/acsomega.8b00575.
136. Wang, Y.; Cheng, X.-D.; Song, W.-L.; Ma, C.-J.; Bian, X.-M.; Chen, M. Hydro-sensitive Sandwich Structures for Self-tunable Smart Electromagnetic Shielding. *Chem. Eng. J.* **2018**, *344*, 342–352. doi:10.1016/j.cej.2018.03.097.
137. Wang, Z.; Wei, R.; Liu, X. Fluffy and Ordered Graphene Multilayer Films with Improved Electromagnetic Interference Shielding over X-Band. *ACS Appl. Mater. Interfaces*. **2017**, *9*, 22408–22419. doi:10.1021/acsami.7b04008.
138. Yuan, J.-K.; Yao, S.-H.; Sylvestre, A.; Bai, J. Biphasic Polymer Blends Containing Carbon Nanotubes: Heterogeneous Nanotube Distribution and Its Influence on the Dielectric Properties. *J. Phys. Chem. C.* **2012**, *116*, 2051–2058. doi:10.1021/jp210872w.
139. Chen, J.; Teng, Z.; Zhao, Y.; Liu, W. Electromagnetic Interference Shielding Properties of Wood–plastic Composites Filled with Graphene Decorated Carbon Fiber. *Polym. Compos.* **2018**, *39*, 2110–2116. doi:10.1002/pc.24173.
140. Nan, C.-W. Physics of Inhomogeneous Inorganic Materials. *Prog. Mater. Sci.* **1993**, *37*, 1–116. doi:10.1016/0079-6425(93)90004-5.
141. Kashi, S.; Hadigheh, S.; Varley, R. Microwave Attenuation of Graphene Modified Thermoplastic Poly(Butylene Adipate-co-terephthalate) Nanocomposites. *Polym.* **2018**, *10*, 582.
142. Zha, X.-J.; Li, T.; Bao, R.-Y.; Bai, L.; Liu, Z.-Y.; Yang, W.; Yang, M.-B. Constructing a Special 'sosatie' Structure to Finely Dispersing MWCNT for Enhanced Electrical Conductivity, ultra-high Dielectric Performance and Toughness of iPP/OBC/MWCNT Nanocomposites. *Compos. Sci. Technol.* **2017**, *139*, 17–25. doi:10.1016/j.compscitech.2016.12.011.
143. Nan, C.-W.; Shen, Y.; Ma, J. Physical Properties of Composites near Percolation. *Annu. Rev. Mater. Res.* **2010**, *40*, 131–151. doi:10.1146/annurev-matsci-070909-104529.
144. Wen, B.; Cao, M.-S.; Hou, Z.-L.; Song, W.-L.; Zhang, L.; Lu, M.-M.; Jin, H.-B.; Fang, X.-Y.; Wang, W.-Z.; Yuan, J. Temperature Dependent Microwave Attenuation Behavior for Carbon-Nanotube/Silica Composites. *Carbon* **2013**, *65*, 124–139. doi:10.1016/j.carbon.2013.07.110.
145. Cao, M.-S.; Song, W.-L.; Hou, Z.-L.; Wen, B.; Yuan, J. The Effects of Temperature and Frequency on the Dielectric Properties, electromagnetic Interference Shielding and Microwave-absorption of Short Carbon Fiber/silica Composites. *Carbon* **2010**, *48*, 788–796. doi:10.1016/j.carbon.2009.10.028.

146. Ryvkina, N.; Tchmutin, I.; Vilčáková, J.; Pelíšková, M.; Sáha, P. The Deformation Behavior of Conductivity in Composites Where Charge Carrier Transport Is by Tunneling: theoretical Modeling and Experimental Results. *Synth. Met.* **2005**, *148*, 141–146. doi:10.1016/j.synthmet.2004.09.028.
147. Rahaman, M.; Chaki, T. K.; Khastgir, D. Development of High Performance EMI Shielding Material from EVA, NBR, and Their Blends: Effect of Carbon Black Structure. *J. Mater. Sci.* **2011**, *46*, 3989–3999. doi:10.1007/s10853-011-5326-x.
148. Yilmaz, A. C.; Ozen, M. S.; Sancak, E.; Erdem, R.; Erdem, O.; Soin, N. Analyses of the Mechanical, electrical and Electromagnetic Shielding Properties of Thermoplastic Composites Doped with Conductive Nanofillers. *J. Compos. Mater.* **2018**, *52*, 1423–1432. doi:10.1177/0021998317752503.
149. Chung, D. D. L. Materials for Electromagnetic Interference Shielding. *J. Mater. Eng. Perform* **2000**, *9*, 350–354. doi:10.1361/105994900770346042.
150. Arjmand, M.; Apperley, T.; Okoniewski, M.; Sundararaj, U. Comparative Study of Electromagnetic Interference Shielding Properties of Injection Molded versus Compression Molded Multi-walled Carbon Nanotube/polystyrene Composites. *Carbon* **2012**, *50*, 5126–5134. doi:10.1016/j.carbon.2012.06.053.
151. Dakin, T. W. Conduction and Polarization Mechanisms and Trends in Dielectric. *IEEE Electr. Insul. Mag.* **2006**, *22*, 11–28. doi:10.1109/MEI.2006.1705854.
152. Vas, J. V.; Thomas, M. J. Electromagnetic Shielding Effectiveness of Layered Polymer Nanocomposites. *IEEE Trans. Electromagn. Compat.* **2018**, *60*, 376–384. doi:10.1109/TEMC.2017.2719764.
153. Mondal, S.; Das, P.; Ganguly, S.; Ravindren, R.; Remanan, S.; Bhawal, P.; Das, T. K.; Das, N. C. Thermal-Air Ageing Treatment on Mechanical, Electrical, and Electromagnetic Interference Shielding Properties of Lightweight Carbon Nanotube Based Polymer Nanocomposites. *Compos. Part A.* **2018**, *107*, 447–460. doi:10.1016/j.compositesa.2018.01.025.
154. Sahoo, B. P.; Naskar, K.; Tripathy, D. K. Conductive Carbon Black-Filled Ethylene Acrylic Elastomer Vulcanizates: Physico-Mechanical, Thermal, and Electrical Properties. *J. Mater. Sci.* **2012**, *47*, 2421–2433. doi:10.1007/s10853-011-6065-8.
155. Mondal, S.; Ganguly, S.; Das, P.; Khastgir, D.; Das, N. C. Low Percolation Threshold and Electromagnetic Shielding Effectiveness of Nano-structured Carbon Based Ethylene Methyl Acrylate Nanocomposites. *Composites, Part B.* **2017**, *119*, 41–56. doi:10.1016/j.compositesb.2017.03.022.
156. Ameli, A.; Jung, P. U.; Park, C. B. Electrical Properties and Electromagnetic Interference Shielding Effectiveness of Polypropylene/carbon Fiber Composite Foams. *Carbon* **2013**, *60*, 379–391. doi:10.1016/j.carbon.2013.04.050.
157. Pawar, S. P.; Pattabhi, K.; Bose, S. Assessing the Critical Concentration of NH2 Terminal Groups on the Surface of MWNTs towards Chain Scission of PC in PC/SAN Blends: Effect on Dispersion, Electrical Conductivity and EMI Shielding. *RSC Adv.* **2014**, *4*, 18842–18852. doi:10.1039/c4ra01610f.
158. Pawar, S. P.; Marathe, D. A.; Pattabhi, K.; Bose, S. Electromagnetic Interference Shielding through MWNT Grafted Fe3O4 Nanoparticles in PC/SAN Blends. *J. Mater. Chem. A.* **2015**, *3*, 656–669. doi:10.1039/C4TA04559A.
159. Biswas, S.; Panja, S. S.; Bose, S. A Novel Fluorophore-Spacer-Receptor to Conjugate MWNTs and Ferrite Nanoparticles to Design an Ultra-Thin Shield to Screen Electromagnetic Radiation. *Mater. Chem. Front.* **2017**, *1*, 132–145. doi:10.1039/C6QM00074F.
160. Im, J. S.; Park, I. J.; In, S. J.; Kim, T.; Lee, Y.-S. Fluorination Effects of MWCNT Additives for EMI Shielding Efficiency by Developed Conductive Network in Epoxy Complex. *J. Fluorine Chem.* **2009**, *130*, 1111–1116. doi:10.1016/j.jfluchem.2009.06.022.
161. Hosseini, H.; Mahdavi, H. Nanocomposite Based on Epoxy and MWCNTs Modified with NiFe2O4 Nanoparticles as Efficient Microwave Absorbing Material. *Appl. Organometal. Chem.* **2018**, *32*, e4294. doi:10.1002/aoc.4294.
162. Kar, G. P.; Biswas, S.; Bose, S. Simultaneous Enhancement in Mechanical Strength, Electrical Conductivity, and Electromagnetic Shielding Properties in PVDF-ABS Blends

Containing PMMA Wrapped Multiwall Carbon Nanotubes. *Phys. Chem. Chem. Phys.* **2015**, *17*, 14856–14865. doi:10.1039/C5CP01452B.

163. Sourav, B.; Prasanna, K. G.; Suryasarathi, B. Simultaneous Improvement in Structural Properties and Microwave Shielding of Polymer Blends with Carbon Nanotubes. *Chem. Nano. Mat.* **2016**, *2*, 140–148.
164. Wu, Y.; Wang, Z.; Liu, X.; Shen, X.; Zheng, Q.; Xue, Q.; Kim, J.-K. Ultralight Graphene Foam/Conductive Polymer Composites for Exceptional Electromagnetic Interference Shielding. *ACS Appl. Mater. Interfaces* **2017**, *9*, 9059–9069. doi:10.1021/acsami.7b01017.
165. Zhang, X.; Wei, S.; Haldolaarachchige, N.; Colorado, H. A.; Luo, Z.; Young, D. P.; Guo, Z. Magnetoresistive Conductive Polyaniline–Barium Titanate Nanocomposites with Negative Permittivity. *J. Phys. Chem. C.* **2012**, *116*, 15731–15740. doi:10.1021/jp303226u.
166. Liang, J.; Wang, Y.; Huang, Y.; Ma, Y.; Liu, Z.; Cai, J.; Zhang, C.; Gao, H.; Chen, Y. Electromagnetic Interference Shielding of Graphene/Epoxy Composites. *Carbon* **2009**, *47*, 922–925. doi:10.1016/j.carbon.2008.12.038.
167. Zhang, H.-B.; Zheng, W.-G.; Yan, Q.; Jiang, Z.-G.; Yu, Z.-Z. The Effect of Surface Chemistry of Graphene on Rheological and Electrical Properties of Polymethylmethacrylate Composites. *Carbon* **2012**, *50*, 5117–5125. doi:10.1016/j.carbon.2012.06.052.
168. Li, C.; Yang, G.; Deng, H.; Wang, K.; Zhang, Q.; Chen, F.; Fu, Q. The Preparation and Properties of Polystyrene/Functionalized Graphene Nanocomposite Foams Using Supercritical Carbon Dioxide. *Polym. Int.* **2012**, *62*, 1077–1084.
169. Hsiao, S.-T.; Ma, C.-C. M.; Tien, H.-W.; Liao, W.-H.; Wang, Y.-S.; Li, S.-M.; Yang, C.-Y.; Lin, S.-C.; Yang, R.-B. Effect of Covalent Modification of Graphene Nanosheets on the Electrical Property and Electromagnetic Interference Shielding Performance of a Water-Borne Polyurethane Composite. *ACS Appl. Mater. Interfaces* **2015**, *7*, 2817–2826. doi:10.1021/am508069v.
170. Hsiao, S.-T.; Ma, C.-C. M.; Tien, H.-W.; Liao, W.-H.; Wang, Y.-S.; Li, S.-M.; Huang, Y.-C. Using a Non-covalent Modification to Prepare a High Electromagnetic Interference Shielding Performance Graphene Nanosheet/water-borne Polyurethane Composite. *Carbon* **2013**, *60*, 57–66. doi:10.1016/j.carbon.2013.03.056.
171. Hsiao, S.-T.; Ma, C.-C. M.; Liao, W.-H.; Wang, Y.-S.; Li, S.-M.; Huang, Y.-C.; Yang, R.-B.; Liang, W.-F. Lightweight and Flexible Reduced Graphene Oxide/Water-Borne Polyurethane Composites with High Electrical Conductivity and Excellent Electromagnetic Interference Shielding Performance. *ACS Appl. Mater. Interfaces* **2014**, *6*, 10667–10678. doi:10.1021/am502412q.
172. Poothanari, M. A.; Abraham, J.; Kalarikkal, N.; Thomas, S. Excellent Electromagnetic Interference Shielding and High Electrical Conductivity of Compatibilized Polycarbonate/Polypropylene Carbon Nanotube Blend Nanocomposites. *Ind. Eng. Chem. Res.* **2018**, *57*, 4287–4297. doi:10.1021/acs.iecr.7b05406.
173. Tian, K.; Su, Z.; Wang, H.; Tian, X.; Huang, W.; Xiao, C. N-doped Reduced Graphene Oxide/waterborne Polyurethane Composites Prepared by in Situ Chemical Reduction of Graphene Oxide. *Compos. Part A* **2017**, *94*, 41–49. doi:10.1016/j.compositesa.2016.11.020.
174. Geng, H.-Z.; Kim, K. K.; So, K. P.; Lee, Y. S.; Chang, Y.; Lee, Y. H. Effect of Acid Treatment on Carbon Nanotube-Based Flexible Transparent Conducting Films. *J. Am. Chem. Soc.* **2007**, *129*, 7758–7759. doi:10.1021/ja0722224.
175. Bhawal, P.; Ganguly, S.; Das, T. K.; Mondal, S.; Choudhury, S.; Das, N. C. Superior Electromagnetic Interference Shielding Effectiveness and Electro-mechanical Properties of EMA-IRGO Nanocomposites through the in-situ Reduction of GO from Melt Blended EMA-GO Composites. *Compos. Part B.* **2018**, *134*, 46–60. doi:10.1016/j.compositesb.2017.09.046.
176. Wu, Z.; Gao, S.; Chen, L.; Jiang, D.; Shao, Q.; Zhang, B.; Zhai, Z.; Wang, C.; Zhao, M.; Ma, Y.; et al. Electrically Insulated Epoxy Nanocomposites Reinforced with Synergistic Core–Shell SiO_2@MWCNTs and Montmorillonite Bifillers. *Macromol. Chem. Phys.* **2017**, *218*, 1700357. doi:10.1002/macp.201700357.

177. Pan, Y.; Liu, X.; Hao, X.; Starý, Z.; Schubert, D. W. Enhancing the Electrical Conductivity of Carbon Black-Filled Immiscible Polymer Blends by Tuning the Morphology. *Eur. Polym. J.* **2016**, *78*, 106–115. doi:10.1016/j.eurpolymj.2016.03.019.
178. Ding-Xiang, Y.; Huan, P.; Ling, X.; Yu, B.; Peng-Gang, R.; Jun, L.; Zhong-Ming, L. Electromagnetic Interference Shielding of Segregated Polymer Composite with an Ultralow Loading of in Situ Thermally Reduced Graphene Oxide. *Nanotechnol.* **2014**, *25*, 145705. doi:10.1088/0957-4484/25/14/145705.
179. Yan, D.-X.; Pang, H.; Li, B.; Vajtai, R.; Xu, L.; Ren, P.-G.; Wang, J.-H.; Li, Z.-M. Structured Reduced Graphene Oxide/Polymer Composites for Ultra-Efficient Electromagnetic Interference Shielding. *Adv. Funct. Mater.* **2015**, *25*, 559–566. doi:10.1002/adfm.201403809.
180. Sumita, M.; Sakata, K.; Asai, S.; Miyasaka, K.; Nakagawa, H. Dispersion of Fillers and the Electrical Conductivity of Polymer Blends Filled with Carbon Black. *Polym. Bull.* **1991**, *25*, 265–271. doi:10.1007/BF00310802.
181. Shahzad, F.; Lee, S. H.; Hong, S. M.; Koo, C. M. Segregated Reduced Graphene Oxide Polymer Composite as a High Performance Electromagnetic Interference Shield. *Res. Chem. Intermed.* **2018**, *44*, 4707–4719. doi:10.1007/s11164-018-3274-7.
182. Wu, H.-Y.; Jia, L.-C.; Yan, D.-X.; Gao, J-f.; Zhang, X.-P.; Ren, P.-G.; Li, Z.-M. Simultaneously Improved Electromagnetic Interference Shielding Andĭ ▫ mechanical Performance of Segregated Carbon Nanotube/polypropylene Composite via Solid Phase Molding. *Compos. Sci. Technol.* **2018**, *156*, 87–94. doi:10.1016/j.compscitech.2017.12.027.
183. C, D. N.; K, C. T.; D, K.; A, C. Electromagnetic Interference Shielding Effectiveness of Conductive Carbon Black and Carbon Fiber-filled Composites Based on Rubber and Rubber Blends. *Adv. Polym. Technol* **2001**, *20*, 226–236.
184. Sumita, M.; Sakata, K.; Hayakawa, Y.; Asai, S.; Miyasaka, K.; Tanemura, M. Double Percolation Effect on the Electrical Conductivity of Conductive Particles Filled Polymer Blends. *Colloid Polym. Sci.* **1992**, *270*, 134–139. doi:10.1007/BF00652179.
185. G, S. B.; F, C. L.; A, S. A.; Tamara, I.; O, B. G. M.; Sebastien, L. Conducting Melt Blending of Polystyrene and EVA Copolymer with Carbon Nanotube Assisted by Phosphonium-Based Ionic Liquid. *J. Appl. Polym. Sci* **2018**, *135*, 45564.
186. Fenouillot, F.; Cassagnau, P.; Majesté, J. C. Uneven Distribution of Nanoparticles in Immiscible Fluids: Morphology Development in Polymer Blends. *Polym.* **2009**, *50*, 1333–1350. doi:10.1016/j.polymer.2008.12.029.
187. Wu, S. *Polymer Interface and Adhesion*; Marcel Dekker: New York; Basel, **1982**.
188. Biswas, S.; Kar, G. P.; Bose, S. Engineering Nanostructured Polymer Blends with Controlled Nanoparticle Location for Excellent Microwave Absorption: a Compartmentalized Approach. *Nanoscale* **2015**, *7*, 11334–11351. doi:10.1039/C5NR01785H.
189. Zhang, J.; Ravati, S.; Virgilio, N.; Favis, B. D. Ultralow Percolation Thresholds in Ternary Cocontinuous Polymer Blends. *Macromol* **2007**, *40*, 8817–8820. doi:10.1021/ma0716480.
190. Jyotishkumar, P.; OZdilek, C.; Moldenaers, P.; Sinturel, C.; Janke, A.; Pionteck, Jrgen.; Thomas, S. Dynamics of Phase Separation in Poly(acrylonitrile-butadiene-styrene)-Modified Epoxy/DDS System: Kinetics and Viscoelastic Effects. *J. Phys. Chem. B.* **2010**, *114*, 13271–13281. doi:10.1021/jp101661t.
191. W, M. C. Morphology Development and Control in Immiscible Polymer Blends. *Macromol. Symp.* **2000**, *149*, 171–184.
192. Willemse, R. C.; Ramaker, E. J. J.; van Dam, J.; Posthuma de Boer, A. Morphology Development in Immiscible Polymer Blends: Initial Blend Morphology and Phase Dimensions. *Polym.* **1999**, *40*, 6651–6659. doi:10.1016/S0032-3861(99)00038-5.
193. Sundararaj, U.; Macosko, C. W. Drop Breakup and Coalescence in Polymer Blends: The Effects of Concentration and Compatibilization. *Macromol* **1995**, *28*, 2647–2657. doi:10.1021/ma00112a009.
194. Pang, H.; Yan, D.-X.; Bao, Y.; Chen, J.-B.; Chen, C.; Li, Z.-M. Super-Tough Conducting Carbon Nanotube/Ultrahigh-Molecular-Weight Polyethylene Composites with Segregated and Double-Percolated Structure. *J. Mater. Chem.* **2012**, *22*, 23568–23575. doi:10.1039/c2jm34793h.

195. Al-Saleh Mohammed, H.; Sundararaj, U. Microstructure, Electrical, and Electromagnetic Interference Shielding Properties of Carbon Nanotube/Acrylonitrile-Butadiene-Styrene Nanocomposites. *J. Polym. Sci. B Polym. Phys.* **2012**, *50*, 1356–1362. doi:10.1002/polb.23129.
196. P, S. D.; I, S. T.; S, R. S. D. A.; O, B. G. M.; Alessandro, P.; G, S. B. Hybrid Composites of ABS with Carbonaceous Fillers for Electromagnetic Shielding Applications. *J. Appl. Polym. Sci.* **2018**, *135*, 46546.
197. Schmitz, D. P.; Ecco, L. G.; Dul, S.; Pereira, E. C. L.; Soares, B. G.; Barra, G. M. O.; Pegoretti, A. Electromagnetic Interference Shielding Effectiveness of ABS Carbon-based Composites Manufactured via Fused Deposition Modelling. *Mater. Today Commun.* **2018**, *15*, 70–80. doi:10.1016/j.mtcomm.2018.02.034.
198. Ji, X.; Chen, D.; Wang, Q.; Shen, J.; Guo, S. Synergistic Effect of Flame Retardants and Carbon Nanotubes on Flame Retarding and Electromagnetic Shielding Properties of Thermoplastic Polyurethane. *Compos. Sci. Technol.* **2018**, *163*, 49–55. doi:10.1016/j.compscitech.2018.05.007.
199. Xu, Y.; Tang, S.; Pan, J.; Bao, J.; Zhang, A. Reversibly Cross-linked SEBS/carbon Hybrid Composite with Excellent Solvent-proof and Electromagnetic Shielding Properties. *Mater. Des* **2018**, *146*, 1–11. doi:10.1016/j.matdes.2018.02.071.
200. Lu, D.; Mo, Z.; Liang, B.; Yang, L.; He, Z.; Zhu, H.; Tang, Z.; Gui, X. Flexible, Lightweight Carbon Nanotube Sponges and Composites for High-performance Electromagnetic Interference Shielding. *Carbon* **2018**, *133*, 457–463. doi:10.1016/j.carbon.2018.03.061.
201. Ma, X.; Shen, B.; Zhang, L.; Liu, Y.; Zhai, W.; Zheng, W. Porous Superhydrophobic Polymer/Carbon Composites for Lightweight and Self-cleaning EMI Shielding Application. *Compos. Sci. Technol.* **2018**, *158*, 86–93. doi:10.1016/j.compscitech.2018.02.006.
202. Nimbalkar, P.; Korde, A.; Goyal, R. K. Electromagnetic Interference Shielding of Polycarbonate/GNP Nanocomposites in X-Band. *Mater. Chem. Phys.* **2018**, *206*, 251–258. doi:10.1016/j.matchemphys.2017.12.027.
203. Bai, X.; Zhai, Y.; Zhang, Y. Green Approach to Prepare Graphene-Based Composites with High Microwave Absorption Capacity. *J. Phys. Chem. C.* **2011**, *115*, 11673–11677. doi:10.1021/jp202475m.
204. Nasouri, K.; Shoushtari, A. M. Fabrication of Magnetite Nanoparticles/polyvinylpyrrolidone Composite Nanofibers and Their Application as Electromagnetic Interference Shielding Material. *J. Thermoplast. Compos. Mater.* **2018**, *31*, 431–446. doi:10.1177/0892705717704488.
205. Chauhan Sampat, S.; Verma, P.; Malik Rajender, S.; Choudhary, V. Thermomechanically Stable Dielectric Composites Based on Poly(ether Ketone) and $BaTiO_3$ with Improved Electromagnetic Shielding Properties in X-Band. *J. Appl. Polym. Sci.* **2018**, *135*, 46413. doi:10.1002/app.46413.
206. Wang, H.; Zheng, K.; Zhang, X.; Wang, Y.; Xiao, C.; Chen, L.; Tian, X. Hollow Microsphere-Infused Porous Poly(vinylidene Fluoride)/Multiwall Carbon Nanotube Composites with Excellent Electromagnetic Shielding and Low Thermal Transport. *J. Mater. Sci.* **2018**, *53*, 6042–6052. doi:10.1007/s10853-017-1964-y.
207. Wang, H.; Zheng, K.; Zhang, X.; Du, T.; Xiao, C.; Ding, X.; Bao, C.; Chen, L.; Tian, X. Segregated Poly(vinylidene Fluoride)/MWCNTs Composites for High-performance Electromagnetic Interference Shielding. *Compos. Part A.* **2016**, *90*, 606–613. doi:10.1016/j.compositesa.2016.08.030.
208. Zhang, K.; Yu, H.-O.; Shi, Y.-D.; Chen, Y.-F.; Zeng, J.-B.; Guo, J.; Wang, B.; Guo, Z.; Wang, M. Morphological Regulation Improved Electrical Conductivity and Electromagnetic Interference Shielding in Poly(l-lactide)/Poly(ε-caprolactone)/Carbon Nanotube Nanocomposites via Constructing Stereocomplex Crystallites. *J. Mater. Chem. C.* **2017**, *5*, 2807–2817. doi:10.1039/C7TC00389G.
209. Zhang, K.; Li, G.-H.; Feng, L.-M.; Wang, N.; Guo, J.; Sun, K.; Yu, K.-X.; Zeng, J.-B.; Li, T.; Guo, Z.; Wang, M. Ultralow Percolation Threshold and Enhanced Electromagnetic Interference Shielding in Poly(l-lactide)/Multi-walled Carbon Nanotube Nanocomposites

with Electrically Conductive Segregated Networks. *J. Mater. Chem. C.* **2017**, *5*, 9359–9369. doi:10.1039/C7TC02948A.

210. Liu, Y.-F.; Feng, L.-M.; Chen, Y.-F.; Shi, Y.-D.; Chen, X.-D.; Wang, M. Segregated Polypropylene/Cross-linked Poly(ethylene-co-1-octene)/Multi-walled Carbon Nanotube Nanocomposites with Low Percolation Threshold and Dominated Negative Temperature Coefficient Effect: Towards Electromagnetic Interference Shielding and Thermistors. *Compos. Sci. Technol.* **2018**, *159*, 152–161. doi:10.1016/j.compscitech.2018.02.041.
211. Bizhani, H.; Nayyeri, V.; Katbab, A.; Jalali-Arani, A.; Nazockdast, H. Double Percolated MWCNTs Loaded PC/SAN Nanocomposites as an Absorbing Electromagnetic Shield. *Eur. Polym. J.* **2018**, *100*, 209–218. doi:10.1016/j.eurpolymj.2018.01.016.
212. Yu, W.-C.; Xu, J.-Z.; Wang, Z.-G.; Huang, Y.-F.; Yin, H.-M.; Xu, L.; Chen, Y.-W.; Yan, D.-X.; Li, Z.-M. Constructing Highly Oriented Segregated Structure towards High-strength Carbon Nanotube/Ultrahigh-Molecular-Weight Polyethylene Composites for Electromagnetic Interference Shielding. *Compos. Part A*. **2018**, *110*, 237–245. doi:10.1016/j.compositesa.2018.05.004.
213. Li, L-y.; Li, S-l.; Shao, Y.; Dou, R.; Yin, B.; Yang, M.-b. PVDF/PS/HDPE/MWCNTs/Fe_3O_4 Nanocomposites: Effective and Lightweight Electromagnetic Interference Shielding Material through the Synergetic Effect of MWCNTs and Fe_3O_4 Nanoparticles. *Curr. Appl. Phys.* **2018**, *18*, 388–396. doi:10.1016/j.cap.2018.01.014.
214. Zha, X.-J.; Pu, J.-H.; Ma, L.-F.; Li, T.; Bao, R.-Y.; Bai, L.; Liu, Z.-Y.; Yang, M.-B.; Yang, W. A Particular Interfacial Strategy in PVDF/OBC/MWCNT Nanocomposites for High Dielectric Performance and Electromagnetic Interference Shielding. *Compos. Part A*. **2018**, *105*, 118–125. doi:10.1016/j.compositesa.2017.11.011.
215. Shi, Y.-D.; Yu, H.-O.; Li, J.; Tan, Y.-J.; Chen, Y.-F.; Wang, M.; Wu, H.; Guo, S. Low Magnetic Field-induced Alignment of Nickel Particles in Segregated Poly(l-lactide)/Poly(ε-caprolactone)/Multi-walled Carbon Nanotube Nanocomposites: Towards Remarkable and Tunable Conductive Anisotropy. *Chem. Eng. J.* **2018**, *347*, 472–482. doi:10.1016/j.cej.2018.04.147.
216. Mao, C.; Huang, J.; Zhu, Y.; Jiang, W.; Tang, Q.; Ma, X. Tailored Parallel Graphene Stripes in Plastic Film with Conductive Anisotropy by Shear-Induced Self-Assembly. *J. Phys. Chem. Lett.* **2013**, *4*, 43–47. doi:10.1021/jz301811b.
217. Hashemi Seyyed, A.; Mousavi Seyyed, M.; Arjmand, M.; Yan, N.; Sundararaj, U. Electrified Single-walled Carbon Nanotube/epoxy Nanocomposite via Vacuum Shock Technique: Effect of Alignment on Electrical Conductivity and Electromagnetic Interference Shielding. *Polym. Compos.* **2018**, *39*, E1139–E1148. doi:10.1002/pc.24632.
218. Yang, Y.; Gupta, M. C.; Dudley, K. L.; Lawrence, R. W. Conductive Carbon Nanofiber-Polymer Foam Structures. *Adv. Mater.* **2005**, *17*, 1999–2003. doi:10.1002/adma.200500615.
219. Wang, C.; Wu, Y.; Li, Y.; Shao, Q.; Yan, X.; Han, C.; Wang, Z.; Liu, Z.; Guo, Z. Flame-retardant Rigid Polyurethane Foam with a Phosphorus-Nitrogen Single Intumescent Flame Retardant. *Polym. Adv. Technol.* **2018**, *29*, 668–676. doi:10.1002/pat.4105.
220. Ghosh, S.; Remanan, S.; Mondal, S.; Ganguly, S.; Das, P.; Singha, N.; Das, N. C. An Approach to Prepare Mechanically Robust Full IPN Strengthened Conductive Cotton Fabric for High Strain Tolerant Electromagnetic Interference Shielding. *Chem. Eng. J.* **2018**, *344*, 138–154. doi:10.1016/j.cej.2018.03.039.
221. Lu, Y.; Biswas, M. C.; Guo, Z.; Jeon, J.-W.; Wujcik, E. K. Recent Developments in Bio-monitoring via Advanced Polymer Nanocomposite-based Wearable Strain Sensors. *Biosens. Bioelectron.* **2018**, *123*, 167–177.
222. Ghosh, S.; Ganguly, S.; Remanan, S.; Mondal, S.; Jana, S.; Maji, P. K.; Singha, N.; Das, N. C. Ultra-light Weight, water Durable and Flexible Highly Electrical Conductive Polyurethane Foam for Superior Electromagnetic Interference Shielding Materials. *J. Mater. Sci: Mater. Electron.* **2018**, *29*, 10177–10189. doi:10.1007/s10854-018-9068-2.
223. Eswaraiah, V.; Sankaranarayanan, V.; Ramaprabhu, S. Functionalized Graphene–PVDF Foam Composites for EMI Shielding. *Macromol. Mater. Eng.* **2011**, *296*, 894–898. doi:10.1002/mame.201100035.

224. Thomassin, J.-M.; Vuluga, D.; Alexandre, M.; Jérôme, C.; Molenberg, I.; Huynen, I.; Detrembleur, C. A Convenient Route for the Dispersion of Carbon Nanotubes in Polymers: Application to the Preparation of Electromagnetic Interference (EMI) Absorbers. *Polymer* **2012**, *53*, 169–174. doi:10.1016/j.polymer.2011.11.026.
225. Xu, X. B.; Li, Z. M.; Shi, L.; Bian, X. C.; Xiang, Z. D. Ultralight Conductive Carbon Nanotube-Polymer Composite. *Small* **2007**, *3*, 408–411. doi:10.1002/smll.200600348.
226. Li, L.; Morris, J. E. Electrical Conduction Models for Isotropically Conductive Adhesive Joints. *IEEE Trans. Comp, Packag, Manufact. Technol. A*. **1997**, *20*, 3–8. doi:10.1109/95.558537.
227. Gadenne, M.; Gadenne, P.; Martin, J. C.; Sella, C. Composition and Electrical Properties of Au@Al2O3 Cermet Thin Films: A Critical Study. *Thin Solid Films* **1992**, *221*, 183–190. doi:10.1016/0040-6090(92)90812-P.
228. Kirkpatrick, S. Percolation and Conduction. *Rev. Mod. Phys.* **1973**, *45*, 574–588. doi:10.1103/RevModPhys.45.574.
229. Wang, G.; Zhao, G.; Wang, S.; Zhang, L.; Park, C. B. Injection-Molded Microcellular PLA/Graphite Nanocomposites with Dramatically Enhanced Mechanical and Electrical Properties for Ultra-efficient EMI Shielding Applications. *J. Mater. Chem. C*. **2018**, *6*, 6847–6859. doi:10.1039/C8TC01326H.
230. Yang, Y.; Gupta, M. C.; Dudley, K. L.; Lawrence, R. W. Novel Carbon Nanotube – Polystyrene Foam Composites for Electromagnetic Interference Shielding. *Nano Lett.* **2005**, *5*, 2131–2134. doi:10.1021/nl051375r.
231. Chen, Z.; Xu, C.; Ma, C.; Ren, W.; Cheng, H.-M. Lightweight and Flexible Graphene Foam Composites for High-Performance Electromagnetic Interference Shielding. *Adv. Mater.* **2013**, *25*, 1296–1300. doi:10.1002/adma.201204196.
232. Xu, L.; Jia, L.-C.; Yan, D.-X.; Ren, P.-G.; Xu, J.-Z.; Li, Z.-M. Efficient Electromagnetic Interference Shielding of Lightweight Carbon Nanotube/Polyethylene Composites via Compression Molding plus Salt-Leaching. *RSC Adv.* **2018**, *8*, 8849–8855. doi:10.1039/C7RA13453C.
233. Yan, D.-X.; Ren, P.-G.; Pang, H.; Fu, Q.; Yang, M.-B.; Li, Z.-M. Efficient Electromagnetic Interference Shielding of Lightweight Graphene/Polystyrene Composite. *J. Mater. Chem.* **2012**, *22*, 18772–18774. doi:10.1039/c2jm32692b.
234. Zhang, H.-B.; Yan, Q.; Zheng, W.-G.; He, Z.; Yu, Z.-Z. Tough Graphene-Polymer Microcellular Foams for Electromagnetic Interference Shielding. *ACS Appl. Mater. Interfaces* **2011**, *3*, 918–924. doi:10.1021/am200021v.
235. Shen, B.; Zhai, W.; Tao, M.; Ling, J.; Zheng, W. Lightweight, Multifunctional Polyetherimide/Graphene@Fe_3O_4 Composite Foams for Shielding of Electromagnetic Pollution. *ACS Appl. Mater. Interfaces* **2013**, *5*, 11383–11391. doi:10.1021/am4036527.
236. Shen, B.; Li, Y.; Zhai, W.; Zheng, W. Compressible Graphene-Coated Polymer Foams with Ultralow Density for Adjustable Electromagnetic Interference (EMI) Shielding. *ACS Appl. Mater. Interfaces* **2016**, *8*, 8050–8057. doi:10.1021/acsami.5b11715.
237. Ling, J.; Zhai, W.; Feng, W.; Shen, B.; Zhang, J.; Zheng, W. g. Facile Preparation of Lightweight Microcellular Polyetherimide/Graphene Composite Foams for Electromagnetic Interference Shielding. *ACS Appl. Mater. Interfaces* **2013**, *5*, 2677–2684. doi:10.1021/am303289m.
238. Zeng, Z.; Jin, H.; Chen, M.; Li, W.; Zhou, L.; Zhang, Z. Lightweight and Anisotropic Porous MWCNT/WPU Composites for Ultrahigh Performance Electromagnetic Interference Shielding. *Adv. Funct. Mater.* **2016**, *26*, 303–310. doi:10.1002/adfm.201503579.
239. Yang, W.; Shao, B.; Liu, T.; Zhang, Y.; Huang, R.; Chen, F.; Fu, Q. Robust and Mechanically and Electrically Self-Healing Hydrogel for Efficient Electromagnetic Interference Shielding. *ACS Appl. Mater. Interfaces* **2018**, *10*, 8245–8257. doi:10.1021/acsami.7b18700.

240. Xing, D.; Lu, L.; Teh, K. S.; Wan, Z.; Xie, Y.; Tang, Y. Highly Flexible and Ultra-thin Ni-plated Carbon-fabric/polycarbonate Film for Enhanced Electromagnetic Interference Shielding. *Carbon* **2018**, *132*, 32–41. doi:10.1016/j.carbon.2018.02.001.
241. Na, R.; Liu, J.; Wang, G.; Zhang, S. Light Weight and Flexible Poly(ether Ether Ketone) Based Composite Film with Excellent Thermal Stability and Mechanical Properties for Wide-band Electromagnetic Interference Shielding. *RSC Adv.* **2018**, *8*, 3296–3303. doi:10.1039/C7RA11675F.
242. Jia, L.-C.; Yan, D.-X.; Liu, X.; Ma, R.; Wu, H.-Y.; Li, Z.-M. Highly Efficient and Reliable Transparent Electromagnetic Interference Shielding Film. *ACS Appl. Mater. Interfaces* **2018**, *10*, 11941–11949. doi:10.1021/acsami.8b00492.
243. Oh, H.-J.; Dao, V.-D.; Choi, H.-S. Electromagnetic Shielding Effectiveness of a Thin Silver Layer Deposited onto PET Film via Atmospheric Pressure Plasma Reduction. *Appl. Surf. Sci* **2018**, *435*, 7–15. doi:10.1016/j.apsusc.2017.11.043.
244. Ozen, M. S.; Sancak, E.; Soin, N.; Shah, T. H.; Zarei, A.; Siores, E. Unprecedented Electromagnetic Shielding Effectiveness of Lightweight Nonwoven Ag/PA66 Fabrics. *Fibers Polym.* **2018**, *19*, 321–330. doi:10.1007/s12221-018-7210-z.
245. Sabira, K.; Jayakrishnan, M. P.; Saheeda, P.; Jayalekshmi, S. On the Absorption Dominated EMI Shielding Effects in Free Standing and Flexible Films of Poly(vinylidene Fluoride)/Graphene Nanocomposite. *Eur. Polym. J.* **2018**, *99*, 437–444. doi:10.1016/j.eurpolymj.2017.12.034.
246. Kim, H. M.; Kim, K.; Lee, C. Y.; Joo, J.; Cho, S. J.; Yoon, H. S.; Pejaković, D. A.; Yoo, J. W.; Epstein, A. J. Electrical Conductivity and Electromagnetic Interference Shielding of Multiwalled Carbon Nanotube Composites Containing Fe Catalyst. *Appl. Phys. Lett.* **2004**, *84*, 589–591. doi:10.1063/1.1641167.
247. Xu, Y.; Yang, Y.; Duan, H.; Gao, J.; Yan, D.-X.; Zhao, G.; Liu, Y. Flexible and Highly Conductive Sandwich Nylon/nickel Film for Ultra-efficient Electromagnetic Interference Shielding. *Appl. Surf. Sci.* **2018**, *455*, 856–863. doi:10.1016/j.apsusc.2018.06.061.
248. Duan, H.; Zhao, M.; Yang, Y.; Zhao, G.; Liu, Y. Flexible and Conductive PP/EPDM/Ni Coated Glass Fiber Composite for Efficient Electromagnetic Interference Shielding. *J. Mater. Sci: Mater. Electron.* **2018**, *29*, 10329–10336. doi:10.1007/s10854-018-9089-x.
249. Wan, X.; Lu, H.; Kang, J.; Li, S.; Yue, Y. Preparation of Graphene-Glass Fiber-resin Composites and Its Electromagnetic Shielding Performance. *Compos. Interfaces* **2018**, *25*, 883–900. doi:10.1080/09276440.2018.1439641.
250. Yang, H.; Yu, Z.; Wu, P.; Zou, H.; Liu, P. Electromagnetic Interference Shielding Effectiveness of Microcellular Polyimide/in Situ Thermally Reduced Graphene Oxide/Carbon Nanotubes Nanocomposites. *Appl. Surf. Sci.* **2018**, *434*, 318–325.
251. Baokang, D.; Yipeng, C.; Ning, Y.; Bo, C.; Qingfeng, S. Effect of Carbon Fiber Addition on the Electromagnetic Shielding Properties of Carbon Fiber/Polyacrylamide/Wood Based Fiberboards. *Nanotechnol.* **2018**, *29*, 195605.
252. Gupta, T. K.; Singh, B. P.; Dhakate, S. R.; Singh, V. N.; Mathur, R. B. Improved Nanoindentation and Microwave Shielding Properties of Modified MWCNT Reinforced Polyurethane Composites. *J. Mater. Chem. A.* **2013**, *1*, 9138–9149. doi:10.1039/c3ta11611e.
253. Verma, P.; Saini, P.; Malik, R. S.; Choudhary, V. Excellent Electromagnetic Interference Shielding and Mechanical Properties of High Loading Carbon-Nanotubes/Polymer Composites Designed Using Melt Recirculation Equipped Twin-Screw Extruder. *Carbon* **2015**, *89*, 308–317. doi:10.1016/j.carbon.2015.03.063.
254. Pawar, S. P.; Stephen, S.; Bose, S.; Mittal, V. Tailored Electrical Conductivity, Electromagnetic Shielding and Thermal Transport in Polymeric Blends with Graphene Sheets Decorated with Nickel Nanoparticles. *Phys. Chem. Chem. Phys.* **2015**, *17*, 14922–14930. doi:10.1039/C5CP00899A.
255. Al-Saleh, M. H.; Sundararaj, U. Electromagnetic Interference Shielding Mechanisms of CNT/Polymer Composites. *Carbon* **2009**, *47*, 1738–1746. doi:10.1016/j.carbon.2009.02.030.
256. Duan, H.; Zhu, H.; Yang, Y.; Hou, T.; Zhao, G.; Liu, Y. Facile and Economical Fabrication of Conductive Polyamide 6 Composites with Segregated Expanded Graphite Networks for

Efficient Electromagnetic Interference Shielding. *J. Mater. Sci: Mater. Electron*. **2018**, *29*, 1058–1064. doi:10.1007/s10854-017-8006-z.

257. George, G.; Simon Sanu, M.; Prakashan, V. P.; Sajna, M. S.; Faisal, M.; Chandran, A.; Wilson, R.; Biju, P. R.; Joseph, C.; Unnikrishnan, N. V. Morphological, Dielectric, Tunable Electromagnetic Interference Shielding and Thermal Characteristics of Multiwalled Carbon Nanotube Incorporated Polymer Nanocomposites: A Facile, Environmentally Benign and Cost Effective Approach Realized via Polymer Latex/Waterborne Polymer as Matrix. *Polym. Compos*. **2017**, *39*, E1169–E1183. doi:10.1002/pc.24689.
258. Li, Y.; Pei, X.; Shen, B.; Zhai, W.; Zhang, L.; Zheng, W. Polyimide/Graphene Composite Foam Sheets with Ultrahigh Thermostability for Electromagnetic Interference Shielding. *RSC Adv*. **2015**, *5*, 24342–24351. doi:10.1039/C4RA16421K.
259. Zhao, B.; Wang, S.; Zhao, C.; Li, R.; Hamidinejad, S. M.; Kazemi, Y.; Park, C. B. Synergism between Carbon Materials and Ni Chains in Flexible Poly(vinylidene Fluoride) Composite Films with High Heat Dissipation to Improve Electromagnetic Shielding Properties. *Carbon* **2018**, *127*, 469–478. doi:10.1016/j.carbon.2017.11.032.
260. Sambyal, P.; Dhawan, S. K.; Gairola, P.; Chauhan, S. S.; Gairola, S. P. Synergistic Effect of Polypyrrole/BST/RGO/Fe_3O_4 Composite for Enhanced Microwave Absorption and EMI Shielding in X-Band. *Curr. Appl. Phys*. **2018**, *18*, 611–618. doi:10.1016/j.cap.2018.03.001.
261. Zhan, Y.; Wang, J.; Zhang, K.; Li, Y.; Meng, Y.; Yan, N.; Wei, W.; Peng, F.; Xia, H. Fabrication of a Flexible Electromagnetic Interference Shielding Fe3O4@reduced Graphene Oxide/Natural Rubber Composite with Segregated Network. *Chem. Eng. J*. **2018**, *344*, 184–193. doi:10.1016/j.cej.2018.03.085.
262. Biswas, S.; Arief, I.; Panja, S. S.; Bose, S. Absorption-Dominated Electromagnetic Wave Suppressor Derived from Ferrite-Doped Cross-Linked Graphene Framework and Conducting Carbon. *ACS Appl. Mater. Interfaces* **2017**, *9*, 3030–3039. doi:10.1021/acsami.6b14853.
263. Biswas, S.; Panja, S. S.; Bose, S. Unique Multilayered Assembly Consisting of "Flower-Like" Ferrite Nanoclusters Conjugated with MWCNT as Millimeter Wave Absorbers. *J. Phys. Chem. C*. **2017**, *121*, 13998–14009. doi:10.1021/acs.jpcc.7b02668.
264. Xu, Y.; Yang, Y.; Yan, D.-X.; Duan, H.; Zhao, G.; Liu, Y. Gradient Structure Design of Flexible Waterborne Polyurethane Conductive Films for Ultraefficient Electromagnetic Shielding with Low Reflection Characteristic. *ACS Appl. Mater. Interfaces* **2018**, *10*, 19143–19152. doi:10.1021/acsami.8b05129.
265. Wang, C.; Guo, R.; Lan, J.; Tan, L.; Jiang, S.; Xiang, C. Preparation of Multi-functional Fabric via Silver/reduced Graphene Oxide Coating with Poly(diallyldimethylammonium Chloride) Modification. *J. Mater. Sci: Mater. Electron*. **2018**, *29*, 8010–8019. doi:10.1007/s10854-018-8807-8.
266. Woo, H. J.; Majid, S. R.; Arof, A. K. Dielectric Properties and Morphology of Polymer Electrolyte Based on Poly(ε-caprolactone) and Ammonium Thiocyanate. *Mater. Chem. Phys*. **2012**, *134*, 755–761. doi:10.1016/j.matchemphys.2012.03.064.
267. Jin, L.; Zhao, X.; Xu, J.; Luo, Y.; Chen, D.; Chen, G. The Synergistic Effect of a Graphene Nanoplate/Fe_3O_4@$BaTiO_3$ Hybrid and MWCNTs on Enhancing Broadband Electromagnetic Interference Shielding Performance. *RSC Adv*. **2018**, *8*, 2065–2071. doi:10.1039/C7RA12909B.
268. Zhang, X.-J.; Wang, G.-S.; Cao, W.-Q.; Wei, Y.-Z.; Liang, J.-F.; Guo, L.; Cao, M.-S. Enhanced Microwave Absorption Property of Reduced Graphene Oxide (RGO)-MnFe2O4 Nanocomposites and Polyvinylidene Fluoride. *ACS Appl. Mater. Interfaces* **2014**, *6*, 7471–7478. doi:10.1021/am500862g.
269. Hua, J.; Li, Y.; Liu, X.; Li, X.; Lin, S.; Gu, J.; Cui, Z.-K.; Zhuang, Q. Graphene/MWNT/Poly (p-phenylenebenzobisoxazole) Multiphase Nanocomposite via Solution Prepolymerization with Superior Microwave Absorption Properties and Thermal Stability. *J. Phys. Chem. C*. **2017**, *121*, 1072–1081. doi:10.1021/acs.jpcc.6b11925.